



DIPARTIMENTO DI INGEGNERIA INDUSTRIALE

Dottorato di Ricerca in Ingegneria Meccanica

XIII Ciclo N.S. (2011-2014)

***“Development and experimental validation of CPOx
reforming dynamic model for fault detection and isolation in
SOFC systems”***

Ing. Arturo Di Filippi

Il Tutor

Ch.mo Prof. Cesare Pianese

Dr. Ing. Marco Sorrentino

Il Co- Tutor

Dr. Ing. Dario Marra

Il Coordinatore

Ch.mo Prof. Vincenzo Sergi

A Giada, amb

Table of Contents

INDEX OF FIGURES

INDEX OF TABLES

ABSTRACT

Chapter 1 – INTRODUCTION	1
1.1 - Motivation and objectives of this work	2
1.2 - The Role of Systems Diagnosis	4
1.3 - Introduction to SOFC system diagnosis	5
1.3.1 - FDI: definitions and background	5
1.3.2 - Diagnosis for SOFC systems	7
1.4 - Hydrogen and syngas generation.	12
1.5 - Hydrogen production in fuel cell systems	13
1.6 - Fuel Reforming for FC applications	18
1.6.1 - Catalytic Partial Oxidation for FC systems	20
1.6.2 - Internal and external reforming in fuel cell systems	21
Chapter 2 – REFORMING SYSTEMS: STATE OF THE ART	27
2.1 - Steam Reforming (SR)	27
2.1.1 - Operating Parameters	31
2.1.2 - Thermodynamic analysis	32
2.2 - Partial oxidation (POx) and Catalytic partial oxidation (CPOx)	36
2.2.1 - Reaction Mechanisms	39
2.2.1.1 - Direct oxidation mechanism	39
2.2.1.2 - Indirect oxidation mechanism	40
2.2.1.3 - Literature debate and trend	41
2.2.2 - CPOx operating parameters	43
2.2.3 - Thermodynamic analysis	47
2.2.4 - Internal CPOx reforming for tubular fuel cell: Acumentrics technology	51
2.3 - Autothermal reforming	57

2.3.1 - Thermodynamic analysis	59
2.3.2 - Reaction Mechanism	61
2.4 - Catalysts and supports for CPOx reforming reactors	63
2.4.1 - Status of Catalytic Partial Oxidation Research	63
2.4.2 - CPOx reactors - literature background	65
2.4.3 - CPOx reactors - Catalysts	67
2.4.4 - CPOx reactors – Supports	70
2.5 - Alternative reactor layouts for fuel cell systems	73
2.5.1 - Compact regenerative reformers with concentric annular catalyst beds	73
2.5.2 - Plate reformers and micro-channel reformers	74
2.5.3 - Membrane reactor	75
2.5.4 - Non catalytic partial oxidation reactors	76
2.6 - Catalyst deactivation	77
2.6.1 – Poisoning	78
2.6.2 - Carbon Formation or Fouling	79
2.6.3 - Sintering	82
2.6.4 - Solid state transformation and physical loss of metal	82
Chapter 3 – EXPERIMENTAL SETUP	85
3.1 - EFESO project	85
3.2 - Tests setup	88
3.2.1 - Tests case a: Internal tests on CPOx reactor integrated in Hot Box	90
3.2.2 - Tests case b: Lab tests on CPOx reforming reactor prototype	94
3.2.3 - Tests case c: Tests on final 1 kW planar μ CHP unit	98
3.3 - Fault events in a CPOx reforming system	106
3.3.1 - Fault 1: Carbon deposition	113
3.3.2 - Fault 2: Catalyst oxidation	118
Chapter 4 – CPOx DYNAMIC MODEL	125
4.1 - Reforming Models in SOFC systems: literature review	125
4.2 - CPOx Modeling approaches	129
4.2.1 Minimization of Gibbs free energy	130
4.3 - CPOx Model theoretical content	131

4.4 - Model parameters	135
4.5 - CPOx model description	136
4.5.1 - Linear Regression	143
4.6 - Reactor Design	145
4.7 - Dynamic Conditions	147
Chapter 5 – MODEL VALIDATION AND APPLICATION	151
5.1 - Model results: x_{out} vs T_{out}	151
5.2 - Model results: λ vs T_{out}	155
5.3 - H_2 , CO Selectivity and CH_4 conversion	159
5.4 - Model validation	162
5.4.1 - Comparison with experimental data of tests case a (ref. section 3.2.1)	163
5.4.2 - Comparison with experimental data of tests case b (ref. section 3.2.2)	167
5.4.3 - Comparison with experimental data of tests c (ref. section 3.2.3)	169
5.5 - Fault 1- Carbon deposition: model based fault detection and isolation	175
5.6 - Fault 2- Catalyst oxidation: model based fault detection and isolation	178
CONCLUSIONS	183
Ringraziamenti	
REFERENCES	

Index of figures

Figure 1.1- FDI scheme	6
Figure 1.2- SOFC CPOx system P&ID (RP20 Acumentrics) [38]	8
Figure 1.3- SOFC steam reformed based μ CHP [37] - P&ID	9
Figure 1.4- Steam reforming plant (Technip)	14
Figure 1.5- Electrolysis scheme	17
Figure 1.6: Operating principle of a solid oxide fuel cell	20
Figure 1.7: External reforming CPOx in tubular SOFC system	22
Figure 1.8: Technology progress for reforming methods in fuel cells	23
Figure 1.9: Direct and Indirect internal reforming in fuel cells	24
Figure 2.1 – Flowchart of a standard steam reforming process	29
Figure 2.2: Steam generator configuration	31
Figure 2.3: effect of reactor temperature (with S/C ratio=1) on the equilibrium composition of a SMR reactor [8]	34
Figure 2.4-effect of S:C ratio on the equilibrium composition of a SMR reactor T = (---) 600°C; (-·-·-) 700°C; (----) 800°C [8]	34
Figure 2.5: effect of the pressure on the equilibrium composition and conversion of a SMR reactor (T= 700°C, S/C=1) [8]	35
Figure 2.6: Thermodynamic representation of the partial oxidation of methane	36
Figure 2.7: Image of a CPOx reactor used in a μ CHP application [38]	38
Figure 2.8: Carbon deposition limit over lambda and temperature (SOFC Power) [37]	45
Figure 2.9: conversion of CH ₄ and selectivity to CO in function of the spatial velocity [36]	47
Figure 2.10: Comparison of heating value and methane conversion of SR, CPOx and ATR reformates for different temperatures (Lambda CPOx = 0.27) [37]	48
Figure 2.11: effect of lambda on the equilibrium composition (reactant pre-heating temperature = 200°C) [8]	49
Figure 2.12: Adiabatic temperature, methane conversion and H ₂ gain over lambda (reactant preheating temperature = 200°C) [8]	49
Figure 2.13-a: effect of pre-heating temperature on the equilibrium	

composition of the reactor (reactant pre-heating temperature T = (---) 20°C; (-·-·-·) 200°C; (-·-·-·) 400°C)	50
Figure 2.13-b: effect of pre-heating temperature on the adiabatic temperature of the reactor (reactant pre-heating temperature T = (---) 20°C; (-·-·-·) 200°C; (-·-·-·) 400°C)	51
Figure 2.14: Fuel Cell Efficiency versus Oxygen to Carbon Ratio in Acumentrics technology [38]	53
Figure 2.15: Acumentrics stack bundle, tubular cells and catalytic injetors[38]	54
Figure 2.16: Air and fuel feeding system in Acumentrics μ CHP	56
Figure 2.17: ATR reactor [11]	58
Figure 2.18: effect of lambda and S/C ratio on the adiabatic temperature and conversion in ATR reactor (reactant pre-heating temperature = 400°C) [8]	60
Figure 2.19: effect of lambda and S/C ratio on mole fractions of H ₂ and CO in ATR reactor (reactant pre-heating temperature = 400°C)	60
Figure 2.20: Scheme of Ni/Al ₂ O ₃ catalyst during ATR at different operating temperatures [56]	62
Figure 2.21: Johnson Matthey HotSpot reactor	65
Figure 2.22: Catalyst powder Ni/Al ₂ O ₃	69
Figure 2.23: Corrugate monolith (left) and cordierite honeycomb monolith 600 CPSI (right)	72
Figure 2.24: Ceramic foam of alumina (left) and carbide silicon (right)	72
Figure 2.25: Haldor Topsoe heat exchange reformer	73
Figure 2.26: Plate reformer concept	75
Figure 2.27: Membrane module [ENEA]	76
Figure 3.1 - Planar and tubular solid oxide fuel cells and stacks [37, 38]	87
Figure 3.2 – 1000 W Hot Box tested at SOFC Power facilities [37]	90
Figure 3.3 – Reactor outlet molar fractions vs CPOx reaction equilibrium temperature for lambda 0.27	91
Figure 3.4 – Reactor outlet temperature vs Reactant inlet temperature for lambda 0.27	92
Figure 3.5 - Reactor outlet molar fractions vs CPOx reaction equilibrium temperature for lambda 0.30	92
Figure 3.6 – Reactor outlet temperature vs Reactant inlet temperature for	

lambda 0.30	93
Figure 3.7 - Reactor outlet molar fractions vs CPOx reaction equilibrium temperature for lambda 0.27	94
Figure 3.8 – CPOx reactor test bench scheme (Hysylab) [102]	95
Figure 3.9 – CPOx reactor test bench setup (Hysylab) [102]	95
Figure 3.10 – Gas chromatograph (Hysylab) [102]	96
Figure 3.11 – Reactor temperatures and molar output fractions for two different operating conditions	97
Figure 3.12 – Planar fuel cell stack (manufacturer SOFC Power) [37]	99
Figure 3.13 – 1 kW μ CHP realized by Ariston Thermo [103]	100
Figure 3.14 – Hot Box Module installed in 1 kW μ CHP: scheme and flowchart	101
Figure 3.15: μ CHP performance: stack, CPOx reactor, post combustor and air temperatures vs time	104
Figure 3.16: μ CHP performance: anode air and fuel flowrates, startup burner flowrate and lambda vs time	104
Figure 3.17: μ CHP performance: cathode air flowrate, fuel consumption, stack voltage and current vs time	105
Figure 3.18- Fault Tree fuel feeding system	112
Figure 3.19- Fault Tree reformer system	113
Figure 3.20- Fault 1 event: stack, CPOx reactor, post combustor and air temperatures vs time	115
Figure 3.21- Fault 1 event: T_{CPOx} , anode air and fuel flows, lambda vs time (period restricted)	115
Figure 3.22- Fault 1 isolation: stack, CPOx reactor, post combustor and air temperatures vs time in the μ CHP startup afterwards the fault occurrence	116
Figure 3.23- Fault 1 isolation: T_{CPOx} , anode air and fuel flows, lambda vs time (period restricted) in the μ CHP startup afterwards the fault occurrence	117
Figure 3.24- Fault 1 isolation: stack voltage in the μ CHP startup afterwards the fault occurrence	117
Figure 3.25- Fault 2 event: T_{CPOx} , anode air and fuel flows, lambda vs time	119
Figure 3.26- Fault 2 isolation: stack, CPOx reactor, post combustor and air	

temperatures vs time in the μ CHP startup afterwards the fault occurrence	120
Figure 3.27- Fault 2 isolation: T_{CPOx} , anode air and fuel flows, lambda vs time (period restricted) in the μ CHP startup afterwards the fault occurrence	121
Figure 3.28- Fault 2 isolation: stack voltage in the μ CHP startup afterwards the fault occurrence	121
Figure 3.29- Fault 2 isolation: temperatures and anode flows in the fourth μ CHP startup afterwards the fault occurrence	122
Figure 3.30- Fault 2 isolation: deltaT stack top-bottom and air flows the fourth μ CHP startup afterwards the fault occurrence	122
Figure 3.31- Fault 2 isolation: cluster cells voltage the fourth μ CHP startup afterwards the fault occurrence	124
Figure 4.1 – Scheme of reformer model with the minimization of Gibbs free energy approach	131
Figure 4.2 – System of final equations	140
Figure 4.3 – CPOx model scheme	141
Figure 4.4 – SR model scheme	142
Figure 4.5 – Honeycomb support structure [9]	146
Figure 4.6 – Standard reactor layout configuration [102]	146
Figure 4.7 – Dynamic model scheme	148
Figure 4.8 – CPOx model temperature output trend	149
Figure 5.1 – x_{out} vs T_{out} and T_{out} vs T_{in} for lambda=0.25	152
Figure 5.2 – x_{out} vs T_{out} and T_{out} vs T_{in} for lambda=0.27	153
Figure 5.3 – x_{out} vs T_{out} and T_{out} vs T_{in} for lambda=0.30	154
Figure 5.4 – x_{out} vs T_{out} and T_{out} vs T_{in} for lambda=0.33	155
Figure 5.5 – x_{out} vs lambda and T_{out} vs lambda for $T_{in}=50^{\circ}C$	156
Figure 5.6 – x_{out} vs lambda and T_{out} vs lambda for $T_{in}=150^{\circ}C$	157
Figure 5.7 – x_{out} vs lambda and T_{out} vs lambda for $T_{in}=230^{\circ}C$	158
Figure 5.8 – x_{out} vs lambda and T_{out} vs lambda for $T_{in}=300^{\circ}C$	159
Figure 5.9 CH_4 conversion, H_2 and CO selectivity vs for T_{out} different lambda	160
Figure 5.10 CH_4 conversion, H_2 and CO selectivity vs lambda for different reactant pre-heating temperature	161
Figure 5.11 – x_{out} vs T_{out} for lambda=0.27: comparison with real data (test	

case a)	163
Figure 5.12 – Correlation between experimental and model results for lambda=0.27	164
Figure 5.13 – x_{out} vs T_{out} for lambda=0.30: comparison with real data (test case a)	164
Figure 5.14 – Correlation between experimental and model results for lambda=0.30	165
Figure 5.15 – T_{out} vs T_{in} for lambda=0.29: comparison with real data	166
Figure 5.16 – x_{out} vs lambda for $T_{in}=230^{\circ}\text{C}$: comparison with real data	167
Figure 5.17 – stack current vs time in μCHP power ramp-up phase: measured data	170
Figure 5.18 – cathode air flow vs time in μCHP power ramp-up phase: measured data	171
Figure 5.19 – anode fuel and air flow vs time in μCHP power ramp-up phase: measured data	171
Figure 5.20 – lambda vs time in μCHP ramp-up phase: measured data	172
Figure 5.21 – T_{out} vs time in μCHP ramp-up phase: comparison between measured and simulated transients	173
Figure 5.22 – Fault 1 detection: T_{CPOx} , anode air and fuel flows, lambda vs time	175
Figure 5.23 – Fault 1 isolation: T_{CPOx} measured and simulated, anode air and fuel flows, lambda vs time in the μCHP startup afterwards the fault occurrence	176
Figure 5.24- Fault 1 isolation: stack voltage in the μCHP startup afterwards the fault occurrence	178
Figure 5.25 – Fault 2 detection: T_{CPOx} , anode air and fuel flows, lambda vs time	179
Figure 5.26 – Fault 2 isolation: T_{CPOx} measured and simulated, anode air and fuel flows, lambda vs time in the μCHP startup afterwards the fault occurrence	180
Figure 5.27- Fault 2 isolation: stack voltage in the μCHP startup afterwards the fault occurrence	181

List of tables

Table 1.1 – Reforming mechanisms comparison	16
Table 2.1: Pro and cons of operating with different lambda	44
Table 2.2: Test results on Acumentrics 1kW μ CHP with low O/C ratios [38, 103]	55
Table 2.3 – catalysts for CPOx reactions- properties and technical features	68
Table 2.4 – supports for CPOx reactions- properties and technical features	71
Table 3.1 - Comparison between planar and tubular fuel cell technology	87
Table 3.2 – Product molar fraction and adiabatic reactor temperature for different lambda	93
Table 3.3 – Planar FC stack specifications and operating conditions	99
Table 3.4 – 1 kW μ CHP startup phases and operating conditions	103
Table 3.5 – Failure Mode and Effect Analysis (FMEA) for a CPOx reforming system	108
Table 3.6 – Fault tree symbols, nomenclature and description	110
Table 4.1 – Linear regression data	144
Table 4.2 – Reactor design data [36]	145
Table 5.1 – Deviation between experimental and model results for lambda=0.27	163
Table 5.2 – Deviation between experimental and model results for lambda=0.30	164
Table 5.3 – Test measurements for different lambda at $T_{in} = 230^{\circ}\text{C}$ [36]	166
Table 5.4 – Comparison between model and test results on CPOx reactor external to Hot Box	168

Abstract

In the present work an investigation of the reforming technologies available for Solid Oxide Fuel Cell (SOFC) systems and their basic concepts has been carried out, with the aim to describe, test and simulate the reforming process for fault diagnosis application.

The final aim of a fault diagnosis activity for SOFC systems is to reach the required criteria for a commercial application, which, besides long lifetime and performance, include high reliability and safety at reasonable costs. The achievement of these targets is necessary to contribute promoting the SOFC technology and finally starting a mass production phase.

In this thesis, the attention has been focused on the reforming reactor, responsible for the conversion of the inlet fuel in hydrogen, suitable source fuel for the SOFC. In particular, the Catalytic Partial Oxidation (CPOx) process has been analyzed.

The CPOx reforming mechanism is the most attractive technology for the production of syngas or hydrogen in small-medium scale SOFC applications and Micro Combined Heat and Power (μ CHP) systems. This is due to the ability of the CPOx reaction to be carried out in compact reactors with rapid dynamic response and with low heat capacity. The reaction is slightly exothermic and therefore does not require external heat to take place. In addition, CPOx technology does not require steam, as the media required for the reforming reaction is air, which is easily available for residential application. This mainly means that CPOx is independent from an external water source and any heating source. The hydrocarbon is both oxidized to CO_2 and H_2O , either partially or completely, and also converted to synthesis gas by endothermic steam reforming (according to the indirect CPOx mechanism).

Despite these advantages, catalytic partial oxidation is less efficient than steam reforming. This indicates that it is most suitable for applications in which the system simplicity has the priority with respect to the hydrogen yield. The high surface temperatures can cause a local loss of activity of the catalyst, leading to the instable performance of the entire reactor. Nevertheless, in the CPOx process even a small difference in the operating

air and fuel flow rates could lead to carbon deposition or oxidation of the catalyst, with serious consequences for the SOFC system and for the stack itself.

It is therefore extremely important to develop a diagnosis tool able to investigate these phenomena and to detect and isolate the faults that may verify inside the reactor. The most common fault events likely to occur inside a CPOx reformer for SOFC applications have been analyzed through a Failure Mode and Effect Analysis (FMEA) and a Fault Tree Analysis (FTA). These analyses are aimed at identifying the main events responsible for the catalyst deactivation, together with their causes and effects on the SOFC system performance.

The Catalytic Partial Oxidation mechanism has then been explored from both modelling and experimental points of view, with the aim to simulate the reforming process and identifying the thermodynamic optimal operating conditions at which natural gas may be converted to hydrogen. At the same time, the main fault scenarios likely to occur during the reforming phase have been analyzed, both in experiments and during simulations, to evaluate the capability of the developed model in performing effective fault detection and isolation for on-board diagnostic application.

The CPOx dynamic model developed is based on the minimization of Gibbs free energy and can be easily reconfigured for describing a steam reforming mechanism. The simulation results give useful indication on how operating parameters such as the input conditions of reactants (inlet compositions and temperature) affect the reaction equilibrium and, in turn, the products composition and reactor outlet temperature. A sensitivity analysis for different operating conditions has been carried out. The transient behavior of the reforming reaction and the information about methane conversion and hydrogen selectivity complete the set of model results.

The dynamic CPOx model has been validated through experimental data and its behavior during transients has been carefully analyzed during the variations in the set-points of operating phases. Both test data and reactor design were part of the activities performed within the EFESO project, funded by the Italian Ministry of Economic Development and led by Ariston Thermo Spa.

The model results demonstrate that the CPOx dynamic model represents a useful tool for fault diagnosis application and its results

provide an interesting benchmark for the design and working parameters of a CPOx reforming system for SOFC application.

CHAPTER 1

Introduction

Modern lifestyles have led to a relentless increase in energy consumption. Traditional ways to generate power include combustion of fossil fuels and coal, hydroelectric and nuclear energy conversion. The most widespread power generation technologies rely on the combustion of fossil fuels (e.g. oil, gas, coal), this leading to the environmental pollution due to the release of combustion products in the atmosphere. In addition, the uneven distribution of the finite fossil fuel sources worldwide causes geopolitical unrest. Therefore, there is a need for better ways to satisfy the energy demands of society. Fuel cells appear as an attractive alternative to traditional power generation methods. A fuel cell is a reactor that generates electrical power through an electrochemical reaction of fuel and oxidant, whereas fossil fuel combustion entails a thermodynamical reaction. Electrochemical power generation has many advantages over fossil fuel combustion, including higher efficiency, zero/low pollution, limited equipment maintenance and modularity. The fuel cell receives the reactants that take place in the energy conversion process in a continuous manner, unlike batteries, which use chemical energy that is stored within the electrodes [2,10].

Since the first demonstration of the fuel cell principle described by Sir William Grove in 1839, many types of fuel cells have been developed. In a first moment, a great attention was focused on proton exchange membrane fuel cells (PEMFC), overshadowing the development activities of other fuel cell types, but in the last decades Solid Oxide Fuel Cells (SOFC) have gathered a large attention, mainly for the potential applications as stationary power generation and auxiliary power generation (APUs) for transportation use (ground, marine, air). SOFC attractiveness lies on both the high energy conversion efficiency and the well-known limited emission levels (only the CO₂ released by the hydrogen production process is a concern). Other advantages are: modularity, fuel flexibility and

low noise [1, 21, 40]. Moreover, the high working temperatures provide additional positive features, such as potential use of SOFC in highly efficient cogeneration applications. SOFC may be also suitable for internally reforming the fuel (e.g. natural gas, propane, methanol, gasoline, Diesel, etc.), to produce the hydrogen for the electrical reaction [2].

Most types of fuel cells, including SOFC, require hydrogen as a fuel source. In the transition to sustainable energy, hydrogen is playing a key role as an energy carrier. Although the oldest and most common element in our universe, pure hydrogen is not a natural resource. All hydrogen on earth is stored in a compound with other molecules. Water, essential for all life processes surrounding us, consists of 66% hydrogen. Currently, hydrogen is the most widely industrial gas used in the refining, chemical and petrochemical industries, and in addition can be directly burned in an internal combustion engine or electrochemically converted to electricity in a fuel cell system. In the last years, hydrogen has been the center of attention of public opinion as a possible ‘pole star’ of a new energy future because it is a clean vector (if burnt, CO₂ is not emitted) [40].

1.1 - Motivation and objectives of this work

At the present, long-term stability appears as the most important requirement for the commercial application of the SOFC technology. For stationary applications, the commercial lifetime requirement is generally more than 40,000 h. In comparison, up to a 20,000 h lifetime with more frequent thermal cycles is required for auxiliary power units in transportation applications [6]. However, these lifetime requirements have not been met yet outside of lab environment [85, 86]: SOFC system prototypes still suffer from a low reliability of both the fuel cell itself and the complete system, not allowing their commercial large scale deployment. It is therefore essential to increase the understanding in SOFC systems degradation and faulty mechanisms [20].

The final aim of a fault diagnosis activity for SOFC systems is to reach the required criteria for a commercial application, which, besides long lifetime and performance, include high reliability and safety at suitable costs. The achievement of these targets will surely contribute to

promote the SOFC technology and finally starting a mass production phase.

In the present work, the attention has been focused on one particular component of the SOFC system, the reforming reactor, responsible of the conversion of inlet gas in hydrogen, suitable source fuel for the SOFC.

Hydrogen can be produced using different, domestic resources including fossil fuels, such as natural gas and coal (with carbon sequestration), nuclear, biomass and other renewable energy technologies, such as wind, solar, geothermal, and hydro-electric power. The overall challenge to hydrogen production is cost reduction. The development of clean, sustainable, and cost-competitive hydrogen production processes is key to a viable future clean energy economy. SOFC systems are fed by hydrogen that only in a few cases (mainly in lab tests) is pure, drawn by hydrogen storages. The widest usage of hydrogen for fuel cell derives from conversion of natural gas. In the sections below the hydrogen production mechanisms for fuel cell system are therefore described, with particular attention to the Catalytic Partial Oxidation (CPOx) process, which is the most suitable reforming mechanism for stationary and mobile application related to the development of a medium to small scale technology for the production of syngas and H₂.

Indeed, Catalytic Partial Oxidation mechanism has been explored from both a modeling and experimental viewpoint, with the aim to simulate the process and identify the thermodynamic favorable operating conditions at which natural gas may be converted to hydrogen. At the same time, the main fault scenarios likely to occur during the reforming phase have been analyzed, first experimentally and then in the model, showing the capability of the model to use fault detection and isolation approaches for diagnostic application.

The dynamic model has been validated on experimental data and its behavior during transients was carefully analyzed during the variations in the set-points of operating phases. Both test data and reactor design were part of the activities performed within the EFESO project, funded by the Italian Ministry of Economic Development and led by Ariston Thermo Spa.

1.2 - The Role of Systems Diagnosis

To guarantee the safe operation of the fuel cell systems and to support the successful deployment of SOFC, it is necessary to use specific computational tools, as well as control and diagnosis strategies, and systematic techniques that allow to increase reliability of this technology [6, 86]. This need is worth for fuel cells and for other mechanical, electrical and chemical engineering systems as well. An introduction to general systems diagnosis is indispensable to understand the importance and advantages that can be achieved performing this task. Designers and users often have interest in preventing the occurrence of failures of a mechanism, a machine or any kind of technical device. To this end, several approaches can be taken, the most obvious of which is to stop the system whenever an abnormal functioning is observed, i.e., a fault is determined as a difference in the performance of the system from its expected behavior. The ability to detect the occurrence of any fault, and identify its cause, is a critical task. Attempting to detect a fault before it becomes a failure is a prerequisite to the elimination of *corrective maintenance*, which leads to bring the maintenance operations forward in time, i.e., before the system fails and needs repair, thus reducing the occurrence of expensive, and unexpected breakdowns. In this sense, the two possible options are *preventive maintenance* and *predictive maintenance* [39].

Preventive maintenance (PM) typically refers to performing regular, scheduled operations that keep the system running reliably. On the other hand, Predictive maintenance (PdM) attempts to defer maintenance operations until they are required. Although sometimes there is confusion between the two strategies, it is more generally acknowledged that PM is concerned with preventing a failure blindly, i.e., without knowing if a fault exists or not, whereas PdM endeavors to detect faults before action is taken. In order to optimize the control actions and degradation prevention capabilities, specific diagnostic methods are needed to determine the actual state of the systems *in real-time*. Fault diagnosis methods aim to satisfy the following requirements: early detection of small faults with abrupt or incipient time behavior, diagnosis of faults in the actuator, process components or sensors, detection of faults in closed loops and supervision of processes in transient states.

1.3 - Introduction to SOFC system diagnosis

1.3.1 - FDI: definitions and background

Diagnosing an engineering system involves three activities [3, 4, 5]:

- a) *fault detection* to indicate the presence of faults and the time of detection;
- b) *fault isolation* to determine the location of the faults after their detection;
- c) *fault identification* to determine the size of the faults and their time-variant behavior.

According to the schemes of Figure 1.1, the process is composed of three phases. First a fault must be found through *fault detection* techniques. Second, the fault is located through a process known as *fault isolation*. The concern of many industrial diagnostic systems focuses on these two activities exclusively, so that their practice has become known as **FDI**. The third and final activity, known as *fault identification*, assesses the severity of the fault, either qualitatively or quantitatively. Sometimes, with the acronym FDI the combination of fault detection, isolation and also identification is indicated, instead of FDII.

FDI schemes are based on the redundancy concept, whose main idea is to increase and complete the information available about the actual system status. Temporal redundancy evaluates the evolution of uncorrelated variable in time, whereas analytical redundancy applies models to simulate the reference system and may provide information about non-measurable variables [5].

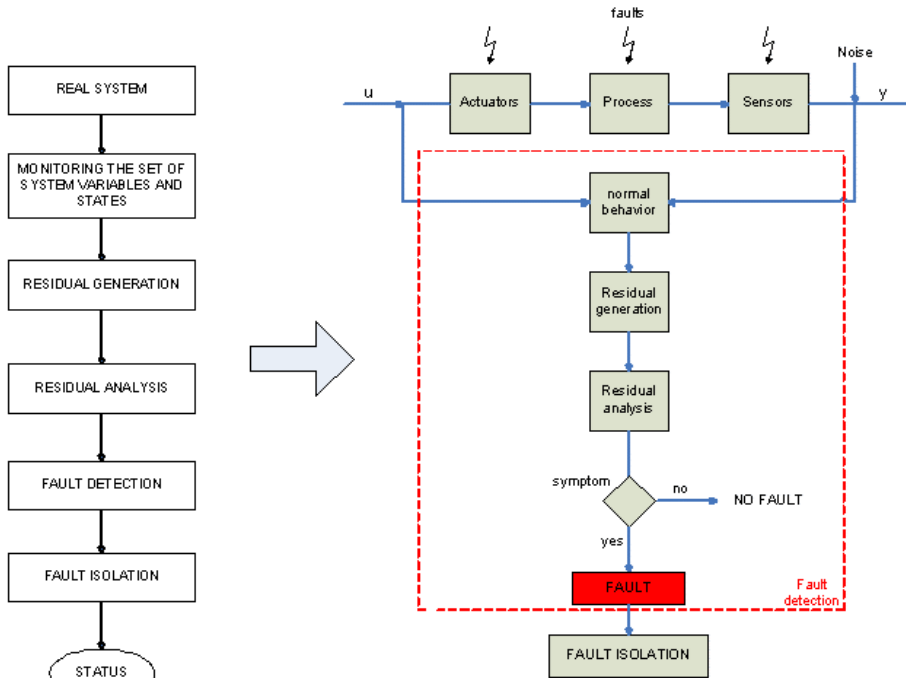


Figure 1.1- FDI scheme

Many approaches have been proposed for fault detection and isolation. The simplest method, used in many industrial applications, consists in limit checking a measured variable. In contrast to this physical redundancy, more sophisticated model-based techniques relying on the concept of analytical redundancy have been developed. In synthesis, the idea behind model-based FDI is to use the redundancy in information obtained from measurement in combination with a process model.

The two principal steps of all FDI algorithms are *residual generation* and *residual evaluation*. The purpose of the first step is to generate a signal, the residual, which is supposed to be nonzero in the presence of one or more faults, and zero otherwise. In general, the residual is obtained by comparing the plant output with the output of a model or several models.

The purpose of the second step of the FDI process is thus to evaluate the residual and draw conclusions regarding the presence of a fault. This is done by comparing some function of the residual to a threshold and then declaring the presence of a fault if the former exceeds the latter [6].

1.3.2 - Diagnosis for SOFC systems

The core of a fuel cell power system is represented by the stack, formed by electrodes, electrolyte and bipolar plate; however, other parts frequently make up a large proportion of the engineering of the fuel cell system. These 'extras' are called *balance of plant (BOP)*.

The fuel cell stack often appears to be quite a small and insignificant part of the whole system, while the extra components required depend greatly on the type of fuel cell, and crucially on the fuel used [7].

Figure 1.2 shows the P&ID (Process and Instrument Diagram) of a typical SOFC system for μ CHP application with catalytic partial oxidation reforming device. Figure 1.3 reports the scheme of a steam reforming system, in which also the heat recovery system is shown in the red box. In contrast to the hydrogen-fueled system, the salient features of these architectures are the use of additional fuel processing equipment:

- Water tank, water pump, water treatment device, steam generator, steam reformer and burner, for steam reforming systems.
- Anode air ventilator, air inlet valve, fuel inlet valve, CPOx inlet valve, differential pressure devices for CPOx reforming systems.

These components are located upstream of the fuel cell stack. For micro combined heat and power (μ CHP) applications, depending on the air cooling system, the heat recovery boiler equipment is placed downstream of the air pre-heater. Low pressure natural gas enters the system and, if required, is compressed and preheated to a temperature suitable for the reforming process (normally pressurization and pre-heating are not needed for residential application where the gas pressure is 20 mbar at ambient temperature).

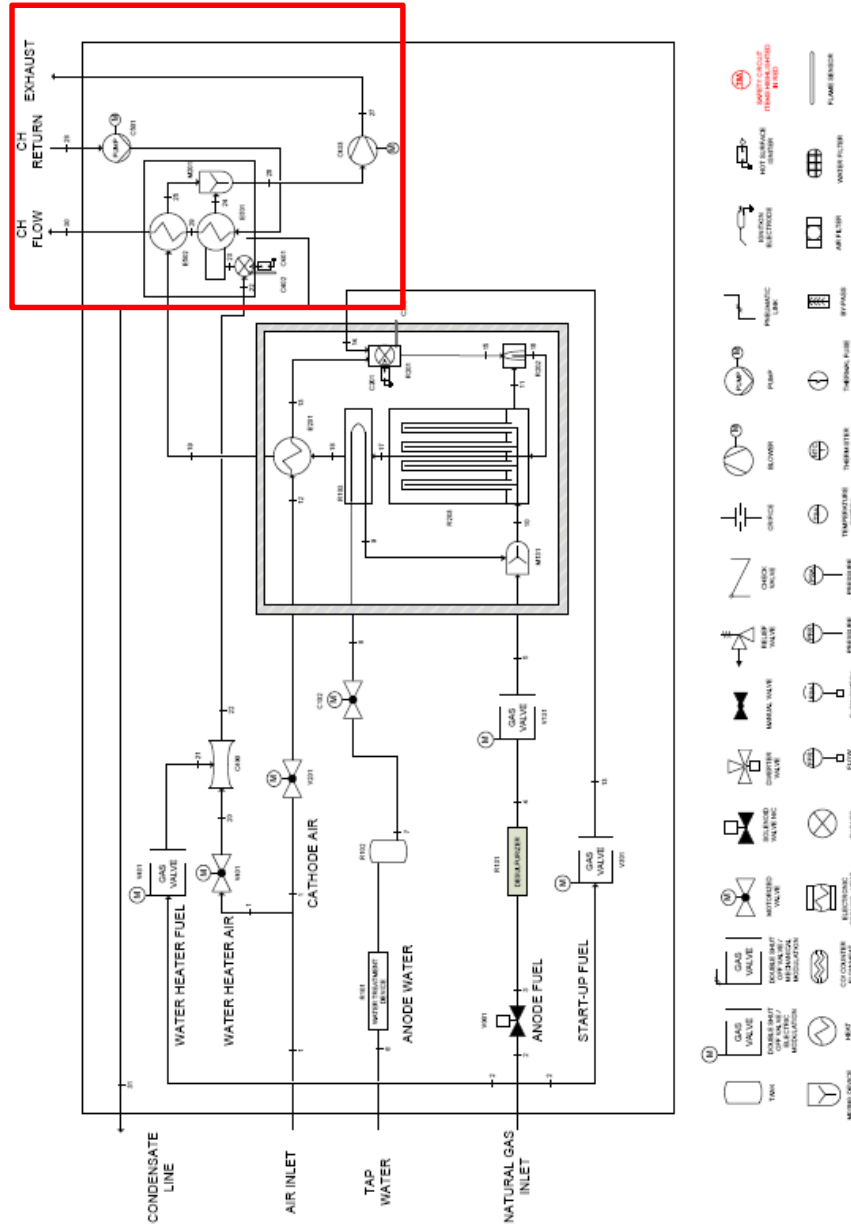


Figure 1.3- SOFC steam reformed based μ CHP [37] - P&ID

Just after entering the system (and after pressurization, if present), natural gas is desulphurized and mixed with either air (CPOx reforming) or with superheated steam (Steam reforming), and delivered to the reformer reactors; the product of the reforming reaction, exiting the reactor, is an hydrogen-rich fuel mixture suitable for the anode compartments of the individual cells. The cathode air, required for both cooling the system and releasing the O_2^- ions required for the fuel cell reaction, is filtered, pressurized and preheated to a temperature approximately $50^\circ C$ below the nominal cell-stack temperature before admittance into the fuel cell stack module. Air is directed into the cathode compartments of the individual cells of the stack through the use of a manifold. The solid oxide fuel cell typically operates at temperatures above $700^\circ C$. At these high temperatures, fast electrochemical reaction kinetics are achieved. After electrochemical oxidation of hydrogen and reduction of oxygen, the direct current (DC) produced in the process is converted to alternating current (AC) by the inverter; a part of this electrical power is used to feed the parasitic loads for the BoP components. The unreacted fuel exiting the fuel cell stack can be recycled to the anode inlet or oxidized with the depleted air exiting the cathode manifold. Typically, oxidation of the fuel is carried out in a catalytic combustion process (post-burner). This offgas burner is also responsible for keeping the stack at sufficient high temperatures during the late startup phase and in standby or idle mode (when the stack is generating only the current needed to feed the parasitic devices). Moreover, it is responsible for the conversion of residual and unreacted species, in order to reduce the formation of pollutant emissions and making the units compliant with international emission standards. The products of the afterburning process are exploited to preheat the fresh air entering the cathode, and are then sent to the external heat recovery device, with the objective to recover their thermal content in the form of hot water or central heating. In both hydrogen- and natural gas-fueled systems, the solid oxide fuel cell temperature is controlled through the excess of air fed to the cathode.

All these components are controlled and actuated by the fuel cell control system, whose development and complexity level depends on the accuracy, performance and safety requirements. For this last issue, many safety devices, such as temperature and pressure switches/controllers, are provided and properly set to allow the fuel cell system working safely at the pre-established optimal operating points.

A fuel cell system is therefore built up by many items, each of which is of course vulnerable to faults that, depending on their gravity, can cause an immediate stop or the late but permanent damage of the fuel cells. For these reasons, the first task to achieve an active tolerant control consists of the inclusion of a fault diagnosis system operating in real-time. The diagnosis system should allow the fault detection, isolation and identification (the fault magnitude estimation).

The model based fault diagnosis compares the current states of the systems with the theoretical optimal values simulated by the model itself. In case a significant discrepancy is detected, the existence of a fault is assumed. The use of measurements and the corresponding model output variables allow to isolate the faults and in some cases to determine their magnitudes. An option could consist in implementing different sensors in the system in order to detect any deviation from nominal operating conditions [5]. However, such approach is problematic for stack and system designers since any addition in system complexity increases costs and reduces reliability. In real systems, there are practical limitations to the number of sensors that can be incorporated. Therefore, diagnosis methods that do not add complexity to the system are needed.

Another approach may be to use the SOFC individual cell voltage responses to estimate their state of health in real time. Nevertheless, the behavior of a fuel cell system is rarely predictable, since a certain degree of variability is often present in operating conditions, system inputs, physical and/or chemical internal processes. A cell voltage decrease can for instance indicate a potential poisoning, a cell leakage, a clogged blower, etc... Commands can therefore be sent by the controller to the subsystem units in order to account for these problems. Therefore, it is necessary to develop a continuous monitoring of devices for detection and diagnosis that could be either used as On Board Diagnostic or as "off-line" diagnosis. In the former case, the tool will send an alarm in order to guarantee installation safety and the respect of regulations, on the basis of the on-line monitoring of variables easy to measure, such as voltage, electric current, temperature. In the latter case, the tool will help the maintenance operations or repairs.

1.4 - Hydrogen and syngas generation

Starting from the sixties of last century, the technologies for the production of energy from fossil fuels had a transition to a new era where the reduction of pollutant was important. This shall be addressed to the fact that combustion of fossil fuels produces high quantities of carbon dioxide and also many chemical species, some of which are toxic for many living organisms. In this scenario, natural gas has gained a position of great importance because of its abundance [9]. Nowadays, increasing efforts are devoted to the development of efficient technologies to exploit the existing resources of natural gas, which consists mainly of methane. In fact, according to the International Energy Agency (IEA) the world's energy demand from natural gas, which consists mainly of methane, is expected to increase by 30-40% in a 25 years perspective. Even though the world has large deposits of natural gas, most is located in remote areas and consequently it must be transported across vast areas to reach its market with high cost of storage and transportation. Therefore, the conversion of methane to more useful and easily transportable chemicals, such as hydrogen/synthesis gas and finally transportable liquids, has been given high priority by scientists.

The hydrogen production from hydrocarbons is not direct, but always goes through a first, intermediate stadium known as synthesis gas (syngas), containing hydrogen and an appreciable amount of carbon monoxide (CO), that shall be in a second step converted in hydrogen by means of water gas shift reaction [8].

Synthesis gas is a very interesting intermediate product in the chemical industry used for a variety of important processes such as ammonia and methanol synthesis, and can be produced from various fossil sources, such as natural gas, naphtha, residual oils, coke from petroleum and coal. Synthesis gas can then be converted to paraffin liquid fuels through Fischer-Tropsch reaction on Fe, Co, Ru and similar metals, or to methanol over Cu/ZnO and then to gasoline by MTG (Methanol-to-Gasoline) process over zeolite catalyst [17]. Synthesis gas is also used for the production of methanol, dimethyl ether, acetic acid and oxoalcohols. Moreover, the synthesis gas is an energy carrier from which hydrogen is often produced.

Hydrogen is the lightest chemical element and offers the best energy

to weight ratio of any fuel. The major drawback to using hydrogen is that it has the lowest storage density of all fuels. However, it is possible to store large quantities of hydrogen in its pure form by compressing it to very high pressure and storing it in containers designed and certified to withstand the pressures involved. With these properties, it can either be stored as a gas or cooled down to its critical point to be stored as a liquid. Hydrogen can also be stored in solid form, in chemical combination with other elements (there are a number of metals which can 'absorb' many times their own weight in hydrogen). The hydrogen is released from these compounds by heating or the addition of water. Among alternative storage mediums investigated, carbon nanotubes and glass microspheres occupy an important role.

1.5 - Hydrogen production in fuel cell systems

Hydrogen is most economically produced from fossil fuels through one of the following reforming reactions [11]:

- **steam-methane reforming (SMR):** Fuel is mixed with steam in the presence of a base metal catalyst to produce hydrogen and carbon monoxide. This method is the most well-developed and cost-effective for generating hydrogen and is also the most efficient, giving conversion rates of 70% to 80% on a large scale. The key challenge in steam reforming is that heat must be transferred from an external source through the reactor walls and throughout the catalyst bed to provide energy for the strongly endothermic reaction. To achieve complete conversion, reforming temperatures of 700 °C or higher are required. In addition, another challenge of steam reforming of liquid hydrocarbon fuels is the carbon formation. Molar steam-to-carbon ratios (S/C) of 2-3 or sometimes higher are typical for conventional steam reformers.
- **partial oxidation (POx):** Partial oxidation can be used for converting methane and heavier hydrocarbons, whereas is rarely used for alcohols. This method involves the reaction of the

hydrocarbon with oxygen to yield hydrogen, and produces less hydrogen for the same amount of fuel than steam reforming. The reaction is, however, exothermic and therefore generates heat. This means that the reaction can be initiated by a simple combustion process leading to quick start-up. Once the system is running, it then requires little external heating to keep the reaction active. This technology is preferred where there is no water source available and for small scale systems.

- **autothermal reforming (ATR):** Autothermal reforming combines the endothermic steam reforming process with the exothermic partial oxidation reaction, therefore balancing heat flow in and out of the reactor. These systems can be very productive, fast-starting and compact, and have been demonstrated with methanol, gasoline and natural gas. A number of automotive and oil companies are also working on proprietary versions of this technology.

Conventional steam-reforming technology is not suited for decentralized synthesis gas production, because steam reformers are large, expensive plants difficult to be scaled down for small-scale operation in remote areas. Figure 1.4 is showing a typical industrial steam reforming plant installed by Technip and its layout.

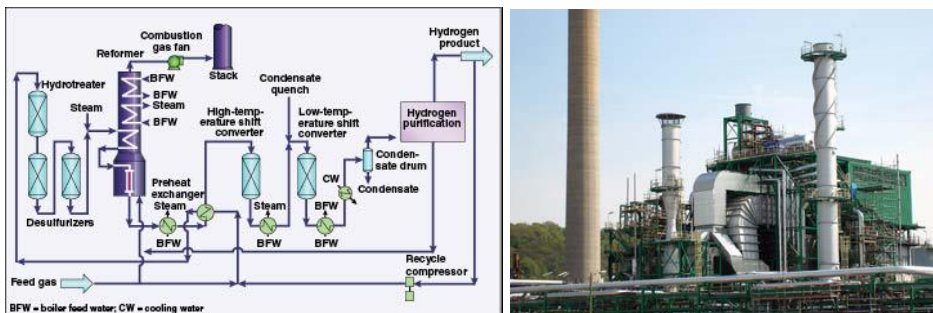


Figure 1.4- Steam reforming plant (Technip)

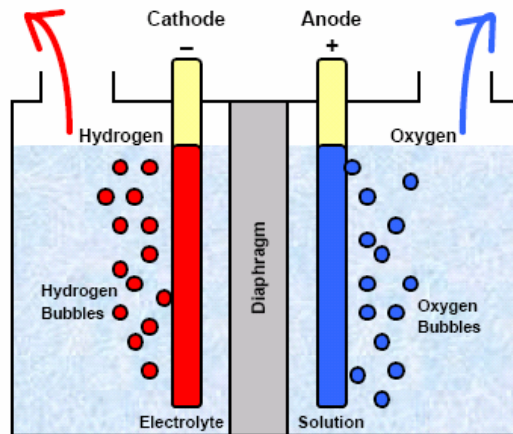
An alternative to steam reforming is the catalytic partial oxidation, which has received a considerable attention during the last 15 years. Indeed, it provides close to 100% methane conversion and syngas yields over 90% in a very fast reaction (millisecond contact times) carried out at high temperatures. Since the catalytic partial oxidation is quick and exothermic, it is suitable to realize compact reformers, which have a rapid response to transient load demands. These aspects make this process suitable for installation in remote areas and also for all stationary and mobile applications related to the recent development of a small-to medium scale technology for the production of syngas and H₂. Potential stationary applications include the production of H₂-rich steams for the fuelling of hydrogen-driven vehicles or residential cogeneration systems, but also for the enhancement of gas turbines performances through the development of H₂ stabilized combustors. On board applications deal with the use of solid oxide fuel cells for auxiliary power units (APUs) on heavy duty vehicles to supply power to auxiliary cab devices and trailers (cryogenic circuits). On-board generation of syngas may also be applied on conventional ICE vehicles to speed up the cold-start phase of catalytic converters and to serve as reducing gas for NO_x trap regeneration and for the SMR of NO_x.

In table 1.1, a summary of the features of steam reforming, catalytic partial oxidation and autothermal reforming is listed.

Table 1.1 – Reforming mechanisms comparison

	Steam reforming	CPOx	Autothermal reforming
Process description	The hydrocarbon (methane) conversion takes place in presence of steam and heat fed by an external heat source (endothermic reaction)	According to the indirect mechanism, the reaction proceeds preferentially at first with a total combustion of CH ₄ with the oxygen sub stoichiometric, and later the H ₂ O generated in this process allows the steam reforming reaction that converts the remaining methane in H ₂ and CO ₂ . The process can either be catalytic (600-800°C) or not	Combination of both previous mechanisms. Similar to the CPOx but in addition steam is fed to the reactor together with air and fuel.
Design parameters	SCR = 2-3 Steam to carbon ratio	Lambda = 0.27-0.3 Ratio between utilized and stoichiometric air	Lambda = 0.2 and SCR = 1
Operating temperature	Reactor T: 600- 1000 °C Pre-heating T: 200- 350°C	Reactor T: 600-800 °C (for CPOx) Pre-heating T: 50- 350°C	Depending on the lambda and SCR
H2 conversion	Up to 70%	Up to 35%	Up to 50%
CO/CO2	approximately 35/3	approximately 1.,5/10	Depending on the lambda and SCR
Heat Requirement	External Heat transfer device is required, therefore results in system complexity and potential higher cost. On the other hand, heat generated from SOFC can be used to drive SR reaction with overall higher system efficiency.	No external heat required. The system is exothermic. The heat generated from the reaction needs to be removed or utilized in the system	May need startup heat, and control systems to switch between lean burning and ATR regimes.
Startup and transients	Needs external igniter to start up although the catalyst bed can be used for catalyst combustion tentatively. Heat transfer efficiency and higher volume makes the start-up extremely slow.	Startup is fast. Transient test is relatively easy to control, but high temperature startup/shutdowns may cause catalyst degradation	Moderate. Can be set up to fast response times by switching between CPOx and ATR (relying in CPOx portion for the faster response time)

Hydrogen can be also produced through the **electrolysis of water**, namely the splitting of water into its elements (fig. 1.5). This process takes place in an electrolyser, which can be described as a 'reverse' fuel cell: instead of combining hydrogen and oxygen electrochemically to produce electricity and water as a fuel cell does, an electrolyser uses electrical current and water to generate hydrogen and oxygen.



Standard Electrolysis

Figure 1.5- Electrolysis scheme

The key issue here is the source of the electrical current. If grid electricity is used, the hydrogen has a carbon footprint associated with it due to the coal or gas that must be burnt to produce the necessary electricity. However, if the electricity is obtained from renewable energy such as wind or solar power, the hydrogen can be produced in a completely carbon-free way. Indeed, many commercial versions of “green” electrolyzers of various capacities are available on the market. A discrete number of companies is currently pushing to promote their spread in the market, in combination with wind or solar power, to produce hydrogen for fuel cells.

Another type of reforming is known as **dry reforming**, or CO₂ reforming. This reaction can be carried out if there is no source of steam available and is defined as through the following [11]:



This reaction may occur in internal reforming fuel cells when anode

exhaust gas containing carbon dioxide and water is recycled to the fuel cell inlet.

Mixed reforming is sometimes refers to a hybrid approach in which both steam and CO₂ are used to reform the fuel. Both dry and mixed reforming have energy and environmental advantages compared with traditional steam reforming. The reactions are catalyzed by nickel, however deactivation due to carbon formation and nickel sintering can be particularly severe, and better catalysts are required.

An alternative to all the above methods of generating hydrogen is to simply heat hydrocarbon fuels in the absence of air (**pyrolysis or thermal cracking**) [47]. The hydrocarbon ‘cracks’ or decomposes into hydrogen and solid carbon. The process is ideally suitable for simple hydrocarbon fuels, otherwise various by-products may be formed. The advantage of thermal cracking is the high purity of the produced hydrogen. The challenge is the removal of carbon that might have formed during the reaction. This can be done by switching off the supply of fuel and admitting air to the reactor to burn off the carbon as carbon dioxide (see section 2.6.2). The principle is simple, but there are real difficulties or issues, among others the safety implications of admitting fuel and air into a reactor at high temperature. Moreover, the control of the pyrolysis is critical to limit the carbon deposition, which can cause irreversible damages on the catalyst. The carbon formation may occur in absence of catalyst as well; in this case, carbon may plug the reactor, meaning that no flow of oxidizing gas can be established to burn off the deposited material. Despite these substantial problems, pyrolysis is being considered seriously as an option for some fuel cell systems. Cracking of propane has been proposed recently to provide hydrogen for small PEM fuel cell systems [11].

1.6 - Fuel Reforming for FC applications

For fuel cell applications, hydrogen can be generated by reforming hydrocarbon fuels such as natural gas, methanol, gasoline or ethanol. These are not necessarily fossil fuels; reforming of bio-ethanol, for instance, is equally possible and this would be a source of renewable hydrogen as well [8, 13].

Fuel processing may be defined as the conversion of the raw primary fuel, supplied to a fuel cell system, into the fuel gas required by the stack. Each type of fuel cell stack has some particular fuel requirements, more stringent when the stack operates at low temperatures. For example, fuel fed to a Phosphoric Acid Fuel Cell (PAFC) needs to be hydrogen-rich with less than 0.5% carbon monoxide. The fuel fed to a PEM fuel cell needs to be essentially carbon monoxide free, while both the Molten Carbonate Fuel Cell (MCFC) and for the SOFC are capable of utilizing carbon monoxide as fuel through the water-gas shift reaction that occurs within the cell. Additionally, differently from PAFC and PEM, SOFC and internal reforming MCFC can utilize methane within the fuel cell themselves.

Natural gas and petroleum liquids contain organic sulphur compounds that normally have to be removed before any further fuel processing can be carried out. In the case of natural gas, the only sulphur compounds may be the odorants that are added to the fuel stream by the utility company for safety reasons. Sulphur is a well-known catalyst poison and, besides the reforming reactor, can easily deactivate the electrodes of all types of fuel cells. Experimental measurement confirm that the catalysts deactivation can occur even if sulphur levels in fuels are below 0.2 ppm. In the particular case of PEM fuel cells, it has been demonstrated that levels of only 1 ppb is enough to permanently poison a PEM anode catalyst. Therefore, sulphur needs to be removed from the inlet stream before the fuel gas flows to the reformer or stack. Desulphurisation will not be detailed in this work as it is assumed that reforming processes always occur with desulphurized gas; it is sufficient to highlight that desulphurization is a well-established process required in many situations, not just for fuel cells.

Considerable research has been carried out in the field of fuel processing and reviews of the key technologies are available in literature [11]. The following sections are intended to provide a basic explanation of the various technologies and related involved materials (e.g. reactors catalysts and supports), focusing on the catalytic partial oxidation, main topic of this thesis.

1.6.1 - Catalytic Partial Oxidation for FC systems

The CPOx is widely used in fuel cell, in particular in molten carbonate fuel cells (MCFC) and in solid oxide fuel cell (SOFC), because these types of cells run on a mixture of hydrogen and carbon monoxide and they have resistance to poisoning by impurities in the fuel. Thus, in both cases it is possible to operate the cell directly on hydrocarbon fuel without the need of a system to remove all traces of CO.

A single solid oxide fuel cell consists of three main components: an anode, a cathode and a solid electrolyte separating the two electrodes. A fuel cell stack consists of many fuel cells, with interconnects that connects the cathode to the anode of the next cell. A gaseous, hydrogen-rich fuel is fed to the anode (negative electrode) compartment and an oxidant is fed to the cathode (positive electrode) compartment. As shown in figure 1.6, under electrical load, at the cathode surface the presence of the catalyst enables oxygen ionization. The solid electrolyte permits the flux of oxygen ions to the anode, where they electro-oxidize hydrogen, thus releasing heat, water and electrons [2, 6]. Since electrolyte material ensures quasi-zero electronic conductivity, electrons are forced to flow through interconnect and external load towards the cathode, thus closing the electrical loop. The theoretical maximum efficiency is very high, in excess of 80%. The SOFC operates at high temperature, conventionally between 800-1000°C.

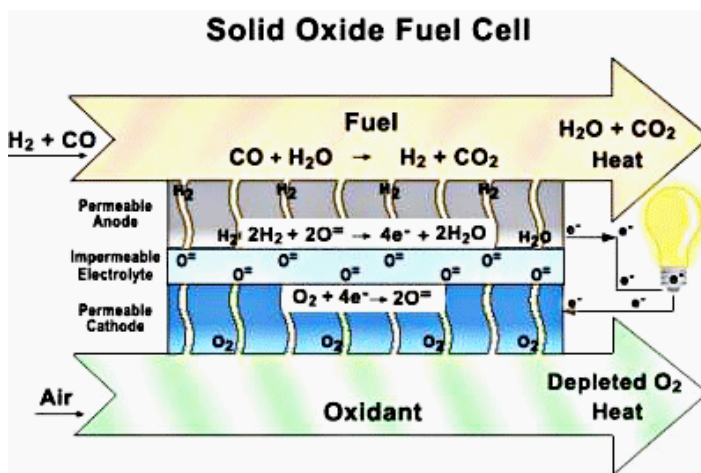


Figure 1.6: Operating principle of a solid oxide fuel cell.

In small-scale devices developed for stand-alone or remote applications, oxygen or air is used as oxidant rather than steam to convert the fuel in syngas. Indeed, the cost and the complexity associated with using large quantities of steam are extremely high, making this system less suitable in small-scale applications. On the other hand, the use of the oxygen, or air, is much simpler and cheaper in terms of configuration and manufacturing [13, 14]. As mentioned before, the CPO reactor is compact and of simple installation, and in fact it is adapt for small scale fuel cell applications, such as residential μ CHP and small auxiliary power unit (APU).

However, when dealing with a catalytic partial oxidation, there is a drop in the efficiency due to the large energy loss in oxidizing the hydrocarbon. Moreover, if excess air is used, a tendency towards a complete oxidation can occur, then consuming all the available oxygen that is converted to H_2O . An advantage of CPOx is the possibility to reform the fuel during all the FC operating range, even at low load. This could not be the case of steam reforming, due to the low heat available at low FC load [7].

1.6.2 Internal and external reforming in fuel cell systems

As mentioned above, the reforming in fuel cell systems can take place either outside of the fuel cell stack or inside the stack itself.

The external reforming is carried out before the fuel reaches the stack cells, in a proper reactor, as shown in figure 1.7. This is the standard configuration for most of the fuel cell systems manufacturer, as it requires less engineering efforts and is extremely easy to implement. The main advantage is the possibility to keep the reforming section and the stack separated, such that no common faults can occur. On the other hand, this solution entails higher costs and lower overall system efficiency respect to the internal reforming solution [8, 23].



Figure 1.7: External reforming CPOx in tubular SOFC system

In external reforming configuration, the reactor can be located in different positions respect to the fuel cell stack: it can be placed either inside the fuel cell module (integrated Hot Box) or within the BoP. For some applications, external reforming is carried out upstream the SOFC system, at a refinery or chemical plant, and the hydrogen is then delivered by pipeline to filling stations.

The internal reforming occurs for high temperature systems such as molten carbonate and solid oxide fuel cells, where it is possible to supply a hydrocarbon (e.g. natural gas or methanol) directly to the fuel cell without prior reforming. The high temperature allows the reforming stage to take place within the fuel cell itself. For SOFC systems, internal reforming is an attractive option offering a significant cost reduction, higher efficiencies and faster load response respect to the traditional external reforming. However, complete internal reforming may lead to several problems which can be avoided with partial pre-reforming of natural gas. This is the reason why in practice, some preliminary reforming or purifying of the fuel is often carried out.

Fuel cell developers have asserted for many years that the heat required to sustain the endothermic reforming of low molecular weight hydrocarbons (e.g. natural gas) can be provided by the electrochemical reaction inside the stack [7]. This has led to various effective internal reforming concepts that have been applied to both SOFC and MCFC, due to their high operating temperatures. This is confirmed by the technology progress related to the fuel reforming techniques, shown in figure 1.8. The present trend is to bring the reforming reaction inside the stack and investigate its benefits.

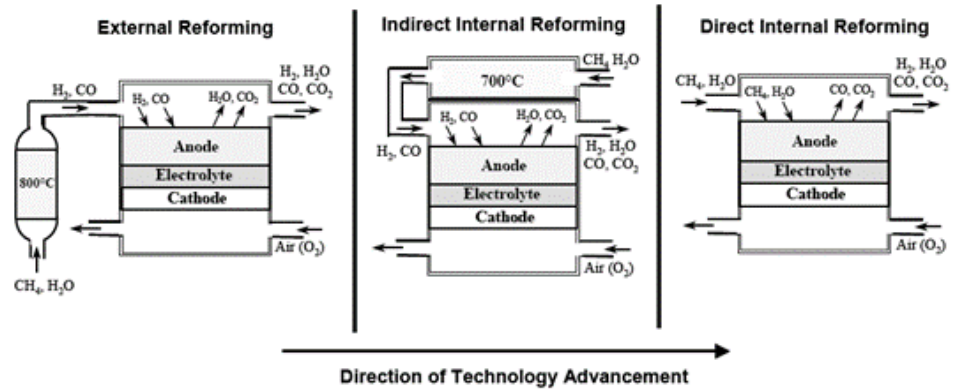


Figure 1.8: Technology progress for reforming methods in fuel cells

It is worth remarking that the internal reforming reactions may be of any type according to the FC operating conditions (temperature, stack current, H_2O generated by the stack); in some cases, catalysts may be added to the anode compartment of SOFC to enhance the occurrence of reforming reaction. Thus, steam reforming, CPOx and autothermal reforming reactions can take place either independently or simultaneously.

In case of steam reforming, in contrast to the endothermic nature of this reaction, the fuel cell reactions are exothermic, mainly because of heat production in the cell caused by internal resistances. The overall heat production is about twice the heat consumed by the steam reforming reaction in an internally reforming fuel cell. Hence, the cooling required by the cell, which is usually achieved by flowing excess air through the cathode in the case of external reforming systems, will be much smaller for internal reforming systems. This has a major benefit on the electrical efficiency of the overall system. The other main advantage of internal reforming is the reduced reforming system cost, since an external reformer is not needed.

Developers of internal reforming fuel cells have generally adopted two approaches, usually referred to as **indirect (IIR)** and **direct (DIR)** internal reforming, even if in some cases, a combination of both approaches has been carried out [11]. Figure 1.9 illustrates the schemes for direct and indirect internal reforming in fuel cells.

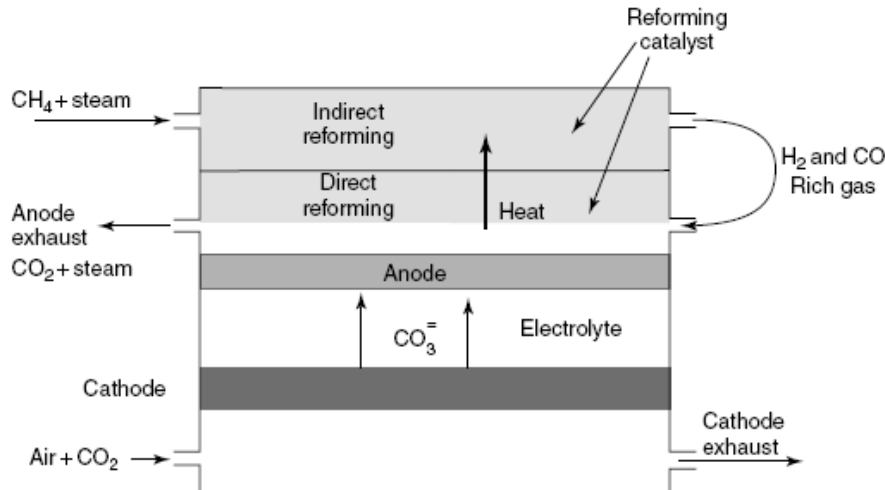


Figure 1.9: Direct and Indirect internal reforming in fuel cells

The Indirect internal reforming, also known as integrated reforming, involves conversion of methane by reformers positioned in close thermal contact with the stack. An example of this type of arrangement alternates plate reformers with small cell packages. The reformat from each plate is fed to neighboring cells. IIR benefits from close thermal contact between stack and reformer but suffers from the fact that heat is transferred well only from cells adjacent to the reformers. In addition, steam for the reforming must be supplied separately. A variation of this type of arrangement locates the reforming catalyst in the gas distribution path of each cell. With IIR, the reforming reaction and electrochemical reactions are separated [30].

In direct internal reforming (DIR), the reforming reactions are carried out within the anode compartment of the stack, taking advantage from the steam generated by the electrochemical fuel cell reaction [84]. This is achieved by placing the reforming catalyst within the fuel cell channels and injectors or directly over the anode layer. A similar layout is easily achievable with tubular fuel cells, where the catalyst is deposited over the anode surface and its large area allows the development of the reforming reaction without need of an external reactor. Indeed, the most significant example of DIR can be found in the Acumentrics tubular SOFC (section 2.2.4). The advantage of DIR is that it offers both good heat transfer and chemical integration, as the product steam from the anode

electrochemical reaction can be used for the reforming without the need for recycling spent fuel. The main drawback is the management of the temperature gradients and the mechanical and thermal design of the stack, which can be highly demanding and time-consuming. Finally, it is important to notice that internal reforming may be applied to several hydrocarbon fuels such as natural gas and vaporised liquids such as naphtha and kerosenes.

CHAPTER 2

Reforming systems: state of the art

In the following sections a description of the three main reforming mechanisms mentioned in chapter 1, namely steam reforming, catalytic partial oxidation and autothermal reforming, is given. For each method, the reactions involved, the main operating parameters and the pros and cons are investigated. Moreover, the thermodynamic and kinetics aspects of the reaction mechanisms are analyzed, with particular focus on the CPOx reforming, which is the topic of this thesis. For this technique, an analysis of reactor catalysts and supports typically used for fuel cell application is carried out. In conclusion, an investigation of the catalyst deactivation phenomena likely to occur during reforming reactions is reported.

2.1 - Steam Reforming (SR)

The first description of a process for the conversion of hydrocarbons with steam was described in 1868 by Tessie du Motay e Marechal using CaO as a medium, resulting in the formation of CaCO₃ and hydrogen [12]. In 1890 Mond and Langer improved the process by using a nickel catalyst; the first industrial application with methane was developed in 1930. Steam reforming technology was subsequently used, in combination with Fisher-Tropsch technology, by Germany during world war II and South Africa during the embargo era for the synthesis of chemical such as fuels and alcohols [11]. Nowadays, steam reforming is a mature technology, practiced industrially on a large scale for hydrogen production, and several detailed reviews of the technology have been published: Van Hook [80], Rostrup-Nielsen [81], while useful data for system design are provided by Twigg (1989) [82]. The basic reforming reaction for a generic hydrocarbon C_nH_m is:



if methane is considered as inlet fuel, the reaction becomes:



The reforming reactions (2.1 and 2.2), more correctly defined *oxygenolysis reactions*, and the associated water-gas shift reaction 2.3 are carried out normally over a supported nickel catalyst at elevated temperatures, typically above 700 °C. In most cases, and certainly with natural gas, the steam reforming reactions are *endothermic*, that is, heat needs to be supplied to drive the reaction forward to produce hydrogen. For the medium and high temperature fuel cells, heat required by the reforming reactions can be provided, at least in part, from the fuel cell itself in the form of exhaust heat; in particular for the SOFC, heat is available from the fuel cell exhaust gases at higher temperatures. SOFC stacks are also hot enough to allow the basic steam reforming reaction (equation 2.1-2.2) to occur within the fuel cell stack [11]. Furthermore, the steam needed for the reaction is also present in the fuel cell, because the product water from the electrochemical reaction appears at the cell anode.

If all this heat is used to promote the reforming reactions (especially when reforming is carried out inside the stack), then the efficiency of these fuel cells can be much higher (typically >50% ref. HHV). The scheme of a typical steam reforming process is shown in figure 2.1.

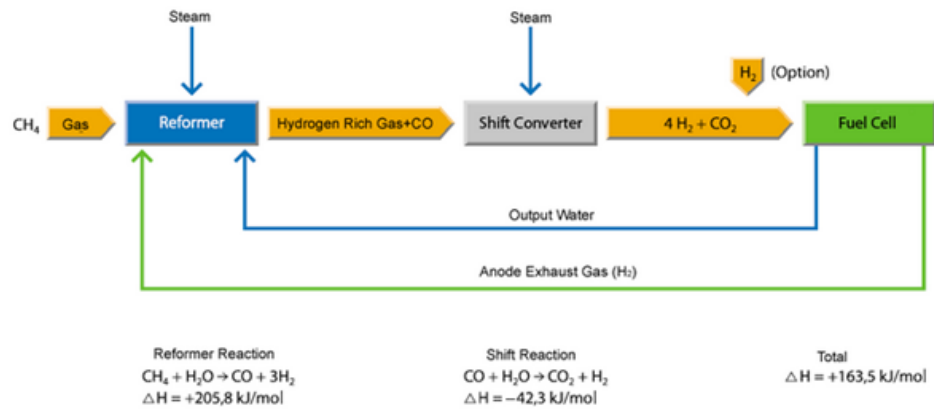


Figure 2.1 – Flowchart of a standard steam reforming process

Reactions 2.2 and 2.3 are reversible and normally reach equilibrium over an active catalyst, as at such high temperatures the rates of reaction are very fast. The water gas shift reaction 2.3 reduces the CO content of the gas by converting it into CO_2 . The combination of the two reactions produces a mixture of carbon monoxide, carbon dioxide, and hydrogen, together with unconverted methane and steam. For some applications, the CO reduction achieved through the water gas shift reaction might not be sufficient. Indeed, even if water-gas shift reaction takes place at the same time of the basic steam reforming reaction, thermodynamics of the reaction are such that higher temperatures favor the production of carbon monoxide and shift the equilibrium to the left ($K = -4.35$). An effective method for reducing the carbon monoxide content of a steam reformed gas stream is to use one or more shift reactors [7]. The first approach is thus to cool the product gas from the steam reformer and to pass it through a reactor containing catalyst, which promotes the shift reaction. This has the effect of converting carbon monoxide into carbon dioxide. Depending on the reformat composition, more than one shift reactor may be needed to reduce the carbon monoxide level to an acceptable level.

There are also some methods for removing the CO_2 produced by the steam reforming in order to maximize the hydrogen gain: the most known are **Pressure Swing Adsorption (PSA)** and **scrubbing with ammine** [11,82]. In the PSA process, the reformer products gas flows through a reactor containing absorbent material. Hydrogen gas is

preferentially absorbed on this material. After a set time, the reactor is isolated and the feed gas is diverted into a parallel reactor. At this stage the first reactor is depressurized, allowing pure hydrogen to desorb from the material. The process is repeated and the two reactors are alternately pressurized and depressurized. PSA is used in the Hyradix fuel processor developed by Eden Energy Ltd.

It is therefore clear that steam reforming process is strongly energy consuming and complex, and high costly alloys are commonly used for catalysts and reactor in order to sustain the high operating temperatures. The steam reforming, in industrial practice, is carried out at 900°C at the pressure of 15-30 atm in a fired tube reformers, which with catalyst filled tubes placed in the radiant part of the heater (nickel supported on oxide carrier, typically Al₂O₃ or ZrO₂) [15]. The superficial contact time is 0.5-1.5 s, which corresponds to residence times of several seconds. The methane conversion, in steam reactions, is typically in the order of 90-92%, with a synthesis gas composition similar to that determined by thermodynamic equilibrium [18]. The principal disadvantages of the steam reforming is that only the 35-50% of the total energy input, given by external combustion of the fuel gas, is absorbed by the reforming process. Therefore, the heat of fuel gas is usually used in the convective part of the reformer by preheating the feedstock and generating steam, thus bringing the overall thermal efficiency over 85%. [9]

Many reforming systems for small scale applications, such as μ CHP, are available in the market. Acumentrics has developed a relatively simple steam generator capable of providing the required steam using the cathode air leaving the stack. It consists of a finned tubes reactor with internal baffles and distribution fittings to achieve steady steam generation of sufficiently high quality. A super-heater section can also be added if necessary. The steam generator is located in the stack cathode exhaust and the super-heater is located in the cathode inlet to the stack, directly downstream of the startup burner. Figure 2.2 shows photographs of the equipment configuration.

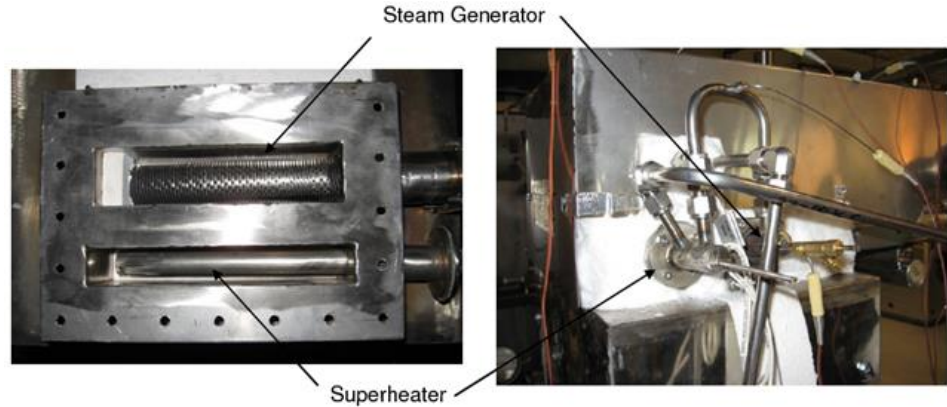


Figure 2.2: Steam generator configuration

The water required for the reforming can be obtained from suitably filtered potable water or from recovered condensate from the fuel cell offgas or from the condensing boiler.

2.1.1 - Operating Parameters

The actual composition of the products from the reformer is then governed by three main operating parameters:

- the temperature of the reactor (product outlet temperature)
- the reactor operating pressure
- the steam to carbon ratio, defined as:

$$\frac{S}{C} = \frac{\text{molar flowrate of steam}}{\text{carbon molar flowrate in } CH_4}$$

indicating the composition of the feed gas and the proportion of steam fed to the reactor.

Graphs and computer models using thermodynamic data are available to determine the composition of the equilibrium product gas for different operating conditions.

It is important to note that although the water gas shift reaction 2.3 occurs at the same time as steam reforming, it is generally exothermic and

promoted at lower temperatures, where the production of CO₂ and H₂ is favored. On the other hand, at high temperatures the formation of CO₂ and H₂ is not promoted, whereas the yield of CO and H₂O according to reaction 2.2 is enhanced. It is worth recalling that steam reforming is not always endothermic, it depends on the fuel. For example, in the case of steam reforming of a petroleum hydrocarbon such as naphtha, the reaction shall be carried out at relatively high temperatures. Indeed, in the case of naphtha at low temperature the reaction may become exothermic (liberates heat). This is because as the temperature is lowered, the reverse of reaction 2.2, namely, the formation of methane, becomes favored and starts to dominate.



Natural gas reforming will invariably be endothermic, and heat must be supplied to the reformer at sufficiently high temperature to ensure a reasonable degree of conversion. Thereby, if the reforming of naphtha is carried out at low temperatures (up to 500–600 °C), then the reactions will tend to yield greater concentrations of hydrogen and the need for external heating will diminish as the reaction becomes exothermic.

2.1.2 - Thermodynamic analysis

The thermodynamic analysis of steam reforming process is useful to identify the most favorable operating conditions at which methane may be converted into hydrogen.

Seo et al. [8] carried out a thermodynamic analysis, based on simulation through the code Aspen Plus and validated with experimental data, aimed to detect the effect of reforming input conditions on the reaction efficiency and output. In particular, for steam reforming the influence of steam to carbon ratio and reactor temperature on the final methane to hydrogen conversion was examined. Both reactant and product reactions were considered at the equilibrium; the reaction products are CH₄, CO, H₂,

C, H₂O, CO₂, while the radicals that could be produced in the reforming reaction were found to be negligible with respect to the main species.

Fig. 2.3 shows the effect of reactor temperature on molar fraction of the reforming products, pointing out the area where the coke formation is likely to occur. It is evident that higher temperatures promote hydrogen formation, however reactor temperatures shall not be higher than 850°C in order to not affect the thermal durability of the catalyst, resulting in a maximum conversion rate of 0.99.

Fig. 2.4 reports the equilibrium composition with respect to the S/C ratio. The simulation shows that, depending on temperature, the conversion is improved as the S/C ratio increases, with H₂ concentration raising and CO lowering. Moreover the energy cost of the reactor for this extra steam generation grows, thereby the choice of S/C ratio must carefully evaluate both aspects.

The simulation indicates that for a reactor temperature of 700°C the S/C should be maintained higher than 2.5 for achieving a conversion of 0.95, while for a temperature of 800°C the conversion is greater than 0.95 starting from S/C ratio of 1.2. Experiments have confirmed that a steam reformer reactor running on natural gas and operating at atmospheric pressure with an outlet temperature of 800°C produces a gas comprising some 75% hydrogen, 15% carbon monoxide, and 10% carbon dioxide on a dry basis.

Despite to CPOx reaction, the equilibrium composition in steam reforming reactor is independent from the pre-heat temperature of the reactants, because the reactor temperature and the steam generation are determined by an external heat transfer.

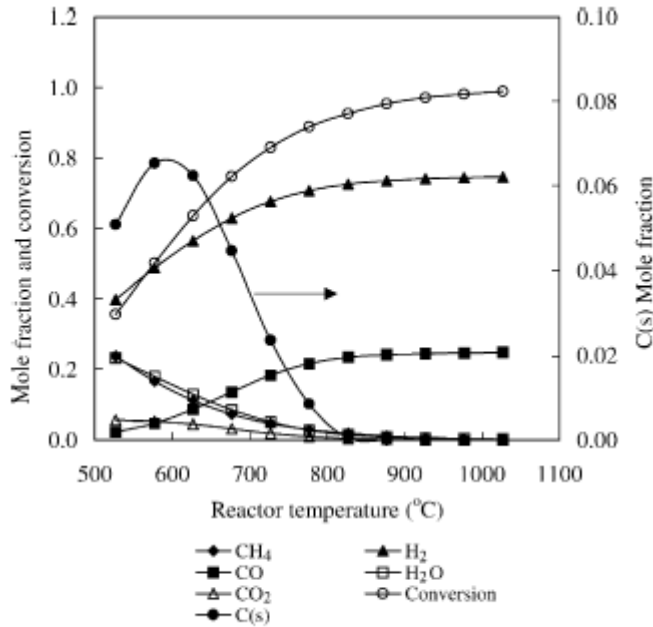


Figure 2.3: effect of reactor temperature (with S/C ratio=1) on the equilibrium composition of a SMR reactor [8]

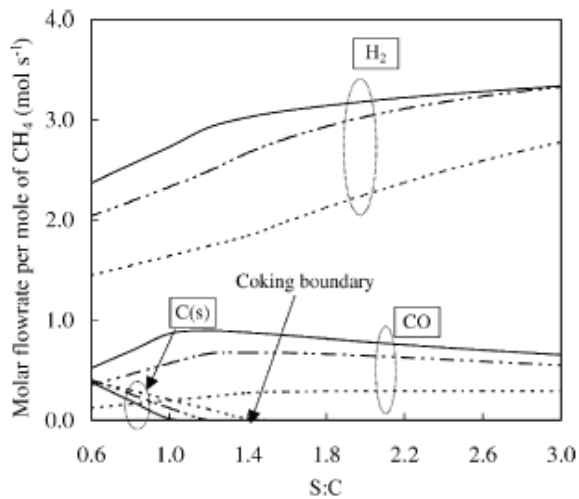


Figure 2.4-effect of S:C ratio on the equilibrium composition of a SMR reactor T = (---) 600°C; (-·-·-) 700°C; (----) 800°C [8]

The effect of varying the pressure on the equilibrium composition and conversion in a SMR reactor is shown in figure 2.5.

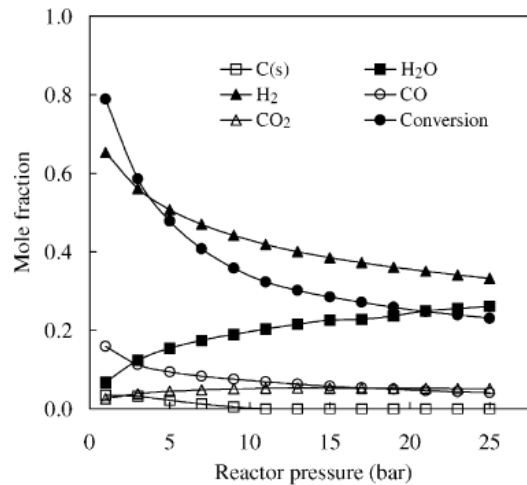


Figure 2.5: effect of the pressure on the equilibrium composition and conversion of a SMR reactor (T= 700°C, S/C=1) [8]

As the pressure is increased, the conversion and the mole fraction of H₂ and CO are rapidly reduced. According to reaction 2.2, there are three molecules of hydrogen and one molecule of carbon monoxide produced for every molecule of methane reacted. According to Le Chatelier's principle, the equilibrium is moved to the right (i.e. in favor of hydrogen) if the pressure in the reactor is kept low. Increasing the pressure will favor formation of methane, since moving to the left of the equilibrium reduces the number of molecules.

These results demonstrate that it is desirable to keep the pressure of the SR reactor as low as possible. The effect of pressure on the equilibrium position of the shift reaction 2.3 is very small.

2.2 - Partial oxidation (POx) and Catalytic partial oxidation (CPOx)

Several studies have been performed with the objective of reducing the steam production in large reactors, this because of its big costs and complexity [19, 20, 24, 25, 26, 27]. As an alternative to steam reforming, methane and other hydrocarbons may be converted to hydrogen via partial oxidation, through the reaction:



Figure 2.6 represents the thermodynamic scheme of the partial oxidation of methane, indicating the reactions involved when considering both direct and indirect mechanisms described in section 2.2.1.

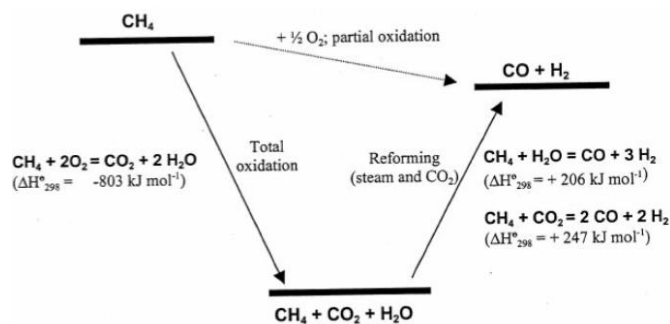


Figure 2.6: Thermodynamic representation of the partial oxidation of methane

Reaction 2.6 is effectively the summation of the steam reforming and oxidation reactions, according to the indirect mechanism described in section 2.2.1.2. About half the fuel entering the reactor is total oxidized through combustion reaction:



to provide heat for the endothermic steam reforming reaction, that occurs until thermodynamic equilibrium is met.

The reaction 2.6 is slightly exothermic, therefore can be performed either with or without the catalyst. In absence of catalyst, the reactor temperature

must be sufficiently high to reach the total conversion of methane (typically 1200–1500 °C), leading to high temperature of the gas at the outlet (1000–1100 °C). In this case the advantage of non catalytic processes is that materials such as sulphur compounds do not need to be removed; although the sulphur has to be removed anyway for fuel cell application before entering the stack [7]. High-temperature partial oxidation can also handle much heavier petroleum fractions than catalytic processes and is therefore attractive for processing diesels, logistic fuels, and residual fractions. Such high-temperature partial oxidation has been carried out on a large scale by several companies but it does not scale down well, and the control of the reaction is critical. If the temperature is reduced, and a catalyst used, then the process is defined as catalytic partial oxidation (CPO_x).

Catalytic partial oxidation has recently received particular attention because it is one of the most attractive technologies for the production of syngas and hydrogen in small to medium scale [9]. Indeed CPO_x can be carried out in compact reactors with rapid dynamic response and with low heat capacity, which is ideal for mobile and stationary small scale production of syngas. Besides, the catalytic partial oxidation has thermodynamic advantages with respect to a steam reforming process [7, 14, 17, 40], as reported below:

1. The reaction is mildly exothermic ($\Delta H_{0\ 298} = -37$ kJ mol⁻¹ to 247 kJ mol⁻¹, depending on the air/carbon ratio), while steam reforming is highly endothermic ($\Delta H_{0\ 298} = 206$ kJ mol⁻¹). Thus, a partial oxidation reactor requires less heat. The reaction takes place in one stage only, differently from steam reforming, and is faster, this means having higher flow rate in smaller reactors and lower startup times. In addition, it can be combined with endothermic reactions, such as steam reforming or dry reforming with carbon dioxide, to make this processes more energy efficient.
2. This technology avoids the need for large amounts of expensive superheated steam, thereby saving costs for the management of the excess H₂O. The media required for the reforming reaction is oxygen or air, which is easily available also for residential application. Moreover, as recalled in previous sections and remarked below, CPO_x reaction is more suitable for small-scale applications, where reduced size and low complexity are preferred.

The main disadvantage of partial oxidation is that it produces less hydrogen per molecule of methane than steam reforming. This means that partial oxidation (either non-catalytic or catalytic) is usually less efficient than steam reforming for fuel cell applications [7]. Furthermore, the catalytic partial oxidation may produce hot spots in the reactor inlet section, which can deactivate the catalyst [21]. Another drawback of partial oxidation is when air is used as the oxidant, as this lowers the partial pressure of hydrogen at the reactor outlet because of the presence of the nitrogen. Though air can guarantee the autothermal operation and is desirable in small scale applications, for SOFC systems this causes a reduction of the Nernst potential of the cell, in turn resulting in a decrease of system efficiency. However, an oxygen separation process, which is also costly, may be required in the cases where nitrogen is undesirable in high-pressure downstream processes.

Despite these negative features, the key advantage of partial oxidation is that it does not require steam. This mainly means that CPOx is free-standing and independent of external water source and heating devices. It may therefore be considered for applications in which system simplicity is regarded as more important than high electrical conversion efficiency, as, for example, small-scale cogeneration, also known as micro-cogeneration, automotive, or for all cases where the steam reforming is not easily applicable (e.g. with liquid hydrocarbons, being here the heating and steam mixing phases more critical).

The image of a standard CPOx reactor installed in a tubular fuel cell module is shown in figure 2.7.



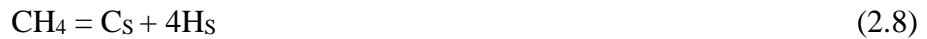
Figure 2.7: Image of a CPOx reactor used in a μ CHP application [38]

2.2.1 - Reaction Mechanisms

The mechanism for the catalytic partial oxidation of methane to synthesis gas has been the subject of a debate which to date is still not completely settled. Two distinct mechanisms have been proposed for explaining the formation of syngas [9]. The more relevant supporters of each process have been Prettre [23] for the indirect mechanism and Schmidt [14,21] for the direct one.

2.2.1.1 Direct oxidation mechanism

This mechanism, also called pyrolysis-oxidation, assumes that H₂ and CO are primary reaction products formed in the oxidation zone at the catalyst entrance, where also a dissociative adsorption of CH₄ with the formation of carbon and hydrogen species occurs [9]. Then surface carbon reacts with surface oxygen to CO and hydrogen atoms combine to H₂. So the basic reactions are:



The by-products CO₂ and H₂O are formed by the combustion between oxygen and H₂ and CO, but also for the reaction of methanation:



The main evidence to confirm the direct path is the observation of syngas at extremely short time with unreacted O₂. H₂O and CO species are in this case interpreted as non-selective oxidation products.

Schmidt et al. [14, 21, 22, 32] have studied the direct oxidation of methane to CO and H₂ at high temperatures over platinum and rhodium catalysts deposited on alumina based monolithic supports. The experimental results were then compared with those given by a model built according to the elementary steps of direct oxidation. Their conclusion was that direct partial oxidation of methane to CO and H₂ occurs through pyrolysis, and the CH₄ adsorption over catalyst surface does not inhibit the dissociation of hydrogen, but excludes the possibility that the following reaction can take place:



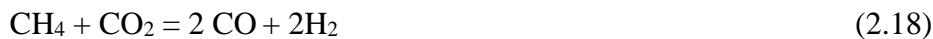
With related formation of H₂O through reaction:



This is confirmed by the high selectivity achievable with the used catalysts.

2.2.1.2 Indirect oxidation mechanism

This mechanism, also called combustion-reforming, postulates the presence of two zones: strongly exothermic CH₄ combustion at the catalyst entrance, followed by strongly endothermic H₂O and CO₂ reforming with not reacted methane downstream. In this reaction mechanism, the primary products are steam and CO₂, while the synthesis gas is the secondary product. Hence the reactions involved are:



Prettre et al. [23, 31] have investigated the partial oxidation of methane over nickel based catalysts. The tests were aimed at determining the reactor

temperature profile and the outlet products composition; test results have then been compared with the species values at the equilibrium, calculated considering that only partial oxidation reaction was occurring inside the reactor. They found out that these values did not match. In addition, as soon as the oxygen/fuel mixture was fed to the reactor, contrary to the features of a pure exothermic reaction, a high rise in temperature was observed, followed by a progressive decrease due to the later development of endothermic reactions inside the system.

In general, the observation of sharp temperature hot-spots at the entrance or on reduced syngas yields and the increase of total oxidation products with decreasing contact time are the major proves of the existence of such an exothermic-endothermic sequence [27].

2.2.1.3 Literature debate and trend

Researchers have followed essentially two approaches to detect whether the mechanism is direct or indirect. One approach is to study methane CPO_x under realistic conditions (high catalyst temperatures and atmospheric or elevated pressure). Typically, in these studies the reaction mechanism is inferred from the outlet concentrations. Such an approach is claimed to be not rigorous for the kinetics analysis, since frequently both direct and indirect scheme can equally justify the data [23, 23, 54]. Another approach exploits well-defined isothermal lower-pressure or diluted conditions. Depending on the experimental conditions, different products are modeled and inferred, then different mechanism conclusions may be drawn.

Many researchers believe that the reaction mechanisms depend on the catalyst used for the reaction (metal and supports) [52, 53, 54], and also on the operating conditions. Weng et al. [52] carried out a study on partial oxidation of methane over two different catalysts, Ruthenium and Rhodium, on the same support (Rh/SiO₂ and Ru/SiO₂). Experimental tests have shown that for Ru/SiO₂ catalyst the reaction occurred according to the mechanism proposed by Prettre [23], while for Rh/SiO₂ the reaction took place according to Schmidt theory [14, 21]. Weng et al. [52] have explained that this is due to the different intensity of chemical bond between metals and oxygen. The strong bond Ru-O inhibits the metal reduction during partial oxidation, thereby promoting the formation of total combustion

products. On the contrary, the bond Rh-O is less intense than facilitating the Rh reduction and promoting the methane dissociation and the yield of partial oxidation products.

The same researchers have also repeated the tests by using two catalysts characterized by the same active elements, but with different supports: Rh/SiO₂ e Rh/Al₂O₃. The result was that partial oxidation is indirect over Rh/Al₂O₃ and direct for Rh/SiO₂ catalysts; this is due to the different interaction existing between active components and their support. It can be resumed that the more the interaction is, the less the metal is reduced (favoring the total oxidation).

On the other hand, Veser et al. [25] affirm that the partial oxidation is always direct, regardless from the catalyst used; the high CO₂ and H₂O quantities observable at the beginning of the reaction shall be addressed to different values of adsorption coefficients for oxygen and methane rather than to an indirect mechanism. Being the oxygen adsorption coefficient higher than methane one, initially the catalytic surface is mainly covered by oxygen, thus promoting the total combustion reaction. When the oxygen partial pressure is decreased sufficiently to balance the gap between the adsorption coefficients of the two species, conditions that promote the partial oxidation development are established over the catalytic surface.

Further studies on catalytic partial oxidation over nickel based catalysts were performed by De Groote e Froment [26]: on the basis of indirect mechanism theory, they created a model where both kinetics of total oxidation of methane (Trimm [34]) and kinetics of steam reforming (Froment [35]) were combined. In order to account for the reaction sequence with steam reforming reaction followed by the combustion one, the percentage of catalyst reduction was considered in the model by multiplying the steam reforming and water gas shift reaction velocity by a reduction factor dependent on the oxygen conversion rate.

Tavazzi and at. [19] carried out a study on the kinetics of CH₄-CPO_x over Rh catalyst at low Rh load using an isothermal tubular reactor. Strong evidences were obtained to classify the scheme as an indirect one. Indeed, they observed the shape of the temperature profiles, which showed a maximum at the beginning of the catalyst, followed by a progressive temperature decrease along the layer. This is consistent with the occurrence of an exothermic-endothermic reaction sequence. Furthermore, the selectivity to H₂ decreased markedly when increasing the GHSV (Gas hourly space velocity). The hotspots on catalyst surface were also observed

by Basile et al. [27] by means of a IR thermo-camera disposed to measure the temperature profile inside the reactor.

In conclusion, the several studies on kinetic mechanism of partial oxidation carried out show that the direct oxidation can occur only over certain catalysts, with short time contact and high reactant mixture temperatures at reactor inlet. The outcome of these studies remarks that **partial oxidation mainly occurs through an indirect mechanism**, and the separation between combustion and reforming zone depends on the catalyst used.

2.2.2 - CPOx operating parameters

The main operating parameters of a CPOx reaction are the lambda value, the inlet reactant pre-heating temperature and the space velocity (GSHV). The influences of these parameters on the CPOx reaction are reviewed afterwards.

lambda

The key parameter in partial oxidation process is the ratio O_2/CH_4 , also known as air ratio, and it is represented through the parameter lambda (λ). It corresponds to half of the ratio O_2/CH_4 and is defined as the ratio between the air utilized by the reaction μ_{air} and the stoichiometric value μ_{stoic} .

$$\lambda = \frac{\mu_{air}}{\mu_{stoic}}$$

In all reactions involving methane and oxygen, this ratio can vary from the partial oxidation theoretical limit ($\lambda = 0.25$) to the value corresponding to the stoichiometric combustion ($\lambda = 1$). As described below, typical values of lambda for the partial oxidation are within the range 0.25-0.35 [36, 37]. The pros and cons of operating at different values of lambda are reported in table 2.1.

Table 2.1: Pro and cons of operating with different lambda

	Pro	Cons
$\lambda = 0.25$	maximizes the yield in hydrogen	high risk of carbon deposition and impossibility to reach high temperatures auto-thermally.
$0.25 < \lambda < 0.30$	reduces the risk of carbon deposition and allows obtaining both equilibrium temperature and hydrogen conversion desired even with low pre-heating of inlet reactant mixture.	less yield in hydrogen respect to the theoretical condition
$\lambda > 0.3$	It is used in the startup phases to stabilize the reactor temperature. It leads to higher methane conversion	a excessive time in this condition can generate overheating and consequent degradation of the catalyst, the hydrogen yield is lower than other conditions.

In equation 2.6, a value of lambda close to 0.25 ($O_2/CH_4 = 0.5$) promotes the formation of partial oxidation products with respect to the total combustion (eq. 2.7), and thereby is the theoretical reference for CPOx. On the other hand, it prevents reaching high temperatures autothermally, in turn, can sustain the reaction without having an external heating source. This implies the risk that the unreacted methane does not react with steam according to reforming reaction 2.2 to yield hydrogen and carbon monoxide, but tends to pyrolysis, forming coke and facilitating the carbon deposition [37]. In order to allow the system to reach high temperatures in auto-thermal regime and to maximize the synthesis gas yield, it is necessary to operate at lambda higher than 0.25. This allows the occurrence of the total combustion reaction responsible for keeping the temperatures high.

The parameter lambda for a catalytic partial oxidation mechanism shall hence be accurately controlled during each phase of the process. A low lambda can theoretically guarantee the highest hydrogen conversion, approaching the steam reforming one, but the risk of undergoing a carbon deposition over catalyst bed (and also anode cell) is high. The inferior limit for lambda to avoid carbon deposition depends on the operating

temperature.

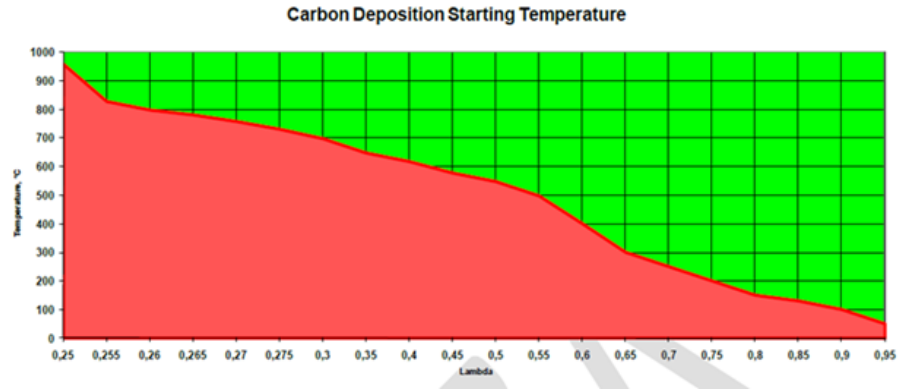


Figure 2.8: Carbon deposition limit over lambda and temperature (SOFC Power) [37]

Figure 2.8 illustrates the carbon deposition limit with respect of lambda and operating temperature according to the experimental data disclosed by SOFC Power, Italian SOFC manufacturer. When working in the red area, the carbon deposition is almost certain. In order to avoid catalyst deactivation, lambda and operating temperature shall be selected within the green area. This information confirms that it is required working at temperatures over 700°C for the lambda range typically adopted in FC applications.

Irrespectively from the carbon deposition phenomenon, as long as the lambda increases, a rise of the temperature together with an higher methane conversion occur. On the other hand, the hydrogen yield is reduced. There is a limit to the increase of lambda that typically is bounded by 0.33-0.35. In fact, the higher the lambda is, the more difficult is to control the temperatures inside the reactor.

Moreover, it is also difficult to control and prevent the total combustion reaction development, which can become unstable, thus causing consistent heating formation. This issue is critical for the applications of CPOx reactor in fuel cells; indeed the reforming feeding system must be designed carefully, especially valves and flow meters that control the supply of air and fuel to the reactor. Even a slight difference in the design operating flow rates could lead to carbon deposition or

oxidization of the catalyst, with serious consequences for the system and for the stack itself.

Experimental data and simulation results of CPOx reaction for different lambda values are shown in the following.

Inlet Reactant pre-heating temperature

In addition to the value of lambda, the other factor that strongly characterizes the partial oxidation reaction is the preheating temperature of inlet air/gas mixture entering the reactor. This temperature can be either designed in the engineering phase or determined experimentally by making some trials and errors when the system is ready for tests. In fuel cell systems with reforming reactor integrated inside the Fuel Cell Module (defined also as Hot Box by many fuel cell manufacturers, see chapter 3) the pre-heating issue is taken into account by properly integrating the reactor inside the Hot Box itself. Experimental tests [24, 25, 27, 36, 37] have shown that the input temperature of reactants may cause an increase of both the CH₄ conversion and the adiabatic temperature of the reactor. To improve the conversion of the reformer, it is advantageous to pre-heat the reactants to a temperature higher than ambient one, also for sustaining the catalytic reaction. However, this increases the adiabatic temperature of the CPOx reactor, which in turn may cause deactivation of the catalyst. In most of SOFC applications, the preheating temperature is included in the range 20-400 °C, depending on several variables such as lambda, reactor, catalyst and integration of the reactor in the system (e.g. for the heat losses). Typical values for CPOx reactors integrated in SOFC Hot Box are restricted to the range 150-300°C [37].

Experimental data and simulation results of CPOx reaction for different inlet reactant temperature values are reported in the following sections.

Space velocity (GHSV)

Another interesting parameter for the catalytic partial oxidation is the spatial velocity, that is nothing else than a way to take into account the contact time of the reactant species over the catalyst surfaces (namely, the GHSV is the inverse ratio of the contact time).

The Gas Hourly Space Velocity (GHSV) is defined by the ratio of

the total volume flowrate of reactant gases entering the reactor in standard conditions (0°C at 1 atm) and the total catalyst useful volume [36]. In the catalytic partial oxidation it is useful to increase the spatial velocity to maximize the hydrogen gain, up to a limit value beyond which the hydrogen yield decreases, and the methane conversion as well. The decrease in hydrogen selectivity with GHSV is indeed one of the drawbacks of catalytic partial oxidation process.

Figure 2.9 reports experimental measures of the conversion of methane and selectivity of carbon monoxide in function of the spatial velocity [36].

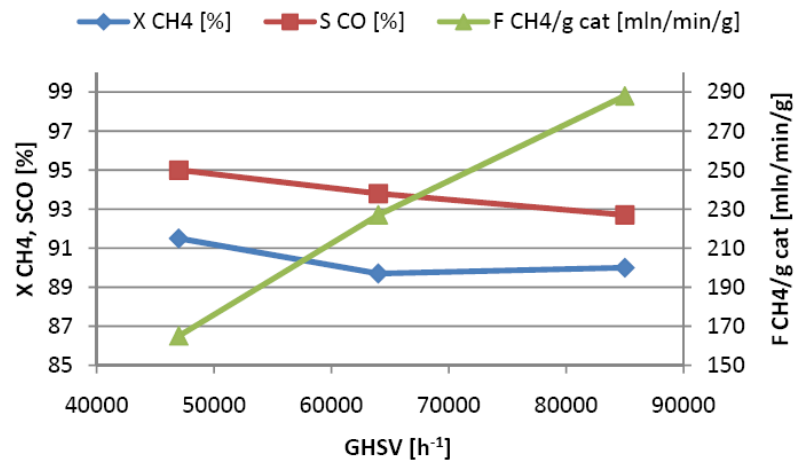


Figure 2.9: conversion of CH₄ and selectivity to CO in function of the spatial velocity [36]

2.2.3 - Thermodynamic analysis

As already stated in previous paragraphs, the main drawback of CPO_x reaction is the low conversion efficiency in hydrogen with respect to other reforming mechanisms. As shown in figure 2.10, this is mainly due to the loss in heating value associated to the partial combustion of gases, which

brings to recommend a minimum temperature for the reactor of 700°C [37].

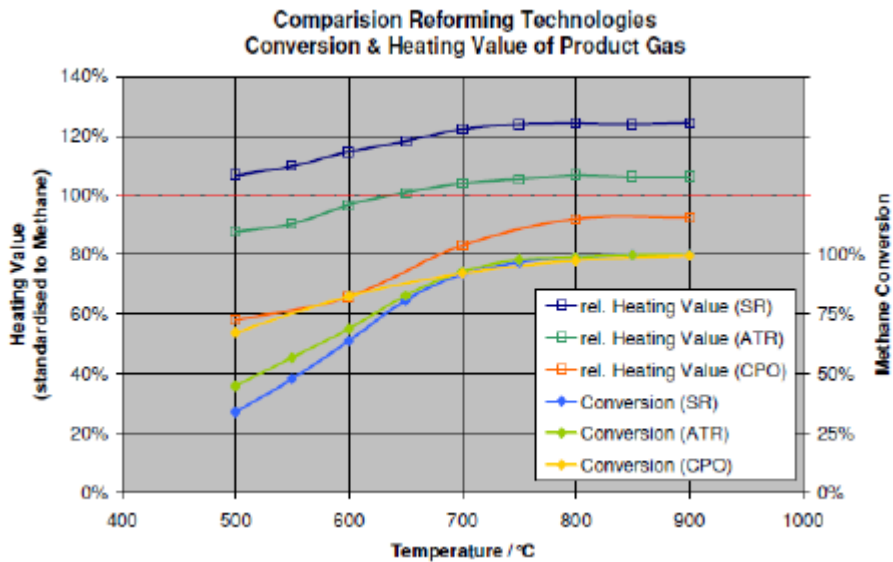


Figure 2.10: Comparison of heating value and methane conversion of SR, CPOx and ATR reformates for different temperatures ($\lambda_{CPOx} = 0.27$) [37]

Seo et al. [8], whose reforming model has already been recalled in paragraphs 2.1 and 2.2, carried out several studies on the partial oxidation reactions for studying the influence of the inlet parameters on the thermodynamics of the reactions. Considering a partial oxidation reaction (i.e. without catalyst and with higher temperature than the typical CPOx method) they reported the results achieved in their model by varying lambda in the range from 0.25 to 0.6 and the inlet reactor pre-heating temperature from 100 to 500°C.

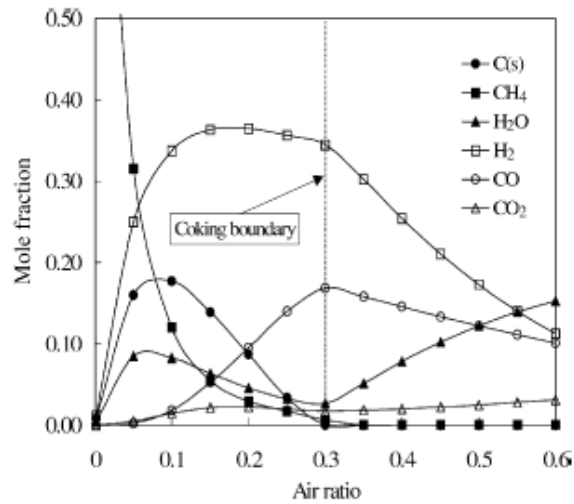


Figure 2.11: effect of lambda on the equilibrium composition (reactant pre-heating temperature = 200°C) [8]

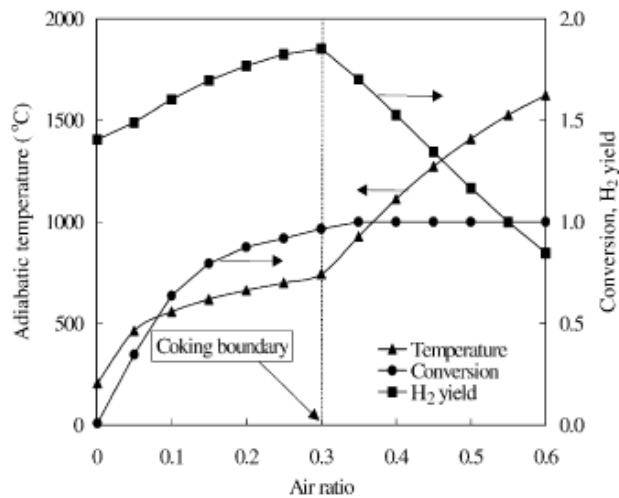


Figure 2.12: Adiabatic temperature, methane conversion and H₂ gain over lambda (reactant preheating temperature = 200°C) [8]

Figure 2.11 reports the concentrations of reaction products at the equilibrium as a function of the lambda, for a preheating reactant temperature of 200°C and pressure 1 atm. It can be noted that for lambda

higher than 0.3 the coke formation is prevented, in spite of a reduction of the H_2 and CO yield.

In Figure 2.12 the increasing trend of methane conversion rate is shown together with the trend of reactor outlet temperature when varying the lambda. The same authors proved that the CPOx (with lambda 0.27) proceeds auto-thermally at temperature of 700°C .

The effects of preheating temperature on the conversion and on the adiabatic temperature of the CPOx reactor are illustrated in figure 2.13-a and 2.13-b. The increase in the input temperature of the reactants causes the rise of both the CH_4 conversion rate and the adiabatic temperature.

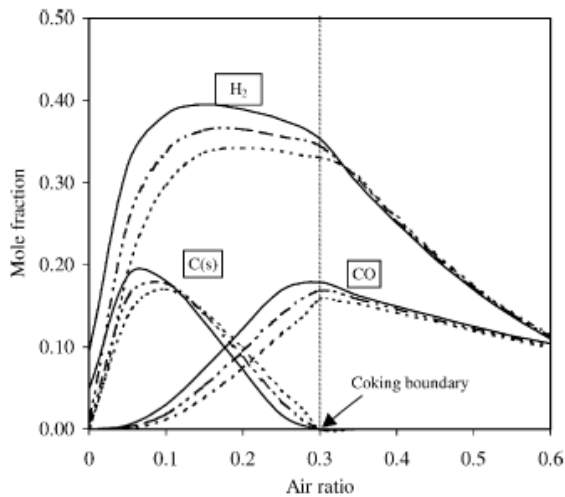


Figure 2.13-a: effect of pre-heating temperature on the equilibrium composition of the reactor
 (reactant pre-heating temperature $T = (---) 20^\circ\text{C}$; $(-\cdot-\cdot-\cdot-) 200^\circ\text{C}$; $(-----) 400^\circ\text{C}$).

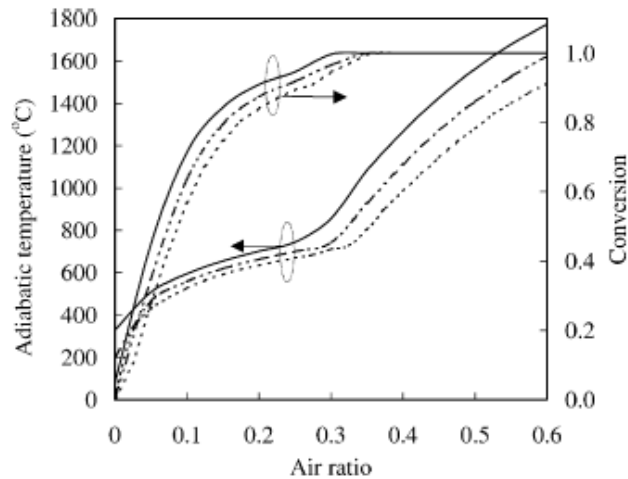


Figure 2.13-b: effect of pre-heating temperature on the adiabatic temperature of the reactor
 (reactant pre-heating temperature $T = (---) 20^{\circ}\text{C}$; $(-\cdot-\cdot-\cdot) 200^{\circ}\text{C}$; $(\cdots\cdots) 400^{\circ}\text{C}$).

However, if the catalyst temperatures need to be maintained below 800°C , the lambda shall be decreased progressively with increasing preheat temperature in order to avoid deactivation of the catalyst. In their analysis, Seo et al. found that the adiabatic reactor temperature increases from 670°C to 857°C when the preheat temperature of reactants was raised from 20 to 400°C at a lambda of 0.3 . In real operation, in order to operate the reactor with a high flow rate of reactants, it is necessary to heat up the reactants sufficiently to maintain the catalytic region.

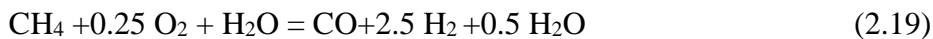
2.2.4 - Internal CPOx reforming for tubular fuel cell: Acumentrics technology

Tubular fuel cells have different design and performance respect to the more used planar ones (section. 3.1). The model developed in this thesis can be adapted to both cases, since it characterizes the reforming reactor that is upstream the stack. The experimental results collected for the model validation are referred to a planar design, that is also most suitable for small

scale application and allows obtaining higher stack and system efficiency, thereby the planar fuel cell layout is assumed for the purpose of this work. Nevertheless, the planar design is of bigger interest for industrial and academic research, due to its higher potentiality in terms of performances, the small footprint and the possibility to stack the cells in modules. However, the experimental tests carried out at Ariston facilities (see section 3.2) have involved also some μ CHP units with tubular design, developed by Acumentrics, hence offering the opportunity to investigate the reforming mechanism used for these systems.

Acumentrics Corporation is an American society leader in the manufacturing and marketing of tubular SOFC. Acumentrics has developed a novel method to reform the natural gas fuel stream, which allows the system to work under partial oxidation reforming conditions at low oxygen to carbon (O/C) ratios [38]. In standard tubular CPOx configurations, including the previous units by Acumentrics, an O/C ratio greater than 1.2 (O/C of 1.2 corresponds to a lambda of 0.3) was required to ensure that soot formation within the fuel piping and cells was avoided. With this new technology, systems can run at O/C ratios as low as 0.5 (lambda 0.125) without dropping carbon. This reduction in O/C ratio results in a significant improvement in the stack operating efficiency, as shown in Figure 2.14. As depicted in the plot, at low O/C ratios the stack efficiency approaches that of a steam reforming configuration.

By using low O/C it is possible to break up the global autothermal reactions into a CPOx over the catalyst surface, followed by steam reforming in the fuel cell using the water produced in the electrochemical reactions. Globally, this leads to an autothermal (ATR) reaction described as follows:



but with a much lower energy penalty as there is no vaporization of water. From thermodynamic consideration, the free energy of the products must be the minimum [101].

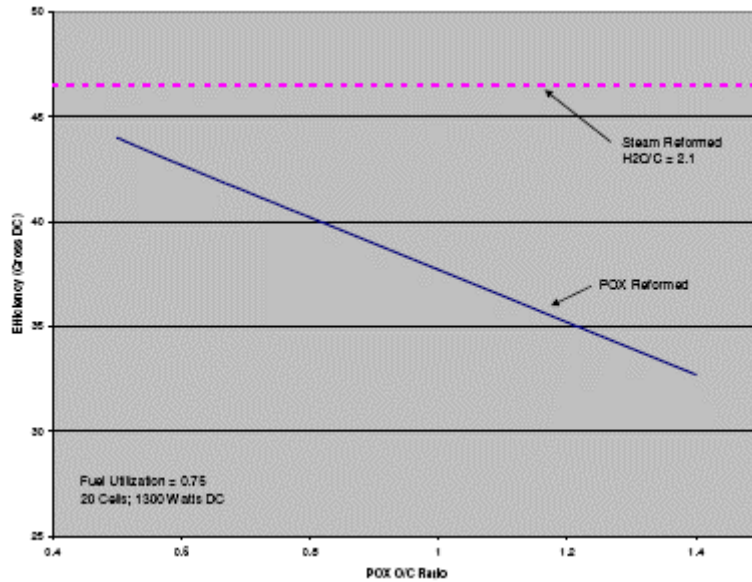


Figure 2.14: Fuel Cell Efficiency versus Oxygen to Carbon Ratio in Acumentrics technology [38]

The new fuel processing technology developed at Acumentrics envisages catalytic coated fuel injectors in conjunction with internal fuel recirculation. This allows to overcome two of the main shortcomings of CPOx operation (fig. 2.14), namely reduced efficiency and lack of an in stack heat sink as compared to in-situ steam reformed operation. This arrangement overtakes the mentioned drawbacks while retaining the general simplicity of a CPOx system. Anode gas processing requires the metering of the air and fuel streams to the correct ratio which for small μ CHP systems is much simpler and less expensive than condensing the offgas stream, metering and re-injecting the water to produce steam. It will also require less maintenance and is less costly than a potable water filtering system.

Figure 2.15 shows some images of the tubular fuel cell stack and the standard layout of Acumentrics fuel cell module, showing the position of each device (i.e. startup burner, recuperator, offgas burner and catalytic fuel injectors) inside the Hot Box. The figure also represents the configuration adopted by Acumentrics for the integration between each fuel injector and tubular cell.

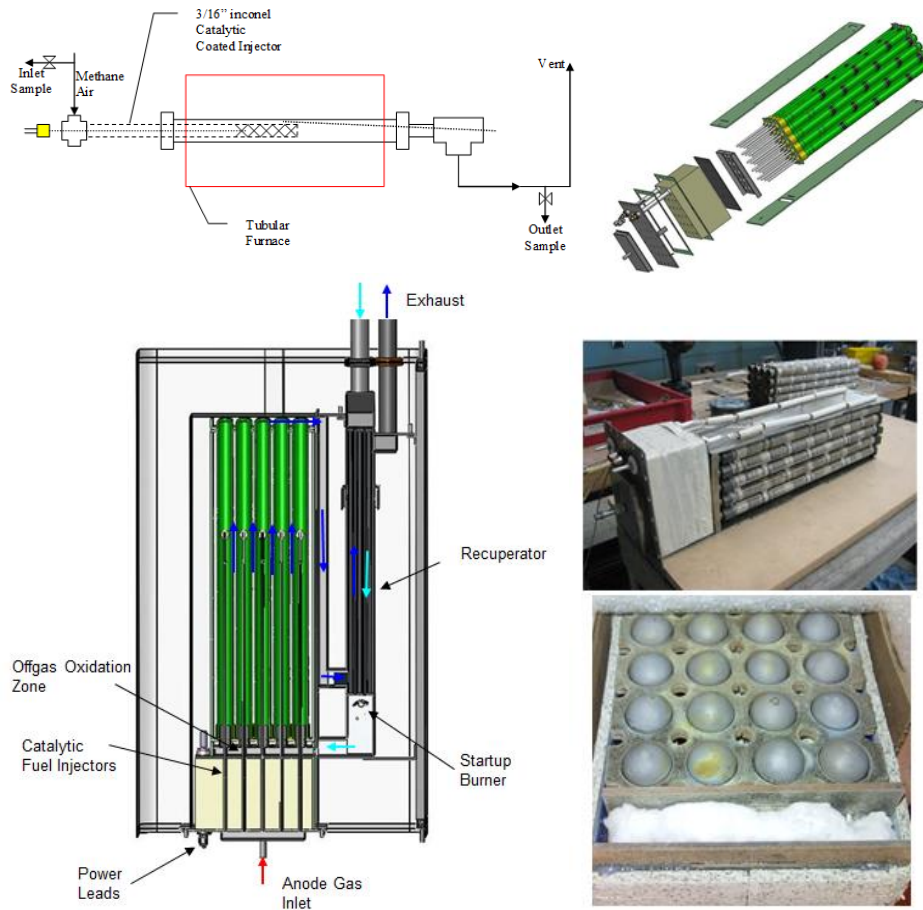


Figure 2.15: Acumentrics stack bundle, tubular cells and catalytic injectors [38]

By adding the catalyst in the injector of each single cell an almost isothermal reformer is created. This is in contrast to the adiabatic reformer most commonly used in different fuel cell systems. The temperature is essentially controlled at the stack level, which is very favorable for the reforming performance, and this makes the reforming system highly tolerant to deviations in O/C, ranging from 0.5 to 1.7 (respectively corresponding to a λ of 0.125 and 0.43). A constant O/C of 1.7 in the long time would burn out the monolith in an adiabatic system. For enabling the reforming reactions to take place, the control system opens the anode

fuel and the anode air valve when the plenum temperature reaches 650 °C. At these conditions, the stack is warm enough to guarantee the required conversion within the injectors of each cell and the cell itself.

The general concern with this solution is that for $O/C < 1$ ($\lambda < 0.25$) the carbon formation is thermodynamically enhanced. Certainly the risk is considerably high, but this phenomenon does not necessary have to occur and can be stopped if kinetic barriers to its formation are in place. The kinetic barriers are always present in the form of activation energies, thus carbon formation is prevented either by removing any catalyst that can lower this activation energy, or by adding catalysts, which decrease the activation energy for the gasification of carbon. The basis of Acumentrics technology and testing is the removal of carbon forming the catalysts, thereby increasing the activation energy for the process and enabling the operating at low O/C for natural gas.

The correct O/C ratio to be used depends on the system and its overall performance. At open circuit and low load conditions (below 30 A of current generated by the stack and generally with low power), the O/C ratio must be approximately 1.2-1.4, for improving the heat balance of the system.

Table 2.2: Test results on Acumentrics 1kW μ CHP with low O/C ratios [38, 103]

Current [A]	Voltage [V]	Stack Power [W]	Uf [%]	η DC [%]	η AC [%]	Fuel cons. [W]	O/C ratio [1]
20	17,71	354	43	25%	16%	1403	1,20
30	16,60	498	56	31%	22%	1627	1,20
40	15,50	620	65	33%	24%	1881	1,20
50	14,14	707	75	35%	25%	2014	1,20
60	13,47	808	70	32%	23%	2553	1,20
60	13,96	838	73	36%	26%	2335	1,00
60	14,13	848	75	40%	30%	2111	0,80
60	14,44	866	75	43%	32%	1996	0,60

At a given percentage of full load (approximately 75%) and above, when the current exceeds 30 A, the O/C can be lowered to approximately 0.5-0.6, in order to be sure that there is enough H₂O and CO for the steam reforming reaction. This is the phase when the reforming mechanism turns

into an autothermal reforming and there are remarkable benefits for the electrical efficiency of the system, as shown in table 2.2 above. The test results demonstrate as the DC electrical efficiency increases from 32% to 43% when the O/C ratio is lowered from 1.2 to 0.6. For O/C ratio lower than 0.5, the risk of having carbon deposition becomes almost certain.

The anode fuel feeding system for the high efficiency CPOx is shown in figure 2.16. It is slightly different with respect to the standard configuration, usually designed to provide a fixed oxygen to carbon ratio achieved through a Venturi based pressure compensation system. For the high efficiency and low O/C system, the oxygen to carbon ratio must be variable to achieve proper operations, and its scale is set according to the load and fuel utilization.

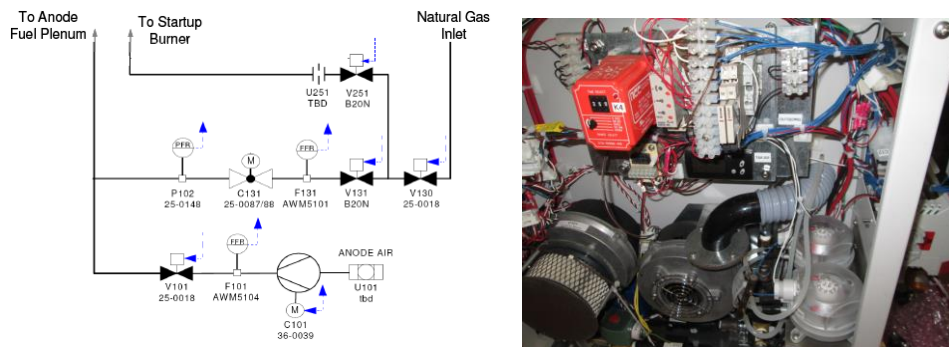
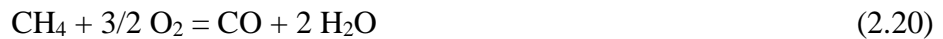


Figure 2.16: Air and fuel feeding system in Acumentrics μ CHP

This variable O/C operation can be achieved in several methods. In the configuration shown in figure 2.16, the anode air flow is controlled by the speed control of an anode blower, and the anode fuel flow is controlled via a modulating fuel valve. Both streams include flow meters to measure the flowrates. This is required to maintain the correct O/C ratio over the entire operating range. It is important to take into account the maximum error of the air flow meter and fuel flow meter (5% tolerance respect to the set point conditions), to avoid any catalyst deactivation phenomena due to the excess of either fuel or air flow. It is also possible that the flow meters can be eliminated by characterizing the fuel flow versus fuel valve position and characterizing the air flow based on anode blower speed and pressure.

2.3 - Autothermal reforming (ATR)

Autothermal reforming (ATR) is another common technique in fuel processing. It was developed by the Danish company Haldor Topsoe at the end of 1950s and usually describes a process in which both steam and oxidant (oxygen, or more normally air) are fed with the fuel to a catalytic reactor [11]. It can therefore be considered as a combination of CPOx and the SR processes already described, as follows:



By gathering together the reactions 2.20, 2.21, 2.22, the equation for ATR can be summarized as:



The basic idea of autothermal reforming is that both the *endothermic* steam reforming reaction (2.2) and the *exothermic* CPOX reaction (2.6) occur together, such that no heat needs to be supplied or removed from the system (adiabatic process). However, there is some confusion in the literature between the terms *partial oxidation* and *autothermal reforming*.

Joensen and Rostrup-Nielsen [47] published in 2002 a review that clarified the issue and explained both definitions in detail. Their analysis was oriented to investigate on the factors that mainly affect the reaction and can determine whether it falls in CPOx regime or in the ATR one. They realized that if steam is added to a fuel/oxidant mixture and passed through a bed of catalyst, the material of the catalyst itself, besides the operating temperature and pressure, determine to what extent the steam reforming reaction occurs.

Several studies [46, 48, 57, 58] have tried to determine the relative rates of the reforming and partial oxidation reactions over different

catalysts; it is generally assumed that the oxidation reaction is brought to equilibrium faster than the steam reforming reaction. This has been termed the *indirect mechanism* of CPOx, explained in chapter 2.2.1.2. In some CPOx processes, both steam and oxidant are fed with the fuel, an example being the Shell partial oxidation process, currently developed by HydrogenSource in the United States [48]. This uses a proprietary reactor design containing a Platinum group catalyst over which CPOx occurs at the top of the bed, whereas further down the bed, the steam reforming and shift reactions bring the gas to equilibrium.

In other examples of CPOx where the steam oxidation and reforming reactions operate in parallel, the rate of the reactions are not limited by mass transfer and are brought to equilibrium without gain or loss of heat. This is true autothermal reforming, and it is what occurs in Acumentrics' tubular fuel cell when the O/C ratio is reduced below 1.0 ($\lambda < 0.25$) and the current drawn by the stack is at least 30 A (section 2.2.4). In this case the steam required for the autothermal reaction is directly brought by the fuel cell reaction.

The advantages of autothermal reforming are that less steam is needed compared with conventional reforming and that all the heat for the reforming reaction is provided by partial combustion of the fuel [42]. This means that no complex heat management engineering is required, resulting in a simple system design.

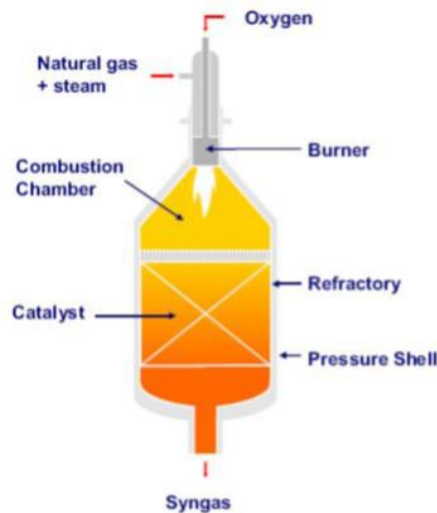


Figure 2.17: ATR reactor [11]

The ATR reactor shown in figure 2.17 consists of a burner, a combustion chamber and a catalyst bed, all of which are contained in a refractory lined pressure shell. A mixture of natural gas and steam is partially converted by pressurized combustion under fuel-rich conditions in the combustion chamber. The temperature in the combustion chamber is in the range of about 1100-1300 °C near the catalytic bed and up to 2500 °C in the flame core, depending on the process conditions. In the combustion chamber also the steam reforming and the water gas shift take place in homogeneous phase due to the high temperature. In reality, a large number of chemical reactions take place in the combustion chamber involving radicals [45].

The oxygen is consumed by the combustion reactions. However, the methane conversion is not complete in the combustion chamber. In fact the final conversion of methane takes place in the catalytic bed, and the synthesis gas leaves the ATR reactor at chemical equilibrium temperature, typically between 850 and 1100 °C.

The ATR reactor is soot free under normal operation. The fuel rich combustion occurs in a turbulent diffusion flame and intensive mixing is required to prevent soot formation. Soot formation is unwanted and would reduce the carbon efficiency of the process, reason why soot particles, if any, should be removed from the synthesis gas.

2.3.1 - Thermodynamic analysis

The most relevant source for the thermodynamic analysis of the ATR reaction is once again given by the paper published by Seo et al. [8]. Figures 2.18 and 2.19 represent the trend of methane conversion and reactor temperature over the air ratio and S/C ratio.

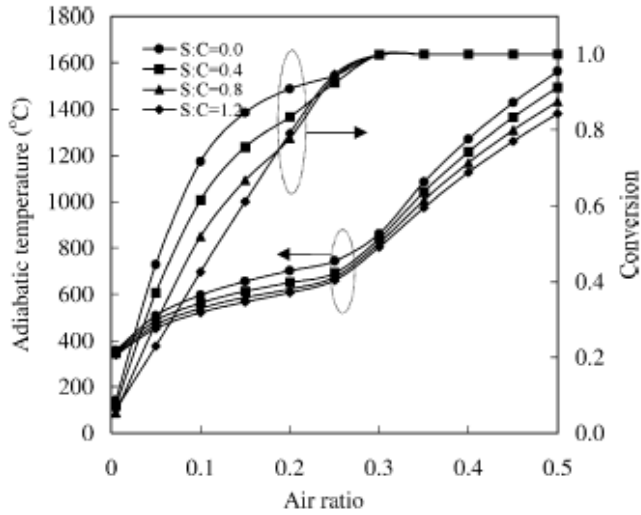


Figure 2.18: effect of lambda and S/C ratio on the adiabatic temperature and conversion in ATR reactor (reactant pre-heating temperature = 400°C) [8]

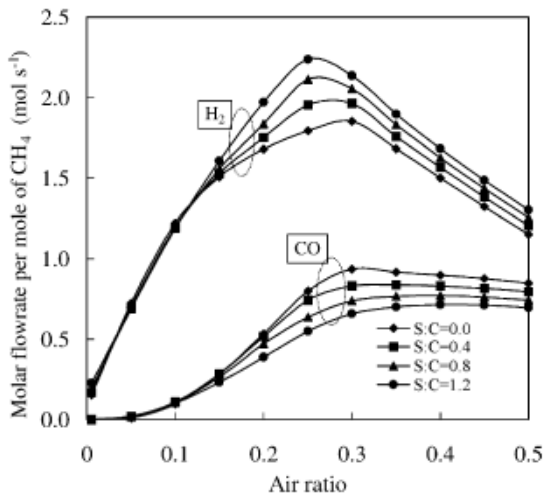


Figure 2.19: effect of lambda and S/C ratio on mole fractions of H₂ and CO in ATR reactor (reactant pre-heating temperature = 400°C)

The methane conversion increases considerably with the air ratio, approaching one when the air ratio is 0.3, whereas the temperature raises also beyond this limit, because even when the methane is all consumed, the

CO can still be oxidized.

On the other hand, by increasing the S/C ratio, both methane conversion and reactor outlet temperature decrease. This can be explained considering that at higher S/C ratios the steam reforming is promoted, with consequent higher heat demand which eventually leads to the cooling of the reactor, decreasing the temperature and reducing the conversion. The benefit of having higher S/C is that the coke formation is prevented and the hydrogen and carbon oxide concentrations increase; however, their trend over the air ratio does not grow up accordingly (the max is around 0.25).

2.3.2 - Reaction Mechanism

In the autothermal reforming it is possible to carry out the oxidation reactions even without catalyst, exploiting the heat and steam coming from the reforming reactions [50]. As alternative, if this is found to be not sufficient, a catalyst may be added to start the oxidation, and this could be the same one used for reforming. Several reactions might occur when steam, air and methane are simultaneously fed to the same reactor. Many studies were performed to investigate on the reaction mechanisms [41-49], similarly to what has been done for the CPOx reaction. The general conclusion is that also in this case the reaction takes place following an indirect mechanism, through the sequence of the total oxidation followed by the reforming phase.

De Grotte and Froment [26] in their research activity demonstrated that the addition of steam to an air/methane mixture determines the reforming reactions to occur in advance, promoting the overlapping of exothermic and endothermic zones, where oxidation and reforming reactions respectively take place. This yields a decrease of the temperature peak over the catalyst bed and in turn a lower deactivation risk for the catalyst. The overlap area between oxidation and reforming depends on the type of catalyst used, as confirmed by the different temperature profiles measured in the reactor when testing several catalysts.

Li et al. [46] and several other researchers [43, 45] tested the autothermal reaction with Rhodium (Rh), Platinum (Pt) and Palladium (Pd) catalysts, when the reactor was heated up to 800°C. The results showed that

Rh catalyst exhibits a temperature peak in the oxidation area lower than Pt and Pd, and in addition the separation of phases proceeds according to the following:

- Pd \approx Pt > Rh: Combustion activity;
- Rh > Pt > Pd: Reforming activity

The high reforming and low combustion activity of a catalyst or vice versa (low reforming and high combustion activity) are reflected in the exothermic/endothemic overlap area: the main result is that the Rh catalyst seems to be the most suitable for the autothermal reforming of methane [50]. However, its high cost and low availability on the market limit its spread and usage (section 2.4.3). On the other hand, the most effective alternative, nickel catalyst, is easy to find in commerce and economic. It is characterized by a lower interaction between exothermic and endothermic zone, due to the stratification occurring on the Ni catalyst during the partial oxidation [34]. Indeed, as demonstrated by Dissanayake et al. [55, 56], the nickel based catalyst exhibits three different zones during the oxidation phase of the autothermal process (figure 2.20)

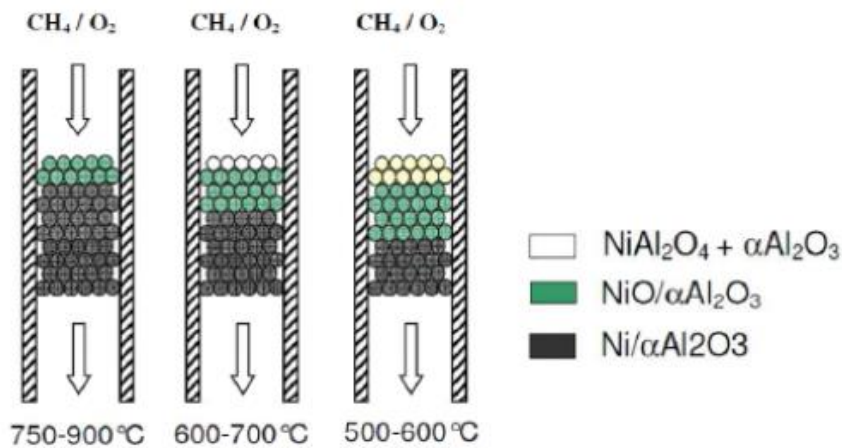


Figure 2.20: Scheme of Ni/Al₂O₃ catalyst during ATR at different operating temperatures [56]

- the first zone is formed by NiAl_2O_4 , characterized by poor tendency to total combustion and nothing for the reformed (white color)
- the second zone is constituted by $\text{NiO} + \text{Al}_2\text{O}_3$, presenting an high activity for total combustion, leading to the total O_2 consumption (green color).
- The third area is made up by metallic Ni, that catalyzes the reforming reaction, leading to CO and H_2 formation (black area)

The existence and weight of each substrate depends on the thermal level of catalytic bed and on the possible pre-reduction process to which the nickel can be subjected.

Many other studies were focused on the evaluation of the effects generated on the autothermal reforming reaction by adding noble metals to the nickel catalyst. In particular, Dias and Assaf in 2004 [57] have analyzed the effects of adding small quantities of platinum and palladium, discovering remarkable benefits for the reaction efficiency. This was confirmed also in the later work carried out by Dias et al. in 2008, and is mainly due to the fact that the addition of noble metals decreases the reduction temperature for the nickel catalyst, bringing it down from 600 °C to 450 °C.

2.4 - Catalysts and supports for CPOx reforming reactors

2.4.1 - Status of Catalytic Partial Oxidation Research

The first papers detailing with the catalytic partial oxidation of methane to synthesis gas were published in 1929 by Liander [61], in 1933 by Padovani and Franchetti [62] and by Prettre [31]. However, high yields of synthesis gas were only obtained at temperatures in excess of 850°C. The latter studies showed that below this temperature non-equilibrium product distributions were observed. However, the carbon formation phenomenon

over the supported catalysts used for tests was not studied in any detail. During the following decades the CPOx mechanism was studied only superficially and many uncertainty factors related to this process were not investigated in detail. Due to these aspects, as well as to the success of the steam reforming process, partial oxidation was left aside for many years. In the late 1980s Green and co-workers [63] began a renaissance in the study of methane partial oxidation. While investigating trends in the behavior of the lanthanides for oxidative coupling using pyrochlores containing noble metals and rare earth metals, they observed high yield of synthesis gas. Their tests revealed that the ruthenium catalyst had an excellent activity for methane partial oxidation. They also performed a high-resolution electron microscopy on the post reaction samples, whose results confirmed that no carbon deposition had occurred. This observation encouraged a detailed investigation of the stoichiometric methane partial oxidation over both noble metals and base metal catalysts by a large number of research groups. The results published in the 1990s were mainly concerned with the catalyst screening, although the effect of the principal system parameters such as operating temperature and pressure were also studied. Later on, many researchers began to shift their investigations towards the improvement of catalyst stability and performance. In this scenario, important results were reported by Hickmann and Schmidt [14,21,64]. They studied the CPOx reaction in an adiabatic reformer with noble metal based catalyst, at atmospheric pressure and in a short-contact time, obtaining conversion results close to the thermodynamic equilibrium. The first simulation of methane partial oxidation over Pt and Rh catalysts surfaces was given by Hickmann et al. [65]. The model consisted of 19 elementary steps including adsorption, desorption and surface reactions.

Currently, the research activities for the process of catalytic partial oxidation mainly concerns the following issues:

- optimization of the catalyst and the support;
- reaction mechanism;
- optimal reactor design.

Besides, the aspects related to the type of fuel to be adopted for each different application are progressively gaining more attention (e.g. logistic fuels such as gasoline and diesel are suitable to be used for on-board and on-site fuel cells). The propane is also drawing higher interest in hydrogen

production studies, since it is a constituent of LPG. The LPG is a commercial gas whose main advantage is the simplicity to be transported and stored on site. Moreover, due to its composition (short aliphatic C₃-C₄ chains and absence of sulphur or other electronegative atoms), LPG is reported to present some significant advantages compared to heavier feedstocks: it exhibits less tendency to the carbon deposition and generates a reaction more exothermic than the methane.

2.4.2 - CPOx reactors - literature background

CPOx reactors can be very simple in design, requiring only one bed of catalyst into which the fuel and oxidant (usually air) are injected [7, 9, 40]. As described in section 2.3, sometimes the steam is added as well, turning the CPOx into an autothermal reforming, where conventional steam reforming also occurs. In this case, depending on the nature of the fuel and on the application, two types of catalyst may be used, one primarily for the CPOx reaction and the other to promote steam reforming. A well-known example of CPOx reactor is the Johnson Matthey HotSpot reactor (Edwards et al., 1998). A schematic representation of an early version of this technology is shown in Figure 2.21.



Figure 2.21: Johnson Matthey HotSpot reactor

It utilizes a platinum/chromium oxide catalyst on a ceramic support. A scaled up reactor of 2 liters capacity successfully demonstrated the

commercial possibilities of this devices for generating hydrogen. The vertical injector pipe penetrated midway into the catalyst bed. The temperature was measured by thermocouples at the mid position.

The novel feature of the reactor is the hot spot caused by point injection of the air-hydrocarbon mixture. This arrangement eliminates the need for pre-heating the reactant mixture during operation, although for the reactor start-up on natural gas the fuel should be warmed up to around 500°C. Alternatively, the reactor can be activated at ambient temperature by introducing an initiating fuel such as methanol or a hydrogen-rich gas, which is oxidized by air at ambient temperature over the catalysts. This oxidation serves to raise the bed to the temperature needed for the natural gas to react (typically over 450 °C).

Several other developers have built CPOx reactors for both mobile and stationary fuel cells applications. Shell has developed their CPOx technology for reforming gasoline within the DaimlerChrysler/Ballard company Excellsis as well as in collaboration with UTC Fuel Cells for stationary applications. CPOx of methanol proceeds with much lower heats of reaction compared with hydrocarbons and a very simple design of the CPOx reactor can be used. An interesting example for a similar application is that developed by Kumar et al. [68] at Argonne National Laboratory. In this method, the methanol is simply mixed with water in liquid form and fed to an igniter, where a controlled flow of air is added. Here a part of the inlet methanol is burnt, producing the heat required to vaporize the water and methanol. The unburnt methanol and the steam generated are then supplied to the reactor, where the catalyst is supported on a honeycomb monolith material (similarly to the automobile exhaust catalysts). More recently, Schmidt [69] has described the catalytic partial oxidation of gasoline on rhodium coated monoliths at 600 °C.

The use of noble metals catalysts in CPOx reactors was studied for the first time by Ashcroft et al. in 1990 [70], followed later by Dong et al [71] and Zhu and Flytzani-Stephanopoulos [72]. These authors investigated the integration of these catalysts with alternative supports such as MgO, ZrO₂, CeO₂. The current studies are focused on the application of silicon carbide SiC supports associated with base metal catalysts (e.g. nickel).

2.4.3 - CPOx reactors - Catalysts

The production of synthesis gas by oxidation reactions can generally be performed in short contact time reactors [60, 61], thereby reducing the reactor volume. Short contact time regimes can be reached by using structured catalytic system where the active materials are deposited over ceramic supports or metallic substrates. As described in section 2.4.4, the supports adopted for the structured catalysts include monoliths with honeycomb structure, ceramic foams and metallic mesh.

Among the different solutions available on the market for the structured catalysts suitable for a CPOx process, it is possible to identify two main groups [59]:

- 1- **Noble Metal Catalysts, or Platinum group metal catalysts (PGM):** catalysts based on noble metals, which can be either self-supporting (mesh, gauzes, knit) or supported by ceramic materials (alumina, silicon, mixed oxides)
- 2- **Base metal catalysts:** typically nickel oxide, but also iron and copper supported by alumina or other ceramic supports.

With reference to the first group, several products are proposed, including those for complete combustion reaction. Their performances are stable and, depending on the material, ensure good methane conversion. Their main drawback is the cost, especially when mixed with platinum elements (e.g. in the complete combustion process for automobiles catalytic converters). On the contrary, the products belonging to the second group are mainly based on nickel over alumina support. This configuration is commonly used for steam reforming reactions. The base metal catalysts are less expensive than noble metals, but have lower activity and are easily deactivated by carbon formation, sulfur poisoning and oxidation [11].

Other types of catalysts, not commonly used for CPOx and generally for SOFC fuel reforming reactions, are the sponge metals (skeletal or Raney nickel). These catalysts are fine-grained metals composed mostly of nickel derived from a nickel-aluminum alloy, typically nickel oxide supported by alumina or other ceramic supports. The Ni-Al alloy is prepared by dissolving nickel in molten aluminum followed by cooling

("quenching") [59].

Table 2.3 lists the main technical features and properties of the catalysts mainly adopted for the CPOx process in fuel cell systems.

Table 2.3 – catalysts for CPOx reactions- properties and technical features

CATALYSTS	Description
Nichel	<p>Commercial catalysts nickel based composed of NiO (average content 15%), deposited over ceramic materials supports α-Al₂O₃, MgO, Zr₂O₃. Additional chemical species entering the final composition:</p> <ul style="list-style-type: none"> - calcium aluminium (10-13% in weight) improves the mechanical resistance of catalysts spheres; - potassium oxide (up to 7% in weight) prevents the coke formation; - Silicium (up to 16% in weight) reacts with potassium oxide to form stable silicates. <p>Advantages: stability, remarkable catalytic activity and low costs. Reactivity: Ni/Al₂O₃ selectivity to CO of 95% and production of H₂ and CO corresponding to the thermodynamic equilibrium values at the reactor outlet temperature (700-900°C).</p>
Ruthenium	<p>The most economic and stable catalyst among those belonging to the transition metals. Supports:</p> <ul style="list-style-type: none"> - If supported by Al₂O₃, at low concentrations (0,015% in weight) is more active and selective than Ni; - If supported by SiO₂ is able to oxidize the methane at low temperatures (400°C); <p>Reactivity: ruthenium based catalysts over rare earth elements based supports have gained methane conversion and selectivity toward CO and H₂ of 56%, 99% and 100% respectively, at pressures of 1 atm.</p>
Rhodium	<p>Platinum based catalysts with rodhium percentage of 2-5%, in the form of mesh, are used in the nytrogen and nitrate production process. Reactivity: rhodium based catalysts guarantee that the product gas compositions are very close to those predicted by the thermodynamic equilibrium. High methane conversion values (more than 90%) and hydrogen selectivity can be achieved.</p>
Platinum-Rodhium	<p>Both Pt/Al₂O₃ and Rh/Al₂O₃ contain an high percentage of noble metals, in the range 0,25-2,0%. Rh and Ni tested at different contact time (0,1-0,5 s) show an higher activity and selectivity toward hydrogen respect to Pt. Reactivity: catalysts Pt-Rh at 10% of Rh led to high oxygen conversion and selectivity toward Co and H₂, even at short time contact and low lambda.</p>

Currently, noble metals, nickel and to a less extent cobalt are mainly used for the CPOx process in fuel cell systems. A worldwide research aimed to identify the best effective catalyst for the reforming process has been encouraged by the recent results achieved in the performance of some metals (Ru, Pd and Rh and Pt-Rh alloys) and lanthanum oxides [20, 21, 27, 52-58].

However, not all these catalysts are stable on long-term activity and the choice of a particular metal is often a balance between several critical parameters. These parameters include [36]:

- the catalytic activity;
- the long-term stability;
- the selectivity towards synthesis gas production;
- a lower tendency towards unwanted side-reactions (especially carbon formation);
- the sensitivity towards sulphur poisoning;
- the cost of the active element.

Nickel catalysts (Figure 2.22) show the highest activity and are attractive due to their low cost. However, they are particularly sensitive to sulphur poisoning and to the thermal sintering.



Figure 2.22: Catalyst powder Ni/Al₂O₃

For CPOx processes, noble metal catalysts are generally recognized as superior in terms of stability compared to nickel catalysts, although there are remarkable differences between the individual noble metals. Palladium is prone to rapid carbon formation at low O/C ratios, as well as the platinum

[40]. A stable catalytic performance with low light-off temperatures ($< 400^{\circ}\text{C}$) can be obtained with rhodium. Indeed, several tests have proved the rhodium to be the best noble metal because of its high selectivity to H_2 , low volatility and resistance to coke formation [36, 37, 64, 65]. On the other hand, the high price makes its usage prohibitive for large-scale facilities. Palladium, ruthenium and iridium catalysts are considerably less active than rhodium but exhibit sufficient activity for many practical applications.

Many critical parameters for the choice of the active phase metal also depend on the choice of the support. The specific metal-support interactions can affect the reducibility of a metal oxide or stabilize the particle dispersion of the metal. The optimal support shall maintain the dispersion of the active phase and ensure thermal stability in severe working conditions. It was proved that $\text{Rh}/\alpha\text{-Al}_2\text{O}_3$ is the catalytic system most suitable and efficient for the partial oxidation of methane to synthesis gas [24, 52, 54, 59]. Widely investigated and used support phases are also ZrO_2 , TiO_2 , CeO_2 and Al_2O_3 .

2.4.4 - CPOx reactors - Supports

Although the main function of the catalyst support is to extend the surface area of the metal, the selection of the best type of support for a particular catalytic metal is fundamental for the CPOx reforming process. Indeed, the support can also substantially alter the rate and course of the reaction. The type of physical support is determined by the nature of the reaction system, since the reaction conditions may limit the choice of support. The support must be stable at the temperature used and shall not react with the solvent, feedstock or reaction products.

Many researchers have evaluated the effect of several supports on the catalytic activity by simply comparing the behavior of nickel catalyst when deposited on different supports: Al_2O_3 , $\text{SiO}_2\text{-Al}_2\text{O}_3$, $\text{SiO}_2\text{-ZrO}_2$ and zeolite [42, 55, 56, 57, 71, 72]. In these studies, the authors observed that the acid supports reduce the catalyst activity, due to the difficulties of nickel to redox in acid environment, with subsequent lack of metallic nickel for the partial oxidation reaction.

There are mainly three different structural layouts for the supports:

- Monolith
- Ceramic foams
- Metallic mesh

Table 2.4 lists the main technical features and properties of the supports mainly used for the CPOx process in fuel cell systems.

Table 2.4 – supports for CPOx reactions- properties and technical features

SUPPORTS	Description
Monolith	Rigid structure in ceramic material where the metallic catalyst is deposited over α -Al ₂ O ₃ through washcoating. The support is characterized by a honeycomb structure, with parallel channels size in order of mm, whose fluid dynamic region is laminar. They differentiate for the materials (conductivity, thermal expansion, ecc..) and for the channel density, measured in cpsi (cells per square inch).
Sponges	Ceramic sponges are derived by various material, such as: Al ₂ O ₃ , SiAlO _x , MgO/SiAlO _x , ZrAlO _x , SiC. The Zr ₂ O ₃ based sponges show an high porosity respect to those that constitute other oxides, this leading to higher selectivity to H ₂ .
Metallic mesh	These structures are characterized by an elevate mass to surface ratio and by a considerably short time contact. The drawback is their huge cost. The Pt meshing shows an high selectivity to CO but, on the other hand, do not permit obtaining an high oxygen conversion and show low selectivity to H ₂ .

The honeycomb monoliths (fig. 2.23) result in much shorter start up time because of their better heat transfer proprieties and lower heat capacity. In addition, at low flowrates honeycombs perform better than packed beds in terms of conversion, selectivity and pressure drops [36]. The effort to minimize the pressure drop over the catalytic system led to the development of corrugates monolithic reactor based on FecrAlloy (Figure 2.23), an alloy containing aluminum (0.5-12%), chromium (20%), yttrium (1-3%), iron and kanthal (an alloy containing aluminum,

chromium, cobalt and iron). Additionally, honeycomb monoliths offer several advantages for experimental investigations and their quantitative analysis, such as the ability to monitor the axial temperature profiles along the channel by means of multiple thermocouple and the reliability of correlation for heat and mass transfer coefficient even at very low Reynolds number. Most of these aspects make honeycombs preferable to foams for the kinetic investigation.

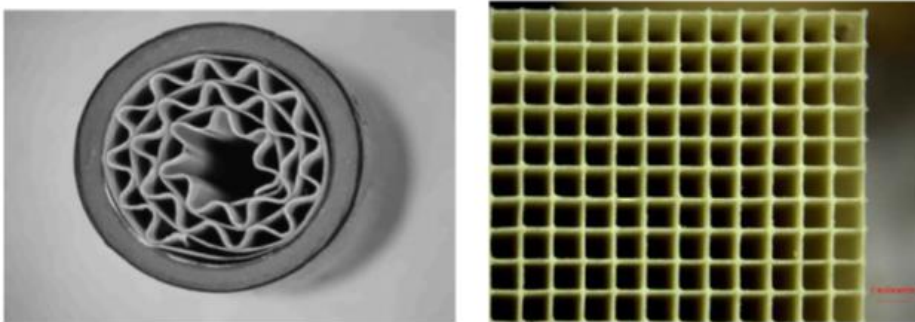


Figure 2.23: Corrugate monolith (left) and cordierite honeycomb monolith 600 CPSI (right)

The ceramic support can also be in foams type: figure 2.24 shows some images of the alumina and silicon carbide foams.

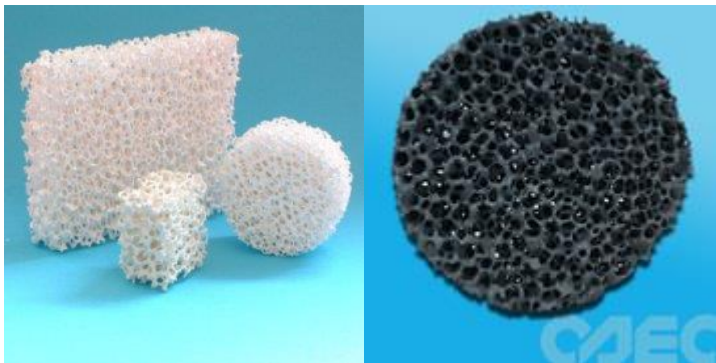


Figure 2.24: Ceramic foam of alumina (left) and carbide silicon (right)

2.5 - Alternative reactor layouts for fuel cell systems

The need to produce hydrogen in de-centralized plants has led many researchers to focus their attention on alternative reactor layouts, applicable to both stream reforming and catalytic partial oxidation, with the target to reduce the overall reactor size and maximize the thermal efficiency of the process. The basic principle of these alternative reactors is to integrate the heat exchange mechanisms and/or separation of H₂ from the other products inside the same reactor [9, 11].

In the following paragraphs the state of the art of non-conventional reactors is described, highlighting their main advantages and drawbacks that obstacle their application.

2.5.1 - Compact regenerative reformers with concentric annular catalyst beds

Figure 2.25 shows an example of a reformer designed by Haldor Topsoe for PAFC systems in which the heat for the reforming reaction is provided by combustion of the lean anode exhaust gas supplemented if necessary by fresh fuel gas [11].

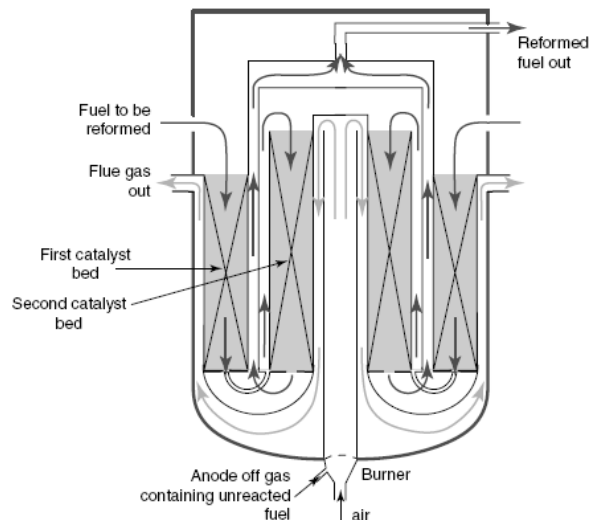


Figure 2.25: Haldor Topsoe heat exchange reformer

In this system, reformer fuel is combusted at a pressure of 4.5 bar in a central burner located in the bottom of a pressure vessel. Feed gas is supplied downwards through the first catalyst bed where it is heated up to around 675 °C by convection from the combustion products and the reformed product gas, both flowing countercurrent to the feed. After leaving the first bed of catalyst, the partially reformed gas is transferred through a set of tubes to the top of the second reforming section. The gas flows down through the catalyst, being heated typically to 830 °C by convection from the co-currently flowing combustion products and also by radiation from the combustion tube. The combination of co-current and countercurrent heat transfer minimizes metal temperatures. The advantages of such a reformer for fuel cell applications are small size and suitability for small-scale use, improved load following and lower cost. Several companies have been developing reformers of this type including Haldor–Topsoe, International Fuel Cells (recently renamed UTC Fuel Cells), Ballard Generation Systems, Sanyo Electric, Osaka Gas, and ChevronTexaco.

2.5.2 - Plate reformers and micro-channel reformers

In the plate reformer, a stack of alternate combustion and reforming chambers are separated by plates [11]. The chambers are filled with suitable catalysts to promote the combustion and reforming reactions, respectively. Alternatively, either side of each plate can be coated with combustion catalyst and reforming catalyst. The heat from the combustion reaction is used to drive the reforming reaction. Plate reformers have the advantage that they can be very compact and furthermore they allow reducing the heat transfer resistance to a minimum. The use of a combustion catalyst means that low heating value gases (e.g. anode exhaust gases) can be burnt without the need for a supplementary fuel.

Plate reformers were first developed by IHI in the 1980s; the catalyst was in the form of spherical pellets located on either side of the heat exchanger surface [75]. More recently, researchers at Gastec designed a plate reformer in which the plates were coated with a ceramic-supported catalyst. This technology has been later acquired by the US fuel cell

company Plug Power. Osaka Gas also built a plate reformer [76], and several other companies hold patents on the technology. The most advanced types of plate reformers use compact heat exchanger hardware in which the catalyst is coated directly onto the exchanger surfaces [77]. The concept is shown in Figure 2.26.

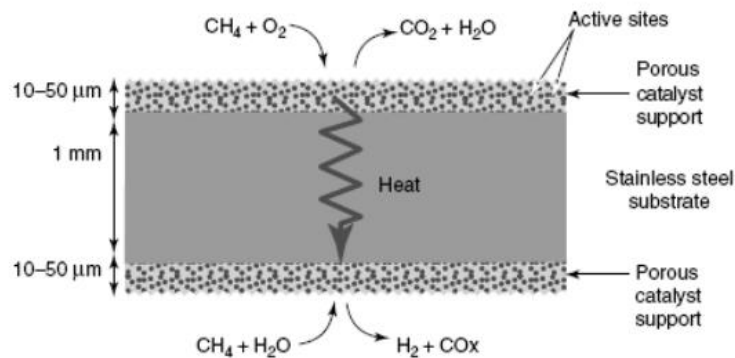


Figure 2.26: Plate reformer concept

Such devices are being developed in the United States by Pacific Northwest National Laboratory, for a 1 kW steam reformer, and by Argonne National Laboratory, for a monolithic catalyst-based reformer for diesel. Several organizations have developed plate reformers for methanol, for example Idatech, Mitsubishi Electric, Innovatek Inc., NTT telecommunications laboratory, and Honeywell [78]. Micro-channel reactor technology could be applied to other parts of a fuel processor such as fuel vaporizers and gas clean-up reactors. However, they suffer from two disadvantages: first, the plugging of the channels due to catalyst degradation and carbon laydown; second, the fact that the catalyst is incorporated into the reactor for life, thereby it is not possible to replace when it becomes degraded.

2.5.3 - Membrane reactor

Hydrogen is able to permeate selectively through palladium or palladium alloy membranes. This has led to the demonstration in the laboratory of

membrane reformers (fig. 2.27), where hydrogen is selectively removed from the reformer as it is produced. This hydrogen removal increases the methane conversion for a given operating temperature above what predicted thermodynamically, and the hydrogen produced is very pure, making it very suitable for PEM fuel cell systems. Some big companies (Exxon, BP, Air Products, and Praxair) are developing membrane reformers for large-scale hydrogen production. It is likely that some of these can be scaled down to meet the needs of fuel cell systems [40].

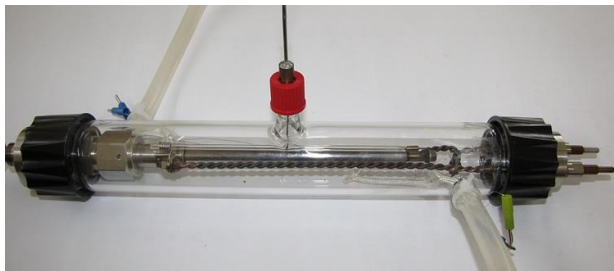


Figure 2.27: Membrane module [ENEA]

Several developers are also known to be working on membrane reformers for fuel cell systems, examples being Praxair, Tokyo Gas, Wellman Defence, Aspen, and Idatech Inc. The systems being developed by IdaTech Inc. are perhaps the most advanced of the small-scale membrane reformer systems for fuel cell applications [83]. The characteristic of the Idatech fuel processor is that it combines an imperfect (but lower cost) membrane filter with a chemical purification system to generate relatively low-cost but high-quality hydrogen. The fuel processor combines the functions of a steam reformer, hydrogen purification, and heat generation into a single device producing 99.8% pure hydrogen with <3 ppm carbon monoxide and <25 ppm carbon dioxide.

2.5.4 - Non-catalytic partial oxidation reactors

Non-catalytic partial oxidation is applied industrially by Texaco and Shell for the conversion of heavy oils to synthesis gas. As explained in section 2.2, in a partial oxidation process, without the catalyst, the reactor operating

temperatures approach 1150-1200 °C. Hence, the reactor has to be made of expensive materials to withstand the high temperatures, and the product gas needs to be cooled to enable unreacted carbon material to be separated from the gas stream. The high temperatures also mean that expensive materials of construction are required for the heat exchangers. In addition, the effluent from non-catalytic partial oxidation reactors invariably contains contaminants (including sulphur compounds), as well as carbon and ash. Due to its complexity and dangerous operating conditions, simple partial oxidation has not been a preferred option for fuel cell applications.

One interesting application of non-catalytic reactors has been the so-called plasma reformer or ‘plasmatron’ [11]. This type of reactor has the advantages of potentially being compact, operating at moderate temperatures with fast start-up capability and good response to load changes. The ‘plasmatron’ is a particular type of small plasma reformer developed by Massachusetts Institute of Technology (MIT) and licensed to ArvinMeritor. It was designed for converting conventional liquid fuels into a hydrogen-rich gas for enhancing the performance of internal combustion engines. Plasma reformers are also being developed by Wangtec, the Idaho National Energy and Environment Laboratory, and by Syngen Inc. All these devices have yet to be scaled up and demonstrated in real fuel cell systems; however, the Syngen process does look promising for the generation of synthesis gas, which has commercial implications for both gas-to-liquids processing and for fuel cell systems.

2.6 - Catalyst deactivation

The knowledge of the chemical and physical aspects of catalyst deactivation is of great importance for the design of deactivation-resistant catalysts, the operation of industrial chemical reactors and the study of specific reactivating procedures. Catalyst deactivation is a phenomenon that occurs when the catalytic activities decrease proportionally to the reduction of the catalyst active surface [36]. Deactivation can occur by a number of different mechanisms, both chemical and physical in nature. These are commonly divided into four classes, namely [11, 60, 82]:

1. **Poisoning;**
2. **Carbon (coke) Formation or Fouling;**
3. **Sintering;**
4. **Phase transformation and physical loss of metal.**

2.6.1 - Poisoning

Poisoning is the loss of activity due to the strong chemisorption on the active sites of impurities present in the feed stream and caused by the irreversible adsorption of species on the catalyst surface [28,59]. Such species include: heavy metals such as lead, copper and zinc; sulfur containing species such as hydrogen sulfide and mercaptans; arsenic; amines and carbon monoxide. In general, it is not possible to remove the poisons by a washing or oxidation procedure (an exception is carbon monoxide).

A poison may act simply by blocking an active site (geometric effect), or may alter the adsorptivity of other species essentially by an electronic effect [40]. Poisons can also modify the chemical nature of the active sites or result in the formation of new compounds (reconstruction) so that the catalyst performance is definitively altered. Usually, a distinction is made between *poisons* and *inhibitors* [60]. *Poisons* are usually substances whose interaction with the active sites is very strong and irreversible, whereas *inhibitors* generally weakly and reversibly adsorb on the catalyst surface. Poisons can be also classified as *reversible* or *irreversible*. In the first case, the poison is not strongly enough adsorbed and accordingly regeneration of the catalyst usually occurs simply by poison removal from the feed. This is the case, for example, of oxygen containing compounds (e.g. H₂O and CO_x) for the ammonia synthesis catalysts. These species hinder nitrogen adsorption, thus limiting the catalyst activity, but elimination of these compounds from the feed and reduction with hydrogen removes the adsorbed oxygen to leave the iron surface as it was before. However, gross oxidation with oxygen leads to bulk changes which are not readily reversed: in this case the poisoning is irreversible, and irreversible damages are produced. In fact, the **oxidation mechanism** likely to occur in a CPO_x reaction (see section 3.3.2) when the lambda is out of the specification range (also a deviation of 10% in the set

point of anode fuel and air can lead to irreversible faults) belongs to the poisoning classification [60]. This phenomenon is easily occurring in Nickel catalysts, whereas the noble metals better contrast it. The oxidation risk is certain at low temperatures (below 500 °C) and is higher than the carbon deposition.

As consequence of the poisoning, the overall catalyst activity may be decreased even without affecting the selectivity. However, most often the selectivity is affected, since some of the active sites are deactivated while others are practically unaffected. This is the case of "multifunctional" catalysts, which have active sites of different nature that promote, simultaneously, different chemical transformations. In some cases, due to the very strong interaction existing between poisons and the active sites, poisons are effectively accumulated onto the catalytic surface and the number of active sites may be rapidly reduced [82].

The main poisoning mechanism likely to occur in SOFC systems with reforming reactor is the **sulfur poisoning**, already mentioned in section 1.6. Its effect on catalyst surface is the same of other deactivation mechanisms, i.e. clogging the catalytic sites and reducing the catalyst activity. As the sulfur poisoning is a simple exothermic reaction, it is more evident at low temperatures: if at 800°C the poisoning of nickel takes place with 5ppm of sulfur, at 500°C only 0.01 ppm are enough to achieve the same goal. A sulfur poisoned catalyst can be regenerated with hydrogen treatment or with oxidation of the catalyst, followed by its reduction.

2.6.2 - Carbon Formation or Fouling

Fouling occurs when the catalyst surface is masked by polymeric materials or tars, and is often referred to as "coking" on fixed-bed particulate catalysts. For catalytic reactions involving hydrocarbons (or even carbon oxides) side reactions occur on the catalyst surface leading to the formation of carbonaceous residues (usually referred to as coke or carbon) which tend to physically cover the active surface [59]. Natural gas, for example, will decompose when heated in the absence of air or steam at temperatures above about 650 °C via pyrolysis reactions of the type:



Another source of carbon formation is from the disproportionation of carbon monoxide via the so-called Boudouard reaction:



Reaction 2.25 is catalyzed by metals such as nickel, reason why catalysts that contain nickel are more vulnerable to this deactivation mechanism.

Coke deposits may amount to variable percentages of the catalyst, and accordingly they may deactivate the catalyst either by covering of the active sites or by pore blocking. Sometimes a distinction is made between *coke* and *carbon*. The difference is however arbitrary: usually carbon is considered the product of CO disproportionation (eq. 2.24), whereas coke is referred as the material originated by decomposition (cracking) or condensation of hydrocarbons.

The coke formation is therefore the result of the deposition of a solid carbon layer, whose thickness depends on the time and chemical species, over the catalytic bed, leading to its deactivation [82]. Carbon deposition may occur in several areas of the system where hot fuel gas is present; therefore, for a fuel cell system, this phenomenon may take place both in the fuel reformer and at cell level [11]. Coke formation evolves in three different ways, depending on the temperature [36]. At lower temperatures (below 500 °C), adsorbed hydrocarbons over the catalyst surface can gather and slowly converting into a polymerized layer of “rubber” not active, that immediately obstructs the catalyst sites. At higher temperatures, the main carbon based product to build up on the catalyst area is the whisker carbon (carbon atoms dissolve into metal elements). At temperatures over 600 °C, the deposit of olefin can be seen, with consecutive encapsulation of catalytic pallets that lead to deactivation [80].

The catalyst support material can also increase the risk of carbon deposition. Indeed, for nickel based reactors, small quantities of alkaline metals are applied to the supports in order to inhibit their acidity, which eventually would promote the cracking of methane and the related carbon formation.

The carbon formation must be prevented for two reasons. Firstly, as already explained, coke deposition on the active sites of the catalyst leads to deactivation. Secondly, carbon deposits can cause total blockage of the reformer tubes or active surface, resulting in the development of ‘hot spots’

[27, 79]. A particular type of carbon formation occurs on metals, known as carburization, leading to spalling of metal in a phenomenon known as ‘metal dusting’.

For steam and autothermal reforming, there is a simple expedient to reduce the risk of carbon formation from reactions 2.23 and 2.24, and that is adding steam to the fuel feed stream [11]. The minimum amount of steam that needs to be added to a hydrocarbon fuel gas to avoid carbon deposition may be calculated, but in practice, a steam/carbon ratio in the range 2-3 is normally employed in steam reforming systems to have a certain margin of safety. The principal effect of increasing the steam is to promote the shift reaction, which has the effect of reducing the partial pressure of carbon monoxide in the fuel gas stream. Since the addition of steam leads to a proportional cost increase, it is preferable to use the lowest steam/methane ratio compatible with the necessity of controlling the formation of carbonaceous residue.

Another procedure to reduce the risk of carbon formation in a fuel cell system is to carry out some **pre-reforming** of the fuel gas before it is fed to the reformer reactor [82]. Pre-reforming is a term commonly used in industry to describe the conversion of high molecular weight hydrocarbons via the steam reforming reaction at relatively low temperatures (typically 250-500 °C). This process step (also known as ‘**sweetening**’ of the gas) is carried out before the main reforming reactions. The advantage of carrying out pre-reforming is that high molecular weight hydrocarbons, which are more reactive than methane, are converted into hydrogen preferentially. The pre-reformer products therefore comprise mainly methane with steam, together with small amounts of hydrogen and carbon oxides, depending on the temperature of the pre-reformer reactor.

Fixed-bed (except carbon supported) catalysts can be reactivated by the controlled combustion of the coke using an inert gas stream and/or steam with a low concentration of air [36]. Powder catalysts can sometimes be reactivated by washing with suitable solvents, treating with oxidizing agents to breakdown the polymeric materials to smaller, more soluble species, and reducing to metal.

2.6.3 - Sintering

Sintering usually refers to the loss of active surface via structural modification of the catalyst. It occurs when crystallite growth of the catalytic metal decreases the metal surface area, causing a loss of activation properties [59, 80]. This is generally a thermally activated process and is physical in nature, taking place for temperatures above $0.5 T_m$, where T_m is the melting temperature of the metal. Thermal sintering can sometimes cause the collapse of the support pore structure [36].

Sintering occurs in both supported and unsupported metal catalysts. In the former case, reduction of the active surface area is caused by the agglomeration and coalescence of small metal crystallites into larger ones with lower surface-to-volume ratios. Small particles are more likely to undergo this reduction in the active phase due to their tendency to be disposed in an ordered pattern, closer to the ideal one. On the other hand, without the presence of the support and a consequent adequate adhesion, the extensive agglomeration of the catalyst occurs in a few seconds.

Two different mechanisms have been proposed for sintering of supported metal catalysts [60]: the atomic migration and the crystallite migration models. In the first case, sintering occurs via escape of metal atoms from a crystallite, transport of these atoms across the surface of the support (or in the gas phase), and subsequent capture of the migrating atoms on collision with another metal crystallite. Since larger crystallites are more stable (the metal-metal bond energies are often greater than the metal-support interaction), small crystallites diminish in size and the larger ones increase. The second model considers sintering to occur via migration of the crystallites along the surface of the support, followed by collision and coalescence of two crystallites. In both cases, the sintering slows down with the time. Catalyst deactivation by sintering is usually irreversible [40].

2.6.4 - *Solid state transformation and physical loss of metal*

Solid-state transformation is a process of deactivation that can be viewed as an extreme form of sintering occurring at high temperatures and leading

to the transformation of one crystalline phase into a different one. These processes may involve both metal-supported catalysts and metal oxide catalysts. In the first case, the incorporation of the metal into the support may be observed. In the case of metal oxide catalysts or supports the transformation of one crystalline phase into a different one can occur [28].

Catalyst deactivation by physical loss of metal can arise in several ways. Metal may dissolve in the reaction medium and be stripped from the support. The support material may be attacked and start to dissolve in some liquid-phase reactions and the insoluble catalyst fines pass through the filter system. Excessive movement of fixed bed catalysts due to pressure fluctuations can cause loss of catalyst fines by abrasion. Certain catalysts may also suffer from loss of active phase. This may occur via processes like volatilization, erosion and attrition [82].

The above forms of catalyst deactivation can be overcome by a more suitable choice of catalyst and/or reaction conditions.

Chapter 3

Experimental Setup

3.1 - EFESO project

The experimental data used for the validation of the reforming model were obtained within the activities carried out for **EFESO** (*Environmental Friendly Energy from Solid Oxide Fuel Cell*) project, financed by the Italian Ministry of Economic Development, led by Ariston Thermo Spa and involving several other industrial and academic partners active in the fuel cell system research and development. **Ariston Thermo** is an international leader in thermic comfort for domestic, commercial and industrial applications, whose range of products includes heating and water heating products (gas and electrical boilers), systems (thermal solar and heat pumps), services and solutions designed to provide the maximum degree of comfort with the minimum use of energy. The R&D division is focused on the design and testing of thermal systems at high energy efficiency which can represent, in the long term scenario, a valid alternative to the common residential boilers. The idea of a combined heat and power generator came out from this contest.

Among the other partners involved in the EFESO project, the key players which have offered an appreciable contribution for this thesis were: **SOFC Power**: Italian solid oxide fuel cell manufacturer, which produce planar FC stacks, FC modules (Hot Box) and high efficiency μ CHP generators. Currently SOFC Power is part of a joint venture which involves also HTC and Solid Cell.

Acumentrics: American tubular fuel cell manufacturer, already introduced in section 2.2.4.

Hsytech: engineering and special process equipment construction company working on chemical processing, traditional and renewable energy, power generation and environment treatment. They are specialized

in manufacturing of reforming systems for fuel cell applications.

Environment Park: public joint-stock company that operates under a system of free competition. Their activities are aimed to offer market solutions for energy saving, waste disposal, clean energy, new materials and fundraising.

The main target of EFESO project was to realize four (4) prototypes of solid oxide fuel cell based μ CHP (μ Combined Heat and Power), to be tested and characterized for in-house application to the aim of evaluating their potentiality and feasibility to enter definitely the market in the mid-term scenario.

The four units realized differ in output power, dimensions and technology, as for the following specifications:

1. unit rated 1 kW electrical outlet power, with planar cell technology and reforming CPOx integrated in the HB (Hot Box and stack by SOFC Power)
2. unit rated 1 kW electrical outlet power, with tubular cell technology and internal CPOx reforming, occurring inside the fuel cell (Hot Box and stack Acumentrics)
3. unit rated 2.5 kW electrical outlet power, with planar cell technology and steam reforming external to the HB (Hot Box and stack by SOFC Power)
4. unit rated 2.5 kW electrical outlet power, with tubular cell technology and internal CPOx reforming (Hot Box and stack by Acumentrics)

Each μ CHP, whose generic P&ID are shown in paragraph 1.3.2, consists of a hybrid electrical-thermal unit which integrates:

- a **fuel cell stack**, supplied by the two fuel cell manufacturers SOFC Power and Acumentrics, planar and tubular configuration respectively. In table 3.1 a comparison between planar and tubular technology is shown, highlighting advantages and drawbacks of both layouts. Figure 3.1 reports some images of both tubular (to the

left) and planar (to the right) cells/stack.

Table 3.1 - Comparison between planar and tubular fuel cell technology

	Tubular	Planar
Start-up Time	< 1h	5-10 h
Shutdown	Time <1h, no need of anode fuel	Time >4h, anode side must be fed until stack temperatures get down 400°C
Thermal Cycles	tolerant to high thermal gradients	Extremely sensible to thermal gradients because of the sealings thermic expansion
Reforming	Internal	External
Current Density	about 250 mA/cm ² (long tubes)	about 500 mA/cm ²
DC Efficiency	42% max	Up to 60% with SR
Thermal losses	Approximately 400W (for 1kW unit)	Approximately 250W (for 1kW unit)
Stack Geometry	Robust, heavy, big size	Compact and light, but complex. HB has almost same size as tubular one
BoP	Simpler, thanks to the low stack pressure losses and more tolerant to the air flow deviations. 10% accuracy on anode flowmeters, apparently small accuracy on cathode air flow	More complex and demanding, it is possible use the same air path for startup and cathode air. Stack has high pressure losses. Accuracy on anode air/fuel flowmeters is 5%, 10% for cathode.



Figure 3.1 - Planar and tubular solid oxide fuel cells and stacks [37, 38]

- a **BoP (Balance of Plant)**, supplied by Loccioni (measurement and control automatic systems manufacturer), that in turn includes air/fuel valves, air/fuel feeding systems, desulphurizers (supplied by Proeng), flow sensors and temperature/pressure measurement.
- a **reforming device**, in particular a CPOx reactor supplied by Hysytech/SOFC Power for the 1 kW planar unit, and steam reforming system by Hysytech/SOFC power for the planar 2.5 kW unit. The Acumentrics tubular systems presents an interesting reforming mechanism, developed and patented by Acumentrics itself, described in section 2.2.4.
- **water and combustion group unit**, same type of those commonly used for domestic gas boilers, supplied by Ariston, that also was the system integrator and thereby responsible for the fabrication and final tests.
- **inverter** for connecting the system to the grid, by ST Microelectronics
- **μ CHP control system**, developed by Loccioni and implemented in Labview environment. The software was used in open loop during the tests, which means the user could set and vary the parameters according to the operating conditions fixed phase by phase in the design reviews.

3.2 - Tests setup

As explained above, in EFESO project both planar and tubular stack have been tested. Although three prototypes of 1 kW μ CHP with tubular layout have awarded the batch approval by Gastec (an international certification agency) enabling their field test activities for residential applications, the experimental data considered for this thesis have all been referred to the planar design. The main reason for this choice was addressed to the layout of the planar system, including a CPOx reactor external to the stack and

located inside the Hot Box. On the contrary, in the tubular Fuel cell Module the reforming mechanism described in section 2.2.4 entails one catalytic fuel injector for each cell. The standard reactor configuration adopted for the planar modules is more appropriate to be used for the validation of the CPOx model described in chapter 4.

In fact, the model has been validated through experimental data gained in three different test cases:

- a) Internal tests on CPOx reactor integrated in the Hot Box
- b) Lab tests on CPOx reactor external to the Hot Box, heated up by electrical resistances
- c) Tests on final 1 kW planar μ CHP unit

Tests a and b were performed respectively at Hysytec/SOFC Power facilities and at Hysylab laboratories (Environment Park). The experimental data measured during test case a are available in the work packages issued by Hysytec and SOFC Power within EFESO project [36, 37, 103], whereas a detailed report of test case b is offered by Environment Park deliverable [102]. During tests performed at Hysylab facilities (tests b) the reactor was separated by the Hot Box, thereby losing information about the thermal integration; however, these tests allowed the measurement of concentrations of the products for different operating conditions.

The tests performed at Ariston Thermo facilities on the μ CHP final units (tests c) were the most complete in terms of set of measured data. Indeed, in addition to the local information directly related to the CPOx reactor, i.e. reactor outlet temperature and lambda, other relevant parameters for the entire SOFC system such as inlet fuel, stack current and cathode air were measured.

3.2.1 - Tests case a: Internal tests on CPOx reactor integrated in Hot Box

The first set of data useful for characterizing the model were offered by SOFC Power and Hysytech, within the activities of EFESO project [36, 37]. The test results were shared among all the partners to attest the positive results achieved in terms of engineering and manufacturing of the integrated CPOx reactor. SOFC Power has setup a test bench in their laboratories finalized to evaluate in detail the temperature distribution inside the reactor and to measure the product gas composition via spectral analysis. The input fuel was natural gas from the grid and the CPOx reactor was integrated in a 1000W Hot Box, shown in figure 3.2. The Hot Box in this case was used as a dummy stack, that means the stack was not generating power during the tests, since the target here was to characterize the reactor properties and its thermal integration inside the enclosure, without focusing on the fuel cell electrical performance. The integration inside the Fuel Cell Module was exploited to reach the reactor operating temperatures required for its activation through the contribution of the startup burner. In addition, the pre-heating properties, namely the heat exchanges occurring inside the hot module and responsible for the warm up of the reactant gas path before entering the reactor, were evaluated. These aspects are better described in the section 3.2.3, where the analysis of the entire μ CHP unit is given.

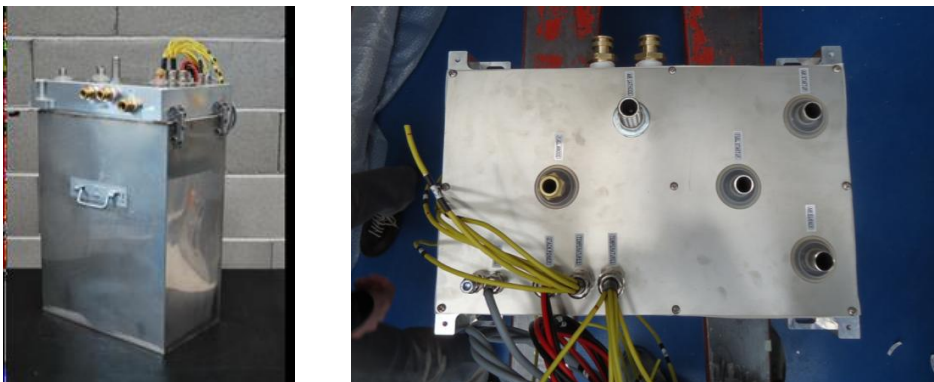


Figure 3.2 – 1000 W Hot Box tested at SOFC Power facilities [37]

The following plots show the experimental measurements carried out during different tests on the CPOx reactor. Figure 3.3 reports the outlet composition (molar fraction) over the adiabatic equilibrium temperature inside the reactor for a lambda of 0.27. The outlet concentrations are measured over the entire operating range of the reaction in order to characterize the trend of each species with the equilibrium temperature. The H₂ concentration is represented through the magenta line; its trend is increasing with the equilibrium temperature, until the maximum hydrogen yield of approximately 0.38 is reached for a reactor temperature around 750 °C. For higher temperatures, the H₂ gain does not rise, as well as the CO molar fraction (green line), which stabilizes slightly below 0.20. The red dotted line represents the nitrogen N₂, which is not consumed by the CPOx reaction, therefore its reduction is due to the balance of the species involved in the reaction. The methane (blue line) is progressively consumed as long as the temperature inside the reactor is increased. Same behavior is offered by the CO₂ (black line) and H₂O (red line), whose output molar fractions tend to zero when the reactor operating temperature exceeds 700 °C. The oxygen O₂ is totally consumed in each condition.

Figure 3.4 depicts the relation between the reactant pre-heating temperature and the temperature of the products at the reactor outlet for the same lambda of 0.27. It might be observed that it is not desirable to work with inlet reactant temperatures higher than 500 °C. Indeed, besides the critical aspects related with the design of the system, above this value the reactor temperature exceeds 800 °C, moving out of the stack operating ranges.

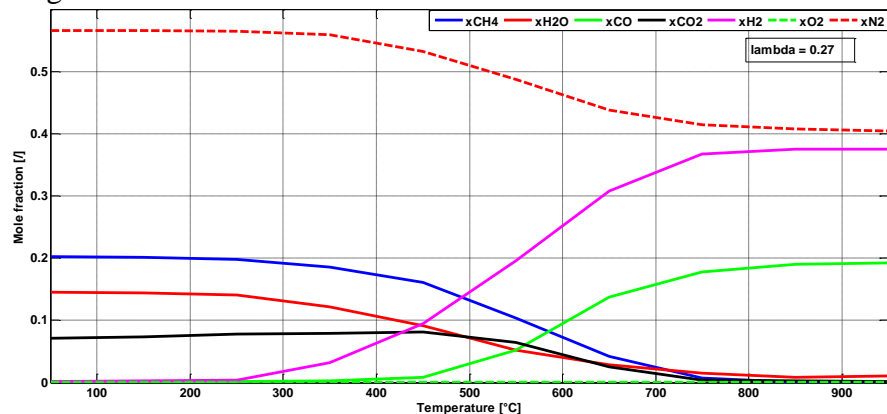


Figure 3.3 – Reactor outlet molar fractions vs CPOx reaction equilibrium temperature for lambda 0.27

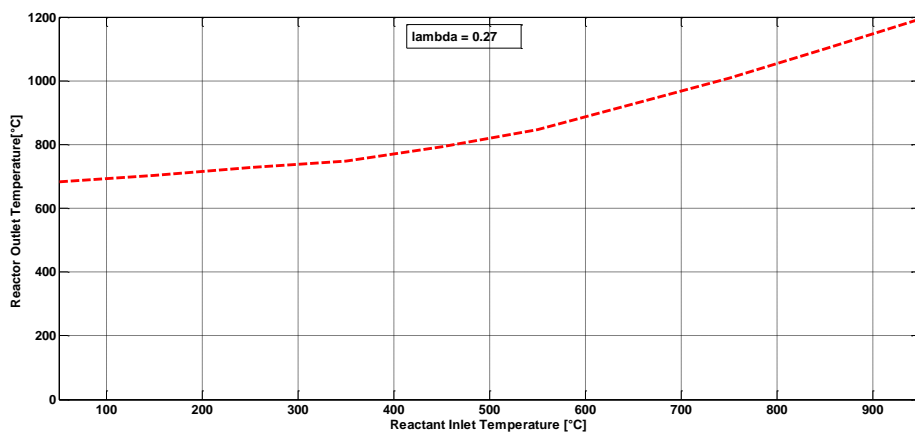


Figure 3.4 – Reactor outlet temperature vs Reactant inlet temperature for lambda 0.27

Figures 3.5 and 3.6 report the same results for a different lambda, 0.30. In this case, both H_2 and CO concentrations approach values slightly lower than the previous condition with lambda of 0.27. On the other hand, the methane conversion is higher, as well as the reactor temperature.

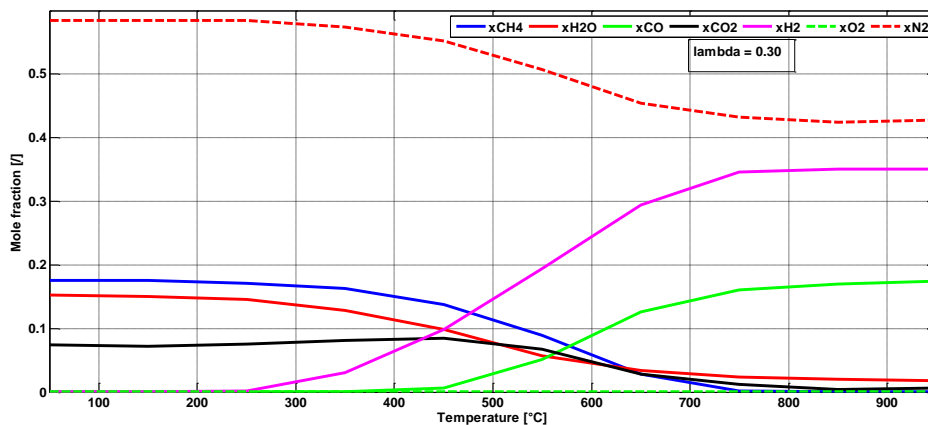


Figure 3.5 - Reactor outlet molar fractions vs CPOx reaction equilibrium temperature for lambda 0.30

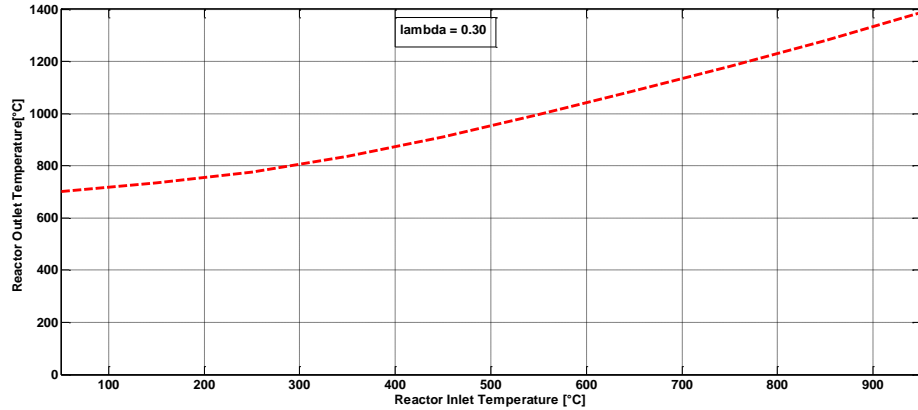


Figure 3.6 – Reactor outlet temperature vs Reactant inlet temperature for lambda 0.30

However, in the two cases (lambda 0.27 and 0.30) the general trends for compositions and temperatures are very similar. A higher lambda allows reaching the optimal equilibrium temperatures and conversions also with reduced reactant pre-heating (below 400°C), while the lower lambda is, the more the reaction moves closer to the theoretical partial oxidation limit, with benefits for the hydrogen conversion.

Similar tests were carried out by Hysytech [36]. Differently from the tests performed by SOFC Power, in this case the reactor was not installed inside the Hot Box, but characterized on a proper test bench. The tests were aimed to identify the reference data for the reactor before its installment inside the Fuel Cell Module. Table 3.2 reports the equilibrium composition and adiabatic reaction temperature for different lambda and with same pre-heating mixture temperature.

Table 3.2 – Product molar fraction and adiabatic reactor temperature for different lambda

	Tin = 230°C						
lambda	CH4	CO	CO2	H2O	N2	H2	Tout
0.25	4,4%	15,65%	2%	2,36%	42%	34,42%	673,5
0.27	2,80%	16,16%	2%	2,52%	42,65%	33,87%	688,71
0.3	1%	16,39%	2%	2,85%	43,78%	33,97%	721,77

The data reported in the table 3.2 are aligned with the results of the previous tests shown in figures 3.3 and 3.5. The outlet reactor temperature

depends on the pre-heating contribution for the reactant species. In this case, for a lambda of 0.25 the low pre-heating effect determines a lower methane conversion (residual CH₄ is 4%). Tests with lambda of 0.27 were carried out at different reactant inlet temperatures. For this condition, the plot in figure 3.7 represents the thermodynamic analysis of the reactor temperature over the products outlet composition. At 750 °C the methane conversion amounts to 93%.

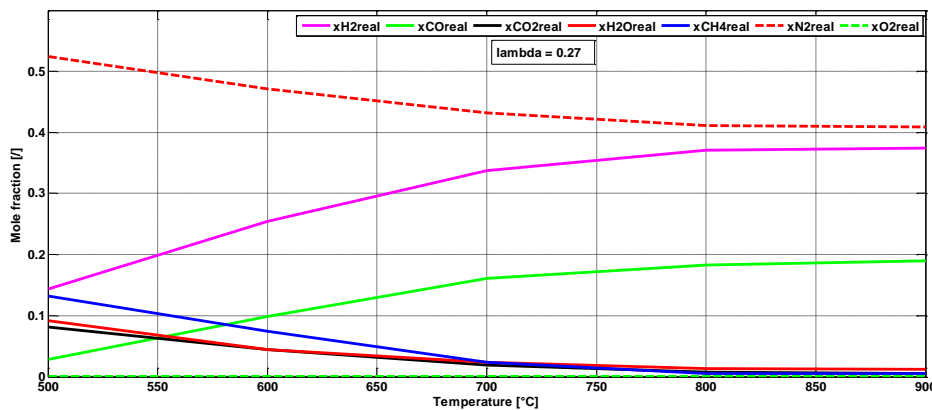


Figure 3.7 - Reactor outlet molar fractions vs CPOx reaction equilibrium temperature for lambda 0.27

3.2.2 - Tests case b: Lab tests on CPOx reforming reactor prototype

For the EFESO project, EnviPark was appointed to investigate about the state of art of reforming technologies for SOFC systems and to bench testing the CPOx reactor to be adopted for 1kW SOFC system [102]. With relation to this activity, a proper test arrangement has been prepared at Hysylab facilities; figure 3.8 and 3.9 show respectively the test bench scheme and setup. The test stand included, beyond the reactor itself, a series of sensors and actuators disposed to measure pressure, temperatures and air/methane flowrate, a gas chromatographs to analyze the outlet composition, a condenser for depriving the outlet products of their water content, being the gas analyzer based on dry measurements, and an hardware/software interface for parameters control.

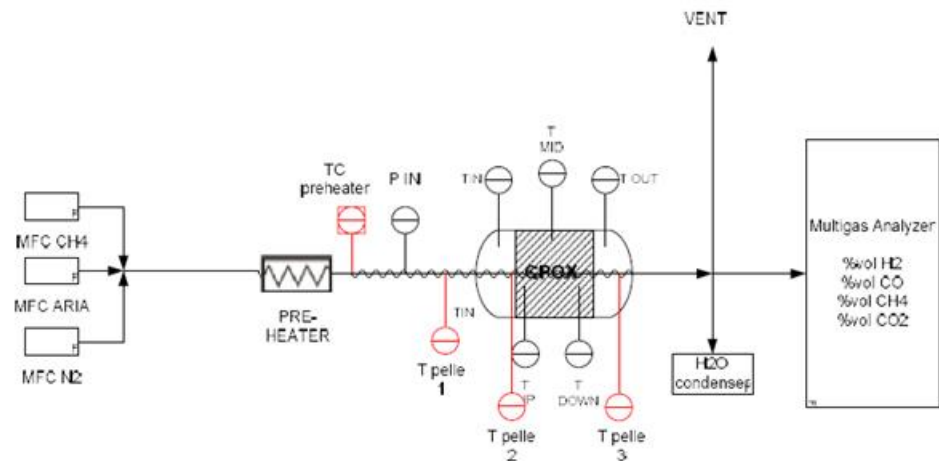


Figure 3.8 – CPOx reactor test bench scheme (Hysylab) [102]



Figure 3.9 – CPOx reactor test bench setup (Hysylab) [102]

In order to approach the appropriate operating temperature for the

CPO_x reaction, the mixture entering the reactor and the reactor itself were heated up by means of three electrical resistances. The first one, with pre-heating function, was disposed upstream the reactor to warm up the reactant mixture. The other resistances were wrapped to the reactor metal housing to permit the activation of the catalyst and enable the reforming reaction. The reactor was duly insulated for approaching adiabatic conditions. Five thermocouples were installed inside the reactor, laid down the monolith channels, in order to measure the temperature in different positions (inlet/outlet of the reactor, up/middle/down of the catalyst). In addition, several thermocouples were used along the feeding path with monitoring purpose and for controlling the set point of the electrical resistances. The concentrations of the products species were measured through the gas analyzer shown in figure 3.10.

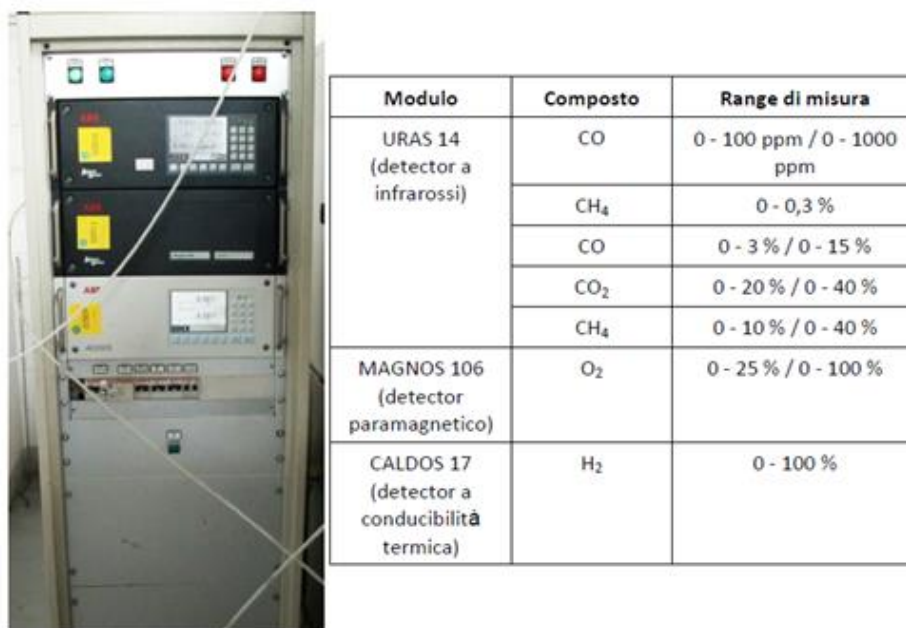


Figure 3.10 – Gas chromatograph (Hysylab) [102]

The tests were carried out by varying the input and control parameters as following:

- Air/methane ratio (λ), in the range 0.29-0.4

- Input fuel (and hence gas hourly space velocity), between 0.8 and 3 kW.
- Pre-heating temperature, between 300 and 450 °C
- Reactor external temperature, at 450 °C and 700 °C.

The high purity of the methane used for the tests made unnecessary the usage of desulphurizers upstream the reactor. Figure 3.11 shows the main results extracted by the test session and taken into account for the model validation (see par. 5.4.2).

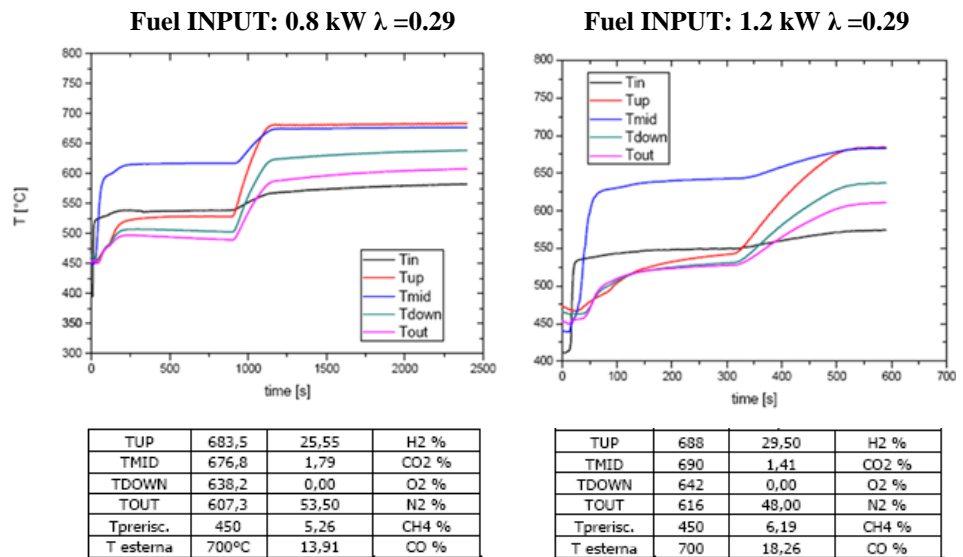


Figure 3.11 – Reactor temperatures and molar output fractions for two different operating conditions

For a same lambda (0.29), the effects of different inlet fuel flowrate, namely 0.8 and 1.2 kW, were evaluated. The plots show the trend of the temperatures measured in different locations of the reactor over the time. The reactor temperatures are directly increasing with the inlet fuel. The temperature of products exiting the reactor is always lower than the temperature at reactor middle position, symptom of the fact that the products suffer a cooling downstream the reactor. In both cases, it might be observed a boost in the temperatures occurring when the mixture is lighted up and the reaction is enabled. For higher fuel flowrate, corresponding in turn to higher gas hourly space velocity, the mixture lights up earlier. For

the same lambda (0.29), the hydrogen conversion improves with increasing input fuel, due to the higher reaction temperatures.

Many tests were carried out at very high lambda, i.e. 0.4 and 0.5; these values are not usually adopted for the SOFC based systems, exception made for the first phases of reaction, when the system shall be warmed up and stabilized. It was already pointed out that an excessive lambda (higher than 0.35) could lead to extremely high temperatures during the steady state conditions, causing problems from both a mechanical and thermal point of view. This is the reason why the results of these tests do not reproduce properly the conditions assumed for the CPOx model developed and described in chapter 4. Furthermore, the reactor used for these tests had different design with respect to what is considered for the model. A more detailed explanation about the impossibility to evaluate all the set of results for the model validation is given in paragraph 5.4.2.

3.2.3 - Tests case c: Tests on final 1 kW planar μ CHP unit

The interest of Ariston Thermo for the cogeneration systems take its roots in a deep and long analysis carried out by the R&D department with the aim to offer an high efficiency and low cost alternative to the standard gas boilers. Since many years Ariston was trying to investigate the μ CHP market, to evaluate its potentialities, feasibility, benefits and drawbacks, starting with Stirling based μ CHP and then switching to tubular fuel cell based units. The goal was to develop a system able to generate electrical power to be consumed in-house or to be fed to the grid, and simultaneously to guarantee the thermal output proper of a conventional gas boiler. The continuous research in this area and the need to stress the electrical output from the fuel cell system, in order to remark the benefit respect to a traditional thermal system and therefore to justify the big initial investment, has led to move toward the planar fuel cell layout, potentially able to offer higher electrical efficiencies.

The last set of experimental data useful for evaluating the effectiveness of the CPOx model described in chapter 4 were made available through the tests performed at Ariston Thermo facilities on the 1 kW μ CHP and stand-alone Hot Box/BoP group [103].

Table 3.3 reports the specifications and operating conditions of the planar S-design stack developed by SOFC Power for EFESO project and included in the Hot Box installed in the 1 kW μ CHP unit. Figure 3.12 illustrates some photos of the stack drawn from SOFC Power website. It is characterized by low pressure drops and can achieve power densities of 400 mW/cm² with electrical efficiencies over 45%. The stacks can be fuelled with reformed natural gas, reformat gas or hydrogen.

Table 3.3 – Planar fuel cell stack specifications and operating conditions

S-design Stack Specs and Operating conditions			
Nominal Stack Power	1000 W	Nominal operating voltage per cell	0.75 V
Max Stack Power	1250 W	Minimum operating voltage per cell	0.6 V
Operating current range	0-40 A	Stack voltage range	35-80 V
Cell footprint	152 mm x 70 mm	Ideal stack operating temperature	800 °C
Active area per cell	80 cm ²	Max. stack operating temperature	850 °C
Stack Depth	290 mm	Operating pressure	Atmospheric
Stack Length	400 mm	Fuel	Hydrogen or reformat
Stack Height	600 mm	Stack air inlet temperature	700-800 °C
Cell numbers	60	Stack fuel inlet temperature	700-800 °C
Auxiliaries power	120 W	Nominal stack pressure drop	< 15 mbar
Min. DC electrical efficiency	34%	Thermal cycles /year	20-30



Figure 3.12 – Planar fuel cell stack (manufacturer SOFC Power) [37]

Figure 3.13 shows some images of the 1 kW μ CHP prototype

assembled by Ariston Thermo.



Figure 3.13 – 1 kW μ CHP realized by Ariston Thermo [103]

According to the configuration described in section 3.2.1, the CPOx reactor has been integrated in the Hot Box module, in a position properly engineered to promote the heat exchange toward the stack and heat

exchangers and to optimize the pre-heating of the air/gas mixture in the path going from the HB inlet to the CPOx reactor. A proper thermal integration of the CPOx reactor inside the HB is essential both to reach high electrical and thermal efficiency and to guarantee the correct operation of the reforming system. This prevents the products mixture to approach temperatures which might be dangerous for the catalyst health and for the fuel cell anode element, especially during transient conditions. After defining the pre-heating temperature operating range, SOFC power has designed the best positioning of the reactor inside the Hot Box, carefully evaluating the sealing aspects, the minimization of mechanical stress related to the thermal gradients between Hot Box basement and stack, and the reactor insulating respect to both Hot Box base and cathodic recuperator.

Figure 3.14 reports the scheme and flowchart of the Hot Box installed inside the μ CHP unit, together with the indication of temperature measurement points. The exhaust flue are conveyed to a heat exchanger to recover their thermal residual energy and realize the cogeneration effect.

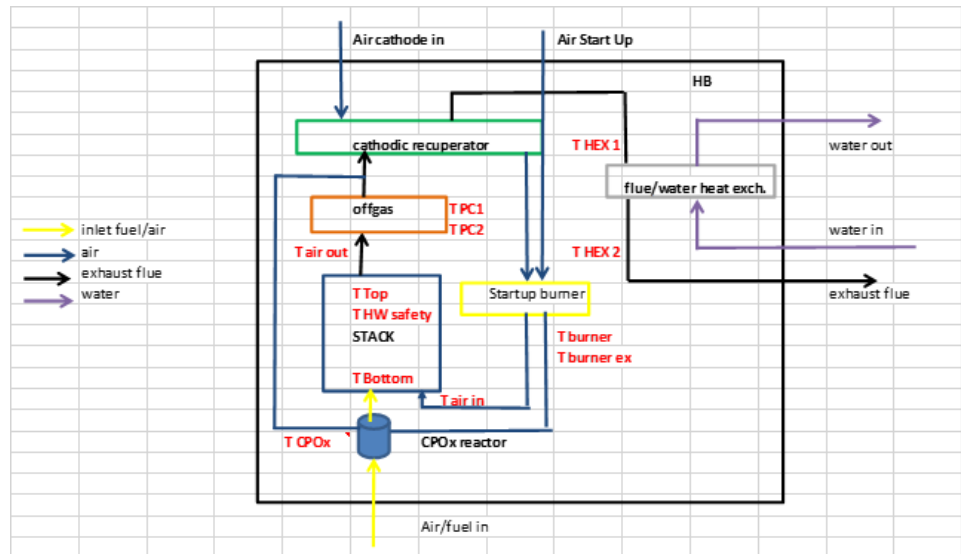


Figure 3.14 –Hot Box Module installed in 1 kW μ CHP: scheme and flowchart

The reactor is heated up through the startup burner during the μ CHP startup phase, together with stack and offgas burner. The startup time falls

between 6-8 hours, according to the thermal gradient set for the warm up, which usually is in the range of 100-120 °C per hour. This slow warm up is necessary to obtain a uniform and stable stack heating and to avoid the risk of thermal shock. The catalyst turns active starting from 400 °C; however, the inlet CPOx air and fuel valves only open when the reactor temperature, measured through a contact thermocouple located inside the reactor, exceeds 550°C. In the startup phase, the air is forced to flow through the ignition burner area before conveying to the reactor housing and stack. Later on, it enters the cathodic recuperator, where the heat exchange allows the warm up of fresh air before the startup flow is directed to the exhaust.

The transition from startup phase to CPOx phase (closing startup fuel valve and opening anode air/fuel valves) occurs when the following set points are achieved:

- 1) The reactor catalyst temperature T_{CPOx} exceeds 550 °C
- 2) The off gas burner temperature, measured on the post-burner surface and index of the combustion quality of unreacted species, shall be higher than 620-650 °C for ensuring a proper combustion in compliance with CO/CO₂ international emission standards.

The average reformate outlet temperature is around 700°C.

Table 3.4 includes the sequence of the design operating phases and related parameters set for the power up of the 1 kW μ CHP unit. As it might be observed by looking at the related column, the lambda set point, for each condition, was determined by SOFC power based on preliminary design studies and experimental in-house testing. The lower limit was fixed to 0.27, as the carbon deposition risk was evaluated too high below this value. Immediately after enabling the inlet fuel valve, the lambda is kept considerably high, around 0.45, in order to speed up the internal heating of catalyst reactor and reach autothermal conditions quickly. When the reactor temperature rises over 600 °C, the lambda can be decreased to 0.31. During the fuel cell operation, when current is drawn from the stack, lambda is decreased down to 0.29 or 0.27/0.28, depending on the desired output (electrical and thermal) conditions.

Table 3.4 – 1 kW μ CHP startup phases and operating conditions

Phase	Set Point Fuel Anode		λ	Set Point Air Anode	Remarks
	Nlpm	KW			
LATE START UP	0,500	0,300	0,455	2,167	fuel/air mixture to CPO _x enabled when T _{CPO_x} exceeds 550°C and Toffgas burner > 650°C
	0,500	0,300	0,410	1,952	
	0,500	0,300	0,360	1,714	
	0,500	0,300	0,330	1,571	
	0,500	0,300	0,310	1,476	
OPERATION	1,000	0,600	0,310	2,952	Run phase (the stack generates electrical current) starting when the average stack temperatures are above 700°C. The more the power generated by the fuel cells is, the more input fuel is required, and the lambda is adjusted accordingly together with other relevant parameters (e.g. cathode air inlet).
	1,500	0,900	0,290	4,143	
	2,000	1,200	0,290	5,524	
	2,500	1,500	0,290	6,905	
	3,000	1,800	0,290	8,286	
	3,500	2,100	0,290	9,667	

Figures 3.15-3.17 report the plots of the main SOFC system parameters versus the time over the entire operating range: startup, early ramp up (or late startup), operation and standby phases. The operating conditions for the run phases were varied according to the values shown in table 3.4. Figure 3.15 shows the temperature trends, measured through the thermocouples positioned as indicated in the Hot Box scheme in figure 3.14. The first plot reports the stack temperatures (top and bottom of the stack, respectively blue and green line) and the temperature measured over the catalyst surface inside the reactor (T CPO_x, red line). The second plot included in Fig. 3.15 represents the offgas burner temperatures (T PC 1, in magenta, and T PC 2, in green) and inlet and outlet air temperatures (T air in, cyan line, and T air out, black line). Figure 3.16 depicts the trends of anode air and fuel flowrates (PV anode air, in blue, and PV anode fuel, in

red), together with the startup burner fuel flowrate (PV startup fuel, green line). The lambda trend is reported in the bottom plot of figure 3.16. In the graph legend, PV stands for Present Value, which indicates the instantaneous parameter value measured through the sensors, whereas SP means Set Point, that is the design operating condition for the same variable. As described in section 3.3, a deviation between PV and SP values out of the range of tolerance indicates a faulty condition. Figure 3.17 includes the plots of cathode air flowrate (PV cathode air, green line), input fuel power (Fuel consumption, red line), stack voltage (in blue) and stack current (in black).

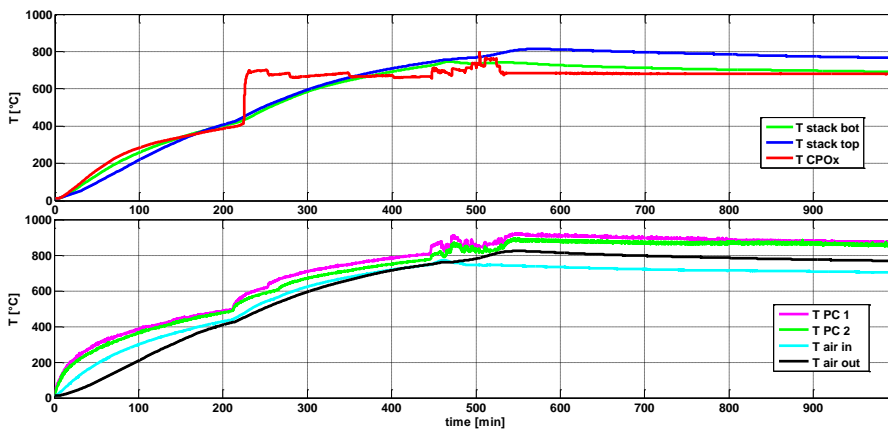


Figure 3.15: μ CHP performance: stack, CPO_x reactor, post combustor and air temperatures vs time

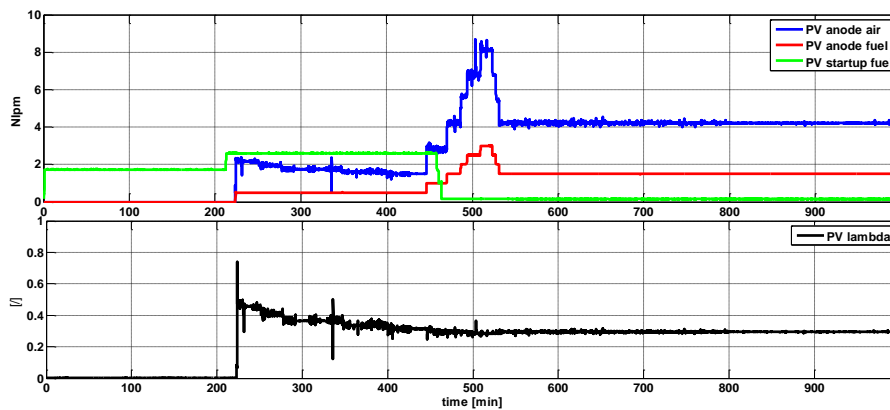


Figure 3.16: μ CHP performance: anode air and fuel flowrates, startup burner flowrate and lambda vs time

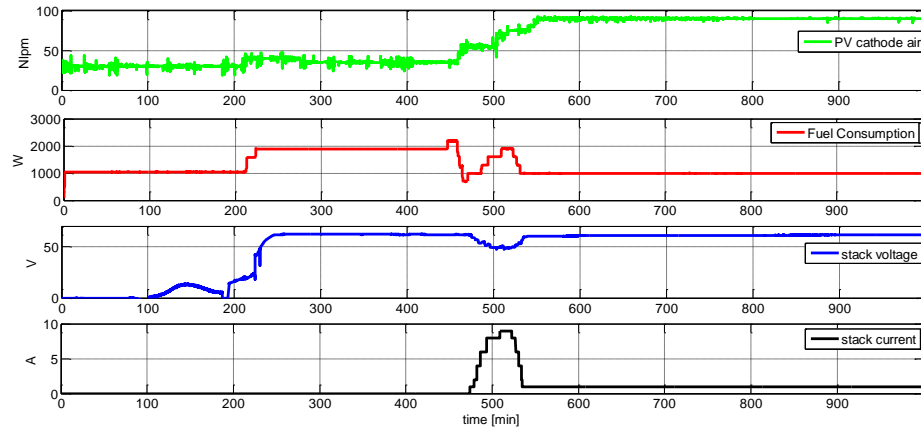


Figure 3.17: μ CHP performance: cathode air flowrate, fuel consumption, stack voltage and current vs time

By analyzing the figure 3.15, it can be observed that during the startup phase the temperatures rise homogeneously, thanks to the heating contribution brought by the startup burner. As soon as the operating temperatures for offgas burner and CPOx reactor mentioned above are reached, the anode line is enabled. This occurs around minute 220, when the opening of the anode fuel and air valves determine the rise in the CPOx temperature, symptom that the CPOx reactor is activated and the reaction enabled. As shown in figure 3.16, in the ramp up phase the lambda value is kept quite higher (in the range 0.45- 0.35) in order to promote the total oxidation reaction responsible for the initial warm up of the CPOx reactor. The lambda is then decreased to the nominal operating value (0.28-0.29) when moving to the run phase. At the same time the anode fuel is activated, the stack starts to generate voltage in open load conditions (Open Circuit Voltage, OCV) (Fig. 3.17). The OCV for the 60 fuel cells stack realized by SOFC Power is fixed to approximately 60 V. As mentioned in the table 3.4, the operation phase, that is when the stack is able to produce electrical power, starts when the average of stack top and bottom temperatures exceeds 700°C. At this point (around minute 460) it is possible to switch off the startup burner, since the system is warm enough to be able to rely on the combination of stack, CPOx and offgas burner reactions for achieving its thermal auto-sustaining. Once concluded the startup phase, in the operation phase the current can be drawn by the stack. As shown in

figure 3.17, progressively with the increase of anode air and fuel flows, the stack current is raised step by step from 1 to 10 A, and the stack voltage decreases accordingly. It is important to note the behavior of stack top and bottom temperatures immediately after the stack begins to produce electrical power. Indeed, with respect to their initial trend, which has seen both top and bottom stack temperatures growing up similarly, they start to diverge and progressively distance each other as long as the electrical performance of the stack are enhanced.

The CPOx temperature mostly oscillates around 700 °C when the current is quite low (early rump up and standby phase), and raises up with increasing current. The power ramp down is done in the same way, only in reverse, until the standby phase is reached (stack only generating small amount of power to auto-thermally sustain itself, i.e. 1 A current).

3.3 - Fault events in a CPOx reforming system

As described in section 2.6, several critical events may occur both in CPOx reactors and in integrated SOFC systems (Hot Box). They could irretrievably damage the catalyst and may also affect the cell performance over time. These events, which are commonly indicated as faults, might be generated after a blackout, a variation in fuel inlet pressure, a fuel or cooling air shutdown, valves or sensors drifting. Each of these faults may lead to either small or catastrophic effects for the related components, such as catalyst deactivation or stack failure.

A detailed description of the faults most likely to occur in a SOFC system, analyzed by means of fault tree analysis and fault diagnosis schemes, was given by the University of Salerno, Department of Industrial Engineering (Eprolab) [6,85,86]. It is briefly reported afterward, with focus on the reforming system, main topic of this thesis.

Fuel reforming catalysts operate at temperatures in the order of 700-800 °C, but in some abnormal conditions may exceed 1000 °C. These high temperatures lead to a variety of degradation mechanisms over time and represent a significant challenge in meeting the durability requirements. Additionally, the fuels can contain variable levels of sulphur, which can lead to the problems described in previous paragraphs. Degradation can be

caused by carbon and particulate build up (fouling), sulfur attack on the reforming catalysts, corrosion/erosion of heat exchange surfaces and thermal induced migration of materials leading to deactivation. The degradation leads to changes in the composition and temperature of the fuel reactants entering into the anode, which in turn results in a variation in fuel cell performance.

FMEA (failure mode and effect analysis)

In Tables 3.5 an FMEA (failure mode and effect analysis) for a SOFC reformer system is reported, listing some possible reformer degradation and failure modes. The FMEA is a formalized method to consider all components, their functions, failure modes and causal system failures. FMEA starts with listing for all the components their operating and failure modes, then considers possible causes for each faulty mode and describes their effects for the unit under consideration and for the complete system. This analysis can be very useful to relate each fault with its causes and effects on the other components and on the overall system. In addition it also accounts for the fault tree construction, because listing the causes that lead to a fault or failure mode it is possible to create a fault tree level, whereas the effects may correspond to the basic events. The strength of FMEA is its completeness, but is often a very time-consuming procedure [6]. Similar analysis for the specific issue of the SOFC reforming system are not easily available in literature. Indeed, apart from the SOFC systems manufacturers, which are required to perform FMEA and hazard analysis to take into account the problems which can be experienced by the end users, only a few researchers in the fuel cell field are focusing their studies on the failure modes and system diagnosis. Therefore, the contribution of the FMEA herein reported is appreciable and represents an important achievement for the present work.

Table 3.5 – Failure Mode and Effect Analysis (FMEA) for a CPOx reforming system



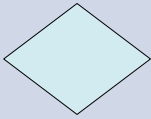
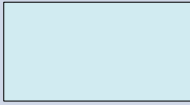
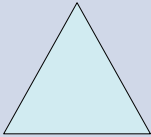


FAILURE-FAULT MODE	CAUSE	EFFECT
Insufficient fuel flow for the reforming reaction	<ul style="list-style-type: none"> - Low flow at the fuel compressor inlet, if present; - Flow control valve malfunction or failure; - Fuel leakage in pipe entering the reformer; - Insufficient methane inlet pressure; - Desulphurizers obstructed; - Mechanical connections issues (e.g. bolts not tightened properly, seal leakages, missing gaskets). 	<ul style="list-style-type: none"> - Changes in reformer outlet composition and temperature of products entering the anode; - Reduction in reactor performance and hydrogen gain, and in turn reduced stack efficiency; - Risk of catalyst oxidation; - Impossibility to reach the nominal stack operating temperatures;
Excessive fuel flow for the reforming reaction	<ul style="list-style-type: none"> - Fuel flow control valve malfunction; - Control system failure; - Sensors/transducers failure; - Air flow into reactor lower than expected. 	<ul style="list-style-type: none"> - Carbon deposition; - Improper fuel conversion and hydrogen gain; - Low reactor temperatures; - Risk of shifting the reforming reaction into the stack cells.
Excessive air flow for the reforming reaction	<ul style="list-style-type: none"> - Air flow control valve malfunction; - Control system failure; - Sensors/transducers failure; - Fuel flow into reactor lower than expected. 	<ul style="list-style-type: none"> - Catalyst oxidation; - Risk of combustion inside the reactor; - Extremely high reactor and stack temperatures; - Risk of combustion into the stack.
Excessive sulfur in fuel stream entering the reformer system	<ul style="list-style-type: none"> - Desulphurizer failure; - Lack of zinc oxide. 	<ul style="list-style-type: none"> - Reduction in the number of active sites for reaction; - Reduction in hydrogen gain and stack electrical performances; - Risk of stack cells poisoning.
Catalyst degradation	<ul style="list-style-type: none"> - Catalyst poisoning of sulphur; - Carbon deposition (fouling); - Catalyst oxidation; - Material migration; - High temperatures inside the reformer. 	<ul style="list-style-type: none"> - Reduction in the number of active sites for reaction; - Reduction in hydrogen gain and stack electrical performances; - Temperature hot spot inside the reactor; - Formation of undesired pollutants .
Excessive preheating of reactant inlet mixture	<ul style="list-style-type: none"> - Inadequate reactor thermal integration; - Malfunction of heat source (e.g. electrical resistance); - A pre-combustion of air/fuel mixture occurs in the feeding system prior entering the reforming. 	<ul style="list-style-type: none"> - High reaction products temperature at stack inlet; - Excessive reformer reaction temperature, with consequent mechanical and thermal stress for the materials involved; - Risk of fire.
Deposition of unburnt hydrocarbons on catalytic surfaces	<ul style="list-style-type: none"> - High carbon level in fuel entering the system; - Few oxygen available. 	<ul style="list-style-type: none"> - Reduction in the number of active sites for reaction; - Increase in pressure drop; - Obstruction in fuel feeding line.
Corrosion/erosion of heat exchange surfaces	<ul style="list-style-type: none"> - High temperatures and sulphur presence. 	<ul style="list-style-type: none"> - Loss in reformer performance.

FTA (Fault Tree Analysis)

The Fault Tree Analysis is a methodology that can support both system design and diagnosis strategies definition. Its target is therefore to generate a fault symptom table for the development of a diagnostic scheme aimed at performing fault isolation process for on-field operating SOFC systems. Starting with a top event, that could be a system/component failure, fault or malfunction, the goal of FTA is to determine, with a top-down approach, all the causes that may lead to it, and the relationships between them. The trees are structured in different levels, such as the top events can be caused by individual or combined lower level failures or events. When a single component fault has to be investigated, the tree levels can comprise both events that are proper of the component itself, i.e. its degradation modes or its materials failure, and events that are located in different parts of the system and are therefore due to other devices malfunctions. At the same time, the top event, which represents the upper tree level, might be an intermediate level for a larger tree that embraces the overall system. Thus, FTA is a methodology for determining the combinations of the component level failures that could result in the occurrence of specific failures at a system level, resulting as an important tool for the fault isolation process [85].

A fault tree mainly consists of some events combined to each other by some logic gates. There are several kinds of primary events (not further developed) in a fault tree: Top Event, Intermediate Events, Basic Events, Undeveloped Events, External Events [6]. AND and OR are the most frequently used gates in fault tree structure. However, other logic gates might also appear in some fault trees, such as XOR, NAND, etc. The legend of symbols used to realize a fault tree is reported in Table 3.6.

Table 3.6 – Fault tree symbols, nomenclature and description

Symbol	Primary Event	Description
	Basic event / Symptom	A basic initiating fault requiring no further development or the corresponding symptom
	Conditioning event	Specific conditions or restrictions that apply to any logic gate
	Undeveloped event	An event which is no further developed either because it is of insufficient consequence or because information is unavailable
Symbol	Intermediate Event	Description
	Intermediate event	A fault event that occurs because of one or more antecedent causes acting through logic gates
Symbol	Transfer	Description
	Transfer	Indicates that the tree is developed at the occurrence in other pages. It is used to avoid extensive duplication in a fault tree
Symbol	Gate	Description
	AND	Output fault occurs if all of the input faults occur
	OR	Output fault occurs if at least one of the input faults occurs

A CPO_x reforming reaction requires precise and strict quantities of both fuel and air; when these amounts are different from the design set points (beyond a tolerance of 5 %) it might be caused by faults in either fuel or air feeding circuit.

In figures 3.18 and 3.19 some examples of fault trees are shown [6,85], each relative to a different top event. When the faulty reformer operation is caused by the lack of fuel entering the reactor, the problem has to be found in the fuel feeding circuit (Figure 3.18). This latter can be caused by any of following faults: fuel leakage in the pipe upstream the reformer inlet point, a fault in the fuel compressor (if present) or a malfunction of the anode fuel control valve regulating the fuel flow entering the system (intermediate events represented by rectangular symbols in the second layer of Fig. 3.18). The undeveloped event symbol (i.e. diamond) stands for a boundary mechanism that does not properly concern the system (i.e. leakage in fuel feeding system upstream the SOFC system inlet).

The fault tree relative to a generic pre-reformer fault is reported in Figure 3.18. Assuming that air and fuel quantities are those required for a nominal and correct reforming reaction, a problem may arise in the component, i.e. catalyst degradation and erosion of heat exchange surfaces. Some symptoms here listed are difficult to be directly observed in a typical SOFC system, due to their complex nature (i.e. NiS, CuS and soot formation), though it is possible to observe their effects on the overall reaction (i.e. blocking of reaction active sites).

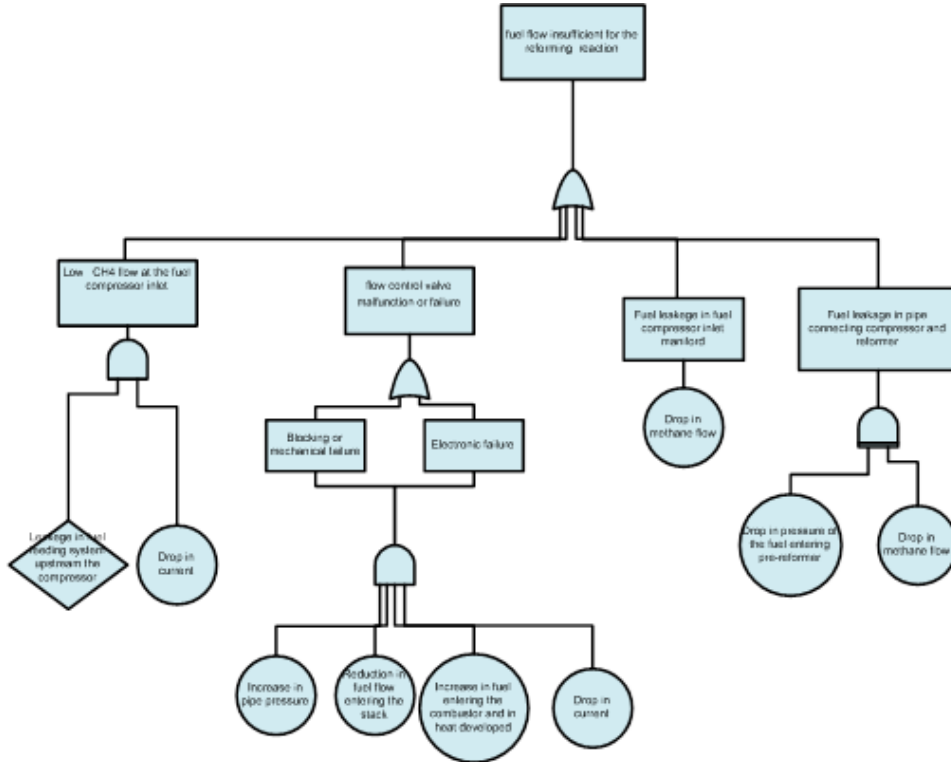


Figure 3.18- Fault Tree fuel feeding system

After the theoretical analysis oriented to offer a general description of the abnormal conditions which may arise when working with a reforming device installed in a SOFC system, some of the faults listed in table 3.5 were verified with the support of the experimental data made available by the tests on μ CHP carried out by Ariston Thermo within the EFESO project. During the test activities on the planar 1 kW μ CHP, two of these faults, namely carbon deposition and catalyst oxidation, occurred, and their effects on the system were evaluated. These faults have then been accounted for in the model described in Chapter 4, with the purpose to test the diagnosis algorithm and to demonstrate that the model can be used as a fault diagnosis tool. As described in chapter 5, by considering the fault events in the model, it is possible to verify whether the real effect of the faults on the reforming reactor parameters is properly reflected by the simulated conditions.

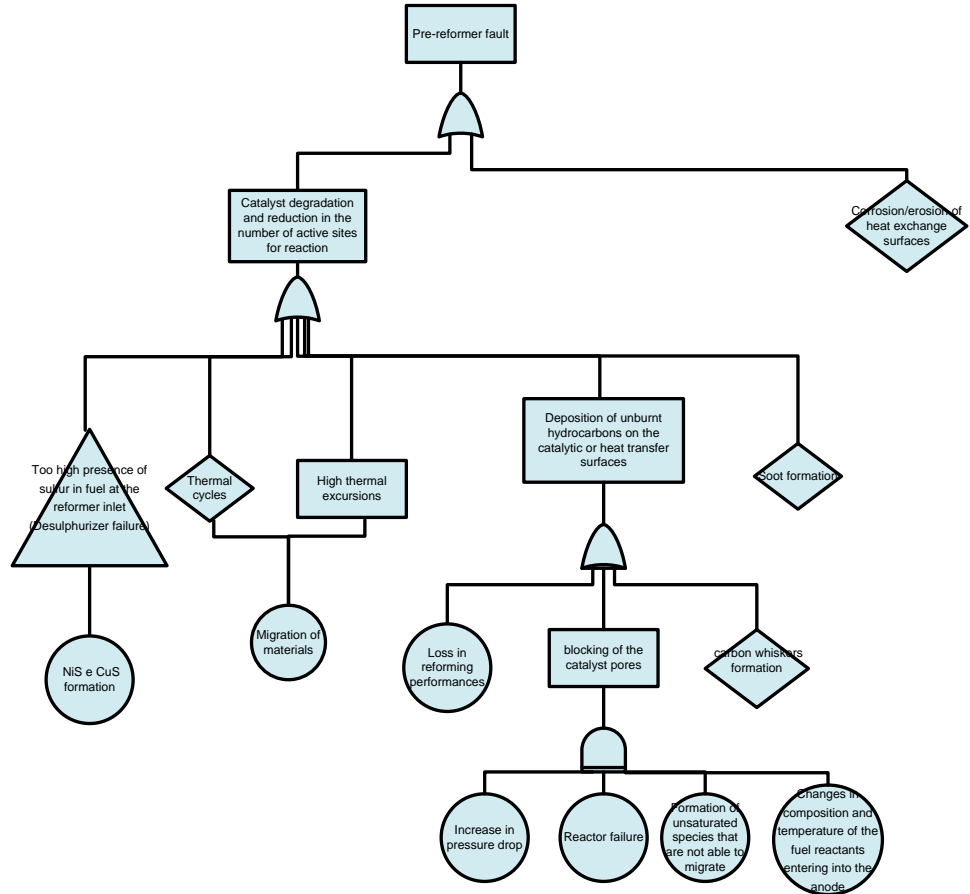


Figure 3.19- Fault Tree reformer system

3.3.1 - Fault 1: carbon deposition

An anode fuel valve drifting occurred during the startup of one μ CHP prototype during the test activities carried out at Ariston Thermo laboratories. In the late startup phase, as soon as the temperatures were sufficiently high to enable the anode air/gas path (with catalyst already active), the set point for lambda was fixed to 0.46 to promote the quick warm up, as reported in table 3.4. The control of the operating phases was

in open loop, this means the operator manually set the input conditions for each parameter and monitored their trend in case of alarms. When giving the signal for both air and fuel valves to open with the designed set point (0.5 Nlpm fuel and 2.2 Nlpm air flow, thereby lambda of 0.46), an offset of the fuel valve, probably due to an improper installation and calibration, caused the fuel flow to be much more than expected, i.e. 3.3 Nlpm. This drifting determined a large decrease in lambda, which dropped to 0.06, well below the minimum value allowed for preventing the carbon deposition, responsible for the deactivation of the catalyst.

Figure 3.20 shows the trends of the temperatures measured in different points inside the Hot Box. It is clear that the startup was not successfully, since the stack temperature never reached the 700°C required for enabling the stack electrical output. As soon as the anode line was opened, the excessive anode fuel flowrate led to a marked decrease in the CPOx temperature, visible around minute 263. In nominal conditions, the CPOx temperature would have exhibit a positive peak at the activation of the reactor. The fault detection appears clear when looking at the plots reported in figure 3.21. Here, the time on x-axis is restricted to the period interested by the fault event. In addition to the detail of the CPOx temperature also shown in figure 3.20, the anode fuel and air flowrates, as well as the lambda value, are reported. For these variables, both the Present Values and the Set Points are represented, to remark the difference between anode fuel SP (green line) and PV (red line). In turn, this deviation is reported to the lambda (blue line against red line in the third plot of the same figure 3.21). The detection time for this fault, intended as the period needed for the supervisory system to receive the signal, elaborate the feedback given by the air/fuel sensors, realize that the system was working out of the design conditions and force the system to shutdown, was extremely short, less than 120 seconds. Nevertheless, the effect was fatal for the catalyst, which was eventually heavily affected by the fuel stream being out of specifications, causing the carbon deposition phenomenon.

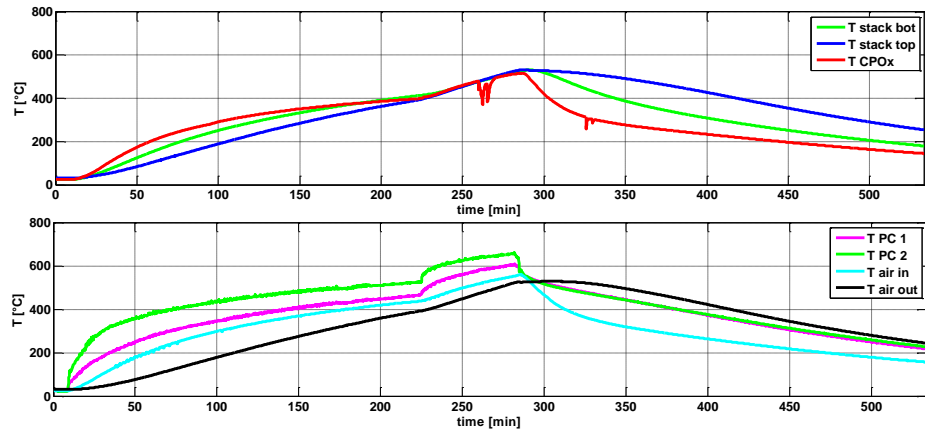


Figure 3.20- Fault 1 event: stack, CPOx reactor, post combustor and air temperatures vs time

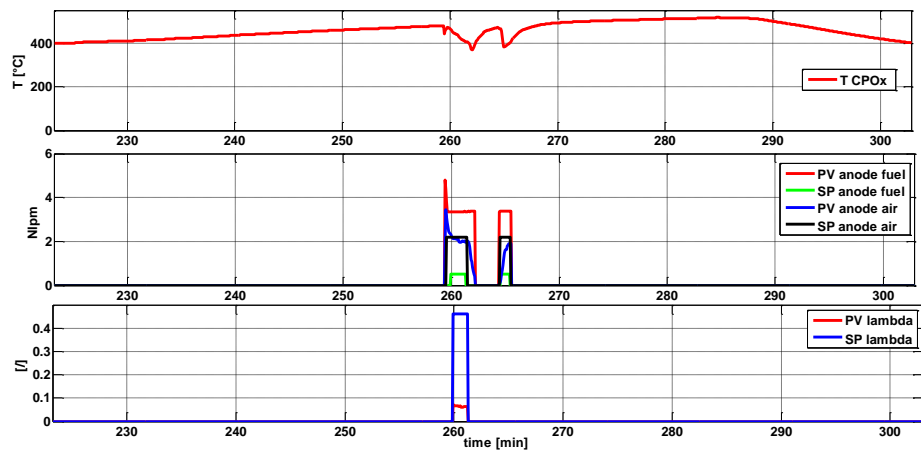


Figure 3.21- Fault 1 event: T_{CPOx} , anode air and fuel flows, lambda vs time (period restricted)

This event was indeed confirmed by the test made afterwards with a second startup attempt for the μ CHP. It was unsuccessful since the reactor temperature never raised above $600\text{ }^{\circ}\text{C}$, as shown in the plots of Figure 3.22. The impossibility of the reactor to approach the nominal operating conditions is a clear symptom of a reduction of the catalyst active surface and, not confirmed but feasible, of the stack cells as well (fault detection). Respect to the nominal operating conditions, it might be observed an uncontrolled increase of the both stack and air outlet temperatures. This

behavior implies that most of the fuel did not react inside the catalyst but downstream into the stack itself and post burner. A detailed explanation of this fault mechanism and its consequences for the system are given in section 5.5.

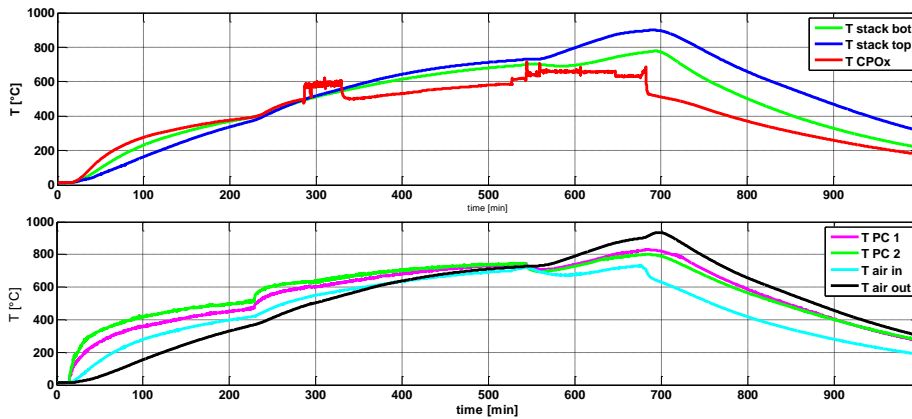


Figure 3.22- Fault 1 isolation: stack, CPOx reactor, post combustor and air temperatures vs time in the μ CHP startup afterwards the fault occurrence

Figure 3.23 reports the trend of anode air and fuel flowrates and lambda value, together with their nominal set points, for the time range between minute 150 and 600. A detail of the CPOx reactor temperature is also given. It may be noted that the present values for both anode air/fuel flowrates and lambda did not deviate from the nominal design set points; however, the reactor temperature did not rise as expected, meaning that the system was not working properly.

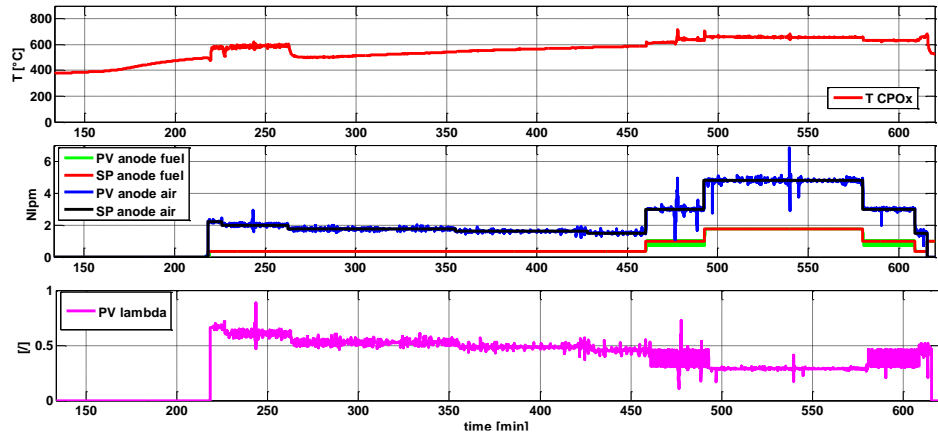


Figure 3.23- Fault 1 isolation: T_{CPOx} , anode air and fuel flows, lambda vs time (period restricted) in the μ CHP startup afterwards the fault occurrence

Additional proof of the faulty behavior of the SOFC unit, which permits the fault isolation, was given by the low stack voltage when in OCV mode. As shown in figure 3.24, the maximum stack Open Circuit Voltage was approximately 6 V, ten times less than the expected value (60 V as reported in figure 3.17). This means that there was not enough hydrogen in the cells to enable the nominal fuel cell reaction and to generate the nominal stack OCV.

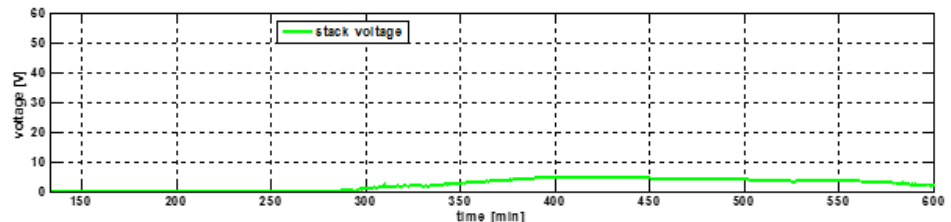


Figure 3.24- Fault 1 isolation: stack voltage in the μ CHP startup afterwards the fault occurrence

When the catalyst reactor is deactivated the methane might flow unconverted through the reforming device and directly burn inside the stack or into the offgas burner. Furthermore, the unreacted fuel might come in contact with the cathode air flow, whose O_2^- ions pass through the electrolyte to reach the anode side. Such phenomena may damage also the stack cells and the sealing.

3.3.2 - *Fault 2: Catalyst oxidation*

During a further session of experimental tests on planar μ CHP prototypes, a similar problem to the fault event described in previous paragraph 3.3.1 was experienced, with the only difference that this time the drift occurred at the anode air valve. The startup and ramp up phases of the μ CHP were successful, and electrical power up to 600 W was generated by the stack (Figures 3.15 - 3.17). As shown in figure 3.17 in section 3.2.3, after the power ramp down the current was reduced to 1 A only, in order to leave the system in standby mode over the night. After a stable phase where all the operating parameters were within design specifications, at a certain moment, suddenly and progressively, the anode air valve started to increase its opening, resulting into more air flow towards the catalyst reactor. On the anode side, the fuel stream remained constant at the desired set point. This strange behavior of the anode air valve might be generated by a fatal error of the control system, which crashed while the system was in standby phase. The reasons why only the anode air control valve failed were investigated after the fault occurrence. They were identified in a bug in the air valve setting configuration. The uncontrolled opening of the anode air valve while the fuel stream remained constant led to a peak of 0.9 for lambda, very close to the stoichiometric combustion ratio. As shown in figures 3.25, the rise in lambda produced an analog peak in CPOx temperature, whose value approached 1200 °C, indicating that a complete combustion occurred inside the reactor.

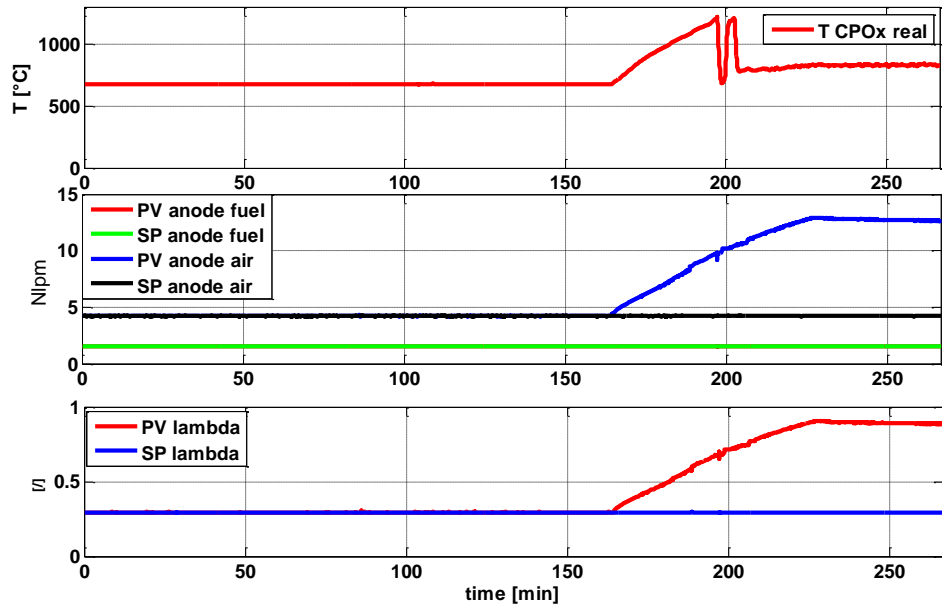


Figure 3.25- Fault 2 event: T_{CPOx} , anode air and fuel flows, lambda vs time

The cooling air flowrate did not change respect to the previous set-point, and the result was an excessive overheating of the CPOx reactor, stack and Hot Box enclosure. The safety thermostat monitoring the CPOx reactor tripped when the threshold temperature was exceeded, leading the system to a forced shutdown.

The consequences were obviously relevant for the CPOx reactor, but not as much catastrophic as those experienced with the carbon deposition event. The excessive amount of air inside the inlet mixture feeding the reforming system generated combustion and most likely the oxidation of several active sites of the catalyst. The severity of catalyst deactivation was linked to the part of the reactor interested by the combustion and by the fault duration (the time the system was running in faulty conditions). Indeed, it is also possible that part of the catalyst can be oxidized before the combustion reaction takes place, but then the ignition of the mixture removes the unreacted oxide obstructions, thereby regenerating some catalyst cells. On the other hand, it is also possible that the combustion may damage both the catalyst and reactor material and insulation, but the active surface can remain unchanged. In this case, the temperature inside the reactor in the subsequent μ CHP startup would be

lower but quite similar to the operating one. A detailed explanation of this fault mechanism and its consequences for the system are given in section 5.6.

As in the previous case, the fault isolation becomes possible when proceeding with a SOFC unit second startup attempt afterwards the fault occurrence. Figure 3.26 shows the trends of stack, reactor, post combustor and air temperatures. The CPOx temperature stabilized around 600 °C and was below 650 °C in the entire operating range, symptom of a faulty behavior of the catalyst reactor. On the contrary, the stack temperatures were not consistently affected by the fault. Indeed, they were not much different from the nominal condition reported in figure 3.15, even if they heavily diverged starting from minute 550, as soon as the system was shutdown, with the stack top temperature approaching dangerous values. Same trend is exhibited by the air outlet temperature. This is due to the thermal inertia of the system, which lasted until the excess heat was all depleted. Figure 3.27 demonstrates that the other relevant parameters, such as anode air/fuel flowrates and lambda, were in accordance to the set points designed for those operating conditions.

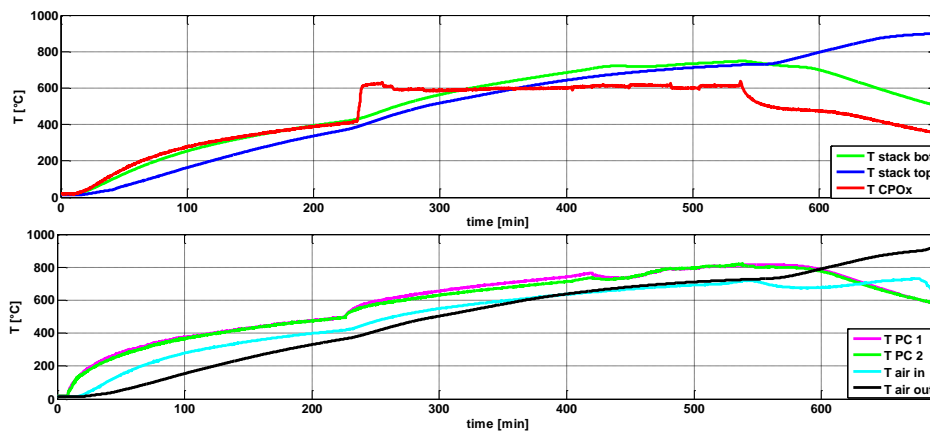


Figure 3.26- Fault 2 isolation: stack, CPOx reactor, post combustor and air temperatures vs time in the μ CHP startup afterwards the fault occurrence

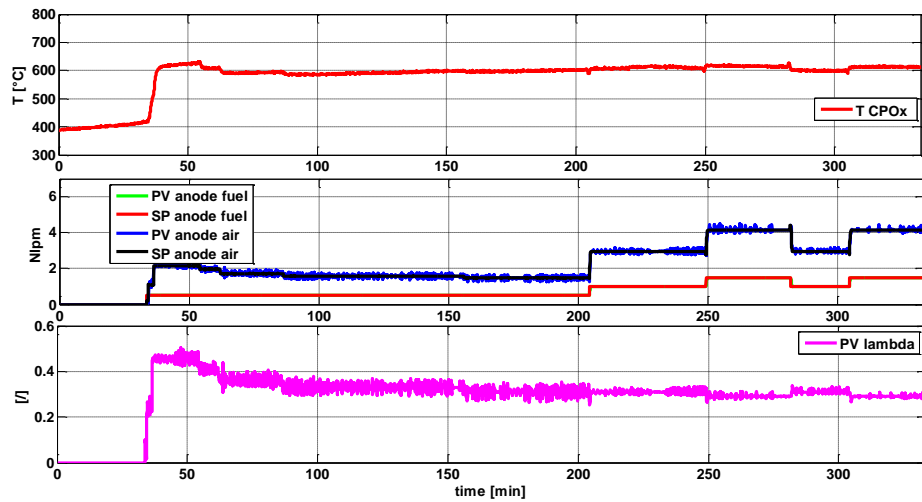


Figure 3.27- Fault 2 isolation: T_{CPOx} , anode air and fuel flows, lambda vs time (period restricted) in the μ CHP startup afterwards the fault occurrence

The main conclusion which can be taken by analyzing the above graphs is that the only variable to clearly indicate a faulty behavior was the CPOx reactor temperature. In fact, as shown in figure 3.28, the stack voltage was only slightly lower than the expected values (OCV slightly below the nominal 60 V displayed in figure 3.17). Electrical power was drawn by the stack up to 400W.

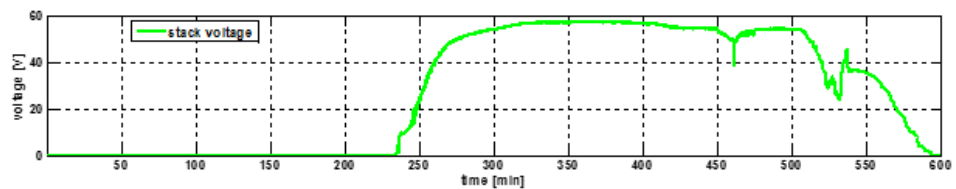


Figure 3.28- Fault 2 isolation: stack voltage in the μ CHP startup afterwards the fault occurrence

However, after operating for some time at these conditions, in the fourth startup subsequent to the fault event the μ CHP performance suffered a drastic worsening and considerably decreased.

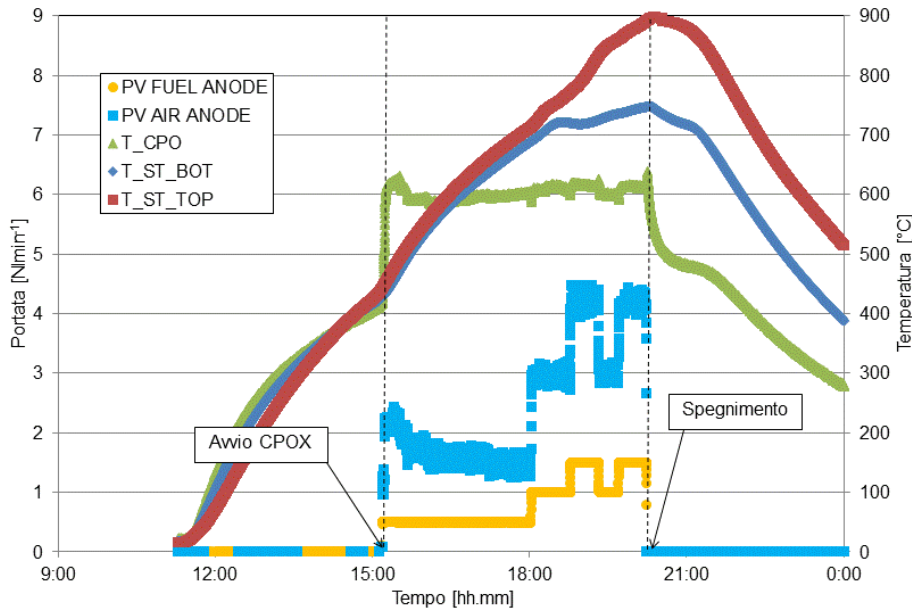


Figure 3.29- Fault 2 isolation: temperatures and anode flows in the fourth μ CHP startup afterwards the fault occurrence

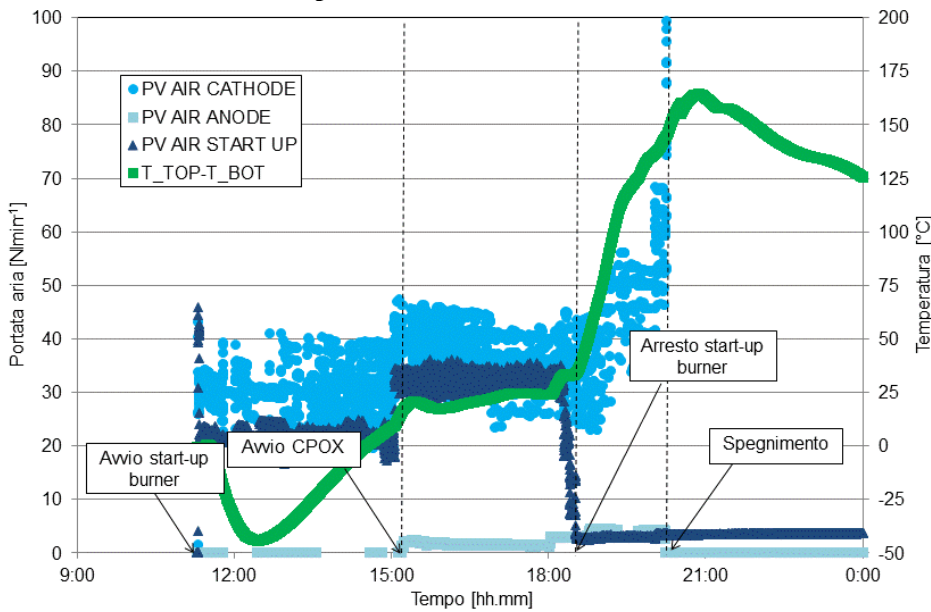


Figure 3.30- Fault 2 isolation: deltaT stack top-bottom and air flows the fourth μ CHP startup afterwards the fault occurrence

As depicted in figures 3.29, 3.30 and 3.31, in this last thermal cycle the CPOx temperature was never able to increase as expected. It oscillated around 600 °C for the entire test. In order to maintain high temperature, without the contribution of the CPOx autothermal reaction, the fuel start up burner was hold ignited until the stack temperature exceeded the designed threshold. The stack temperatures followed a trend similar to what observed in the μ CHP startup after fault 1 (Fig. 3.22). The difference between stack top and stack bottom temperatures was boosting from 20 °C in the late startup phase to the 120 °C corresponding to the end of the power ramp up phase and shut down starting point (fig. 3.29). However, also in this case the CPOx temperature showed a faulty behavior but at the same time the stack was able to generate power, which was remarkably lower than the previous tests. Indeed, in this last test the stack power reached only 100 W, before the excessive air outlet temperature and stack top temperature required a controlled shutdown of the system for safeguarding the operator safety. This indicates that the catalyst had still some active sites, which allowed the generation of a certain quantity of hydrogen able to react inside the fuel cells, opposite to what happened when a carbon deposition fault was detected. Due to the reduced effectiveness of the catalyst, the reaction inside the reformer was not completed. A certain part of the reactant mixture did not react inside the CPOx reactor and reached directly the stack, where both reforming reaction and combustion with the unreacted methane occurred. It is possible to investigate about the state of health of the stack by analyzing the voltage of the single clusters of the SOFC stack, shown in figure 3.31. The clusters are groups of adjacent cells which are electrically connected in series, such that the total stack voltage is computer by summing the voltages of all the clusters. In this case, each cluster is composed by 6 cells, for a total of 60 cells (Table 3.3). As may be observed in figure 3.31, some clusters were finally affected by this faulty phenomenon, as their trend is far from the expected values. As consequence, in addition to the catalyst reactor, it was necessary to re-generate the cell stack as well.

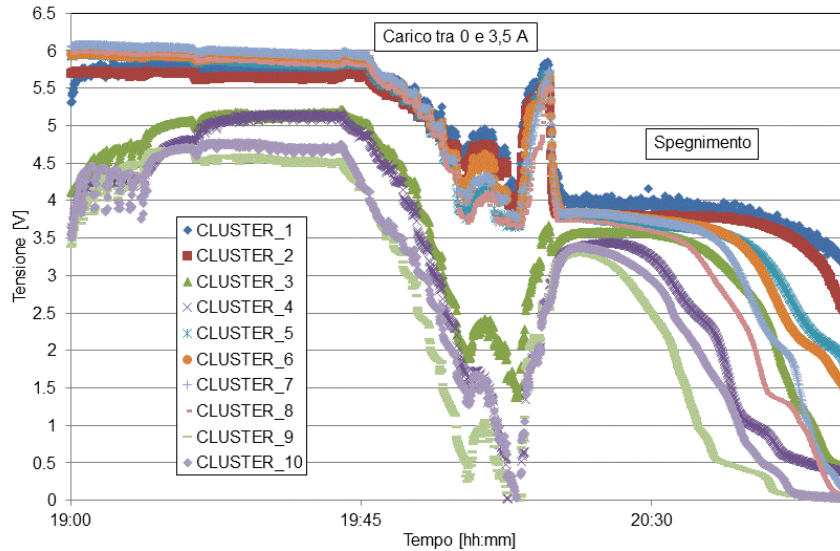


Figure 3.31- Fault 2 isolation: cluster cells voltage the fourth μ CHP startup afterwards the fault occurrence

In conclusion, from a performance point of view the catalyst oxidation fault is less invasive than the carbon deposition, since the SOFC system is still able to operate for a certain time even if out of the nominal range. On the other hand, from an industrial and maintenance perspective, the catalyst oxidation phenomenon may affect also the stack if not detected in the due time, whereas in case of a carbon deposition event, the stack replacement can be avoided. This is a relevant problem for industrial and commercial issues, especially for warranty and maintenance, and indeed is currently strongly investigated by the SOFC systems manufacturers.

Chapter 4

CPOx Dynamic Model

4.1 Reforming Models in SOFC systems: literature review

When referring to the general topic of fuel cell systems, several reforming models can be found in literature for each of the reforming mechanisms described in previous sections (SR, CPOx, ATR). Historically, the most investigated method for fuel reforming in fuel cell has been the steam reforming, and in turn the first mathematical models were developed in respect of this trend. In recent years, though, the large number of studies carried out on CPOx reactors and catalysts species has increased the interest toward these methods. Independently from the type of fuel cell system and reforming technology analyzed, each model can be characterized by several aspects:

- Steady state or dynamic
- Adiabatic or non adiabatic
- Chemical and/or thermodynamic
- Kinetics
- Space dimension
- Control and diagnostics

In most of the cases a reformer model is based on chemical equilibrium. Model inputs generally include the in-flow thermodynamic data (temperature, pressure) and chemical species compositions. The final aim is to calculate the outflow products temperature and pressure, as well as the output chemistry and change in other thermodynamic properties, such as enthalpy, entropy and free energy [29]. In a generic zero-dimensional model [8, 87], the reactants are typically specified by the user by adopting industry-standard quantities, such as the molar steam-to-carbon (S/C) and oxygen-to-carbon (O/C) ratios. The corresponding water and air flow rates

are then calculated as a function of carbon moles in the inlet fuel flow (which is typically varied to satisfy a fuel cell power requirement). In addition, S/C and O/C ratios can be varied to cope with a given enthalpy change requirement, such as a true autothermal mixture, where the net change in enthalpy is zero. Pressure drop and heat losses in the reformer can be either set constant or evaluated via suitable correlation as a function of other operating parameters.

As already recalled in chapter 2, the thermodynamics aspects of the three main reforming methods for fuel cell systems have been largely investigated by Y-S. Seo et al. [8]. The influence of the fuel composition on methane CPOx, has also been analyzed [26, 88, 89, 90], namely through the addition of other chemical species (N_2 , CO_2 or H_2O) to the inlet feed stream. In particular, Donazzi et al. [90] demonstrated experimentally and numerically that by diluting methane/air mixtures having constant O/C ratio with N_2 or CO_2 , the gas temperatures and fuel conversion decrease. On the other hand, the H_2/CO ratio increased for N_2 and decreased for CO_2 dilution.

Jahn and Schroer [29] presented a lumped element model of a natural gas steam reformer being part of a residential fuel cell power plant. The physical laws are represented by ordinary differential equations. The lumped elements are wall, ground plate, burner, reactor and evaporator, and each of them is assigned one uniform temperature. A simple lumped model allows simulating a reduction in active sites available for the reforming reaction, resulting in different composition of flows entering the anode. In addition, faults occurring in the systems that supply water and fuel, thus not concerning the specific reformer reactor, might be taken into account.

Nielsen and Kær [91] gave an example of a steam reformer model for PEM systems. They considered a tubular fixed bed reactor and modeled the thermodynamic, chemical, kinetics and diffusion aspects of the reactions through a two-dimensional partial differential equation (PDE). This model only accounted for processes taking place in the reactor, whereas evaporator and burner were not considered. For the simulation a finite-difference discretization was applied.

With relation to the CPOx modeling, Bizzi and Saracco [16] developed a model of a fixed bed reactor for the catalytic partial oxidation of methane to synthesis gas at short contact time. The transient model, one dimensional in space, accounts for separate energy equations for the gas and solid phases, inter-phase heat and mass transfer, internal radiation within the

fixed bed, longitudinal gas-phase dispersion and detailed surface kinetics. The model is aimed to analyze the influence of the feedstock composition and temperature on reactor conversion and selectivity performance.

Navalho et al. [92] developed a unidimensional heterogeneous mathematical model for catalytic partial oxidation of hydrocarbons, considering a rhodium-based catalyst applied to adiabatic and non-adiabatic honeycomb monolith reactors. The influence of radiative heat losses on the non adiabatic reactor performance was numerically investigated when varying the operating conditions, such as fuel flow rate, air to fuel equivalence ratio and fuel composition.

The knowledge of the intrinsic kinetics is a key issue in numerical modeling endeavors. With a reliable reaction mechanism as well as by accounting for proper heat and mass transport mechanisms the numerical models can support reactor improvements. One dimensional mathematical models have been broadly used in literature to capture the reactor performance in a direct way [93, 26, 88]. Nogare et al. [94] applied a plug flow model and a heterogeneous model, both considering detailed methane CPOx chemistry, and concluded that the former was not adequate to accurately predict species profiles in the first region of the catalyst, while the heterogeneous model gave satisfactory results in the whole range of the catalyst. Maestri et al. [93] applied a heterogeneous dynamic model, considering radiation in solid phase through an effective conductivity and employing global methane CPOx chemistry, to analyze the performance of catalyst supports. They considered spheres, foam and honeycomb monoliths in a packed bed reactor with emphasis on the role of external transport properties on steady-state and start-up regimes. Tavazzi et al. [19] concluded for a packed bed reactor that high feed flow rates and low preheating temperatures contribute to reduce the relative heat losses from the reactor, improving its adiabaticity. For honeycomb monoliths, the flow rate influence on reactor performance was explored numerically by Liu et al. [51] and by Beretta et al. [95].

Radiative heat transfer can play an important role on the overall heat transfer phenomena, mainly due to the high temperature gradients that arise in some sections of a catalytic monolith reactor [96]. The proper study of both thermal radiation and redistribution of the energy released by chemical reactions along the catalyst bed is important to reduce the temperature gradients. In the majority of 1D CPOx heterogeneous models, radiative heat transfer in the solid phase has been considered through an effective

heat conductivity corrected with a radiative contribution. For instance, concerning honeycomb monoliths, Lee and Aris' radiative correlation [96] has been extensively applied. In fact, the diffusion approximation of radiative heat transfer significantly reduces the complexity of the underlying heat transfer mechanism; however, close to the boundaries of a non-adiabatic reactor, where radiative heat losses to surroundings are expected, this approach is not effective enough [97]. Radiative heat losses from the interior of CPOx reactors have received few attention in literature, mostly due to the axial radiative insulation provided by the application of inert heat shields that surround the catalytic structure. However, even with the application of heat shields a perfect insulation is not guaranteed and most of modeling studies only account for radiative losses on boundary conditions [19, 88, 95].

A well-known serious disadvantage during catalytic partial oxidation operation is the occurrence of surface hot spots, which can lead to an unhealthy catalyst thermal behavior. In fact, high catalyst temperatures can cause thermal deactivation mechanisms. Carbon formation, sulphur poisoning and other catalyst deactivation modes were intensively studied in recent years and different approaches were developed for controlling these phenomena. Forzatti et al. [60] have studied the mathematical description of the chemical-physical aspects concerning the various deactivation causes (i.e. poisoning, sintering, coking, solid-state transformation, masking, etc.). Istadi et al. [98] and Trimm [73] did the same but for the specific reforming mechanisms of, respectively, CO₂ reforming and steam reforming. A random carbon deposition and catalyst deactivation model was proposed by Z. Chen, Y. Yan, S.E.H. Elnashaie [28], assuming that the coke deposition rate in general depends on active sites.

More recently, the research focus was moved toward the control of fuel reforming dynamics and parameters and on μ CHP SOFC based systems. Pukrushpan et al. [99] have presented a model-based control analysis and design for a CPOx system that manages natural gas flow and humidified atmospheric air flow in the reactor. The target was to regulate the amount of hydrogen in the fuel cell anode and the temperature of the catalytic partial oxidation reactor during fluctuating power demand phases. Linear feedback analysis and design was used to identify the limitation of a decentralized controller and the benefit of a multivariable controller. Liso et al. [100] have described in both qualitative and quantitative form the

performance of a methane-fed SOFC-based μ CHP system destined to residential applications, also comparing two different types of pre-reforming systems, namely Steam Reforming and Partial Oxidation.

4.2 - CPOx Modeling approaches

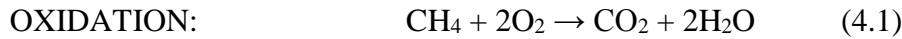
From a theoretical point of view, the reactions involved in steam reforming and catalytic partial oxidation are the same, even if the inlet reactant composition is different for each case. This means that, independently from the type of reforming mechanism considered, one unique model can be adopted for determining the thermodynamic equilibrium in a reforming reactor and calculating the chemical compositions at the reformer outlet. In this thesis, the reforming mechanism is modeled by assuming chemical equilibrium and taking into account the thermodynamic aspect of the reactions occurring inside the reformer. The reforming systems can be modeled through two different approaches, both accurately described in Perry's Chemical Engineers' Handbook [101], where all relevant reactions, together with the list of constants used for calculation of enthalpy and entropy of species, are specified in detail.

The mentioned approaches are as follows:

- 1. Minimization of Gibbs free energy;**
- 2. Equilibrium constants.**

In the present work, the first approach has been used to develop the CPOx dynamic model, as described in detail in section 4.2.1.

The second method is herein briefly described. Differently from the minimization of free Gibbs energy, the equilibrium constants methodology takes into account the reactions occurring inside the reactor. For the CPOx, mechanism the reactions involved, according to the indirect oxidation mechanism (section 2.2.1.2), are:



The model initially resolves the total oxidation reaction (4.1), until all the O_2 is consumed. In a second step, the model takes into account simultaneously the equilibrium reaction for both reforming (4.2) and water gas shift reactions (4.3). The model utilizes an iterative method for calculating the equilibrium constants of reforming and water gas shift reactions; for both reactions, an equilibrium constant is associated to each temperature. In turn, to each temperature corresponds a composition of products at the reactor outlet.

When the number of reactions involved is high, this approach becomes complex and tedious. In addition, the constant equilibrium method makes it difficult to analyze the solid carbon that can be generated during the reforming process. In contrast, a simpler and quicker method, more useful for mathematical computation through commercial software, is represented by the minimization of Gibbs free energy, which for these reasons is normally preferred in fuel-reforming analysis.

4.2.1 Minimization of Gibbs free energy

The approach adopted for the thermodynamic model developed is *zero-dimensional (grey box model)*. The CPOx reactor is represented by only one control volume, while spatial averaging of all dimensions is assumed. Thus, spatial variations are not taken into account. Both global mass and energy balances of input and output species are considered and the resulting system of equations is numerically solved to define the output variables (outlet molar fractions and reactor temperature). The model is dynamic and therefore accounts for the transient variations in input conditions, i.e. air and fuel ratio over the startup and run time, in order to describe the CPOx temperature ramp up. In a dynamic simulation, time is the only independent

variable. A zero-dimensional model is suitable to examine the impact of inlet composition, temperature and reactor geometry when the product gas fractions and the reactor outlet temperatures are required as outputs. However, being the spatial variation of the variables neglected, these models are not suitable to perform prediction. More appropriately, zero-dimensional models are more suited for describing reforming mechanisms, where attention is not focused on the reactor itself but on how it affects the performance of the complete SOFC system. Fuel cell zero-dimensional models are usually based on assumptions, parameters and practical information provided in literature or taken from experimental data.

The Gibbs free energy minimization approach considers that the system reaches the equilibrium condition through a product composition able to minimize the energy of the same system [101]. As shown in figure 4.1, when using this method, it is not necessary to specify the reactions that convert the reactants in products, but it is sufficient to specify the species existing in the system. For CPOx and SR reactions, the interested species are CH₄, CO, CO₂, H₂, H₂O, O₂ and N₂.

The other variable is the reactor outlet temperature, which can be either fixed as operating parameter or calculated through the enthalpy balance. In the model herein described, the outlet reactor temperature represents an output and is determined by numerical computation.

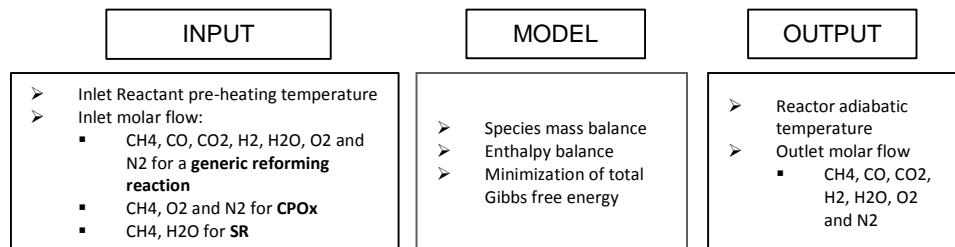


Figure 4.1 – Scheme of reformer model with the minimization of Gibbs free energy approach

4.3 CPOx Model theoretical content

The ideal gas standard Gibbs energy of formation of a chemical compound, ΔG_f^0 , is the increment of Gibbs energy associated with the reaction of

forming that compound in the ideal gas state starting from the constituent elements in their standard state. The standard condition is defined as the existing phase at a temperature of 298.15 K and one atmosphere (101.325 kPa) [101].

For other temperatures, T (K), the Eq. 4.4 may be used:

$$\Delta G_{f,T}^0 = \Delta H_{f,T}^0 - T\Delta S_{f,T}^0 \quad (4.4)$$

Where:

- $\Delta G_{f,T}^0$ is the Gibbs energy of formation at T , kJ/mol;
- $\Delta H_{f,T}^0$ Enthalpy of formation at T , kJ/mol;
- $\Delta S_{f,T}^0$ Entropy of formation at T , kJ/mol K.

In a chemical reaction, chemical equilibrium is the state in which both reactants and products are present in concentrations, which have no further tendency to change with time. Usually, this state results when the forward reaction proceeds at the same rate as the reverse one. The reaction rates of the forward and backward reactions are generally not zero, but equal. Thus, there are no net changes in the concentrations of the reactants and products. Such a state is known as dynamic equilibrium.

At the equilibrium state, differential variations may occur in the system at constant T and P without producing a change in G_t , which means:

$$dG_{P,T}^t = 0 \quad (4.5)$$

The minimization of the total Gibbs energy G_t in accordance with Eq. 4.5 is limited to gas-phase reactions, for which the problem is to find the equilibrium composition for given T and P and for a given initial feed.

A description of the steps involved in the minimization method is given as follows:

1. Formulate the constraining material-balance equations, based on the conservation of the total number of atoms of each *element* in a system comprised of w elements. Let subscript k identify a particular atom, and define A_k as the total number of atomic masses of the k th element in the feed. Further, let a_{ik} be the number of atoms of the k th element present

in each molecule of chemical species i . The material balance for element $k=1,2,\dots,w$ is then

$$\sum_i n * a_{ik} = A_k \quad (4.6)$$

2. Multiply each element balance by λ_k , a Lagrange multiplier:

$$\lambda_k * (\sum_i n * a_{ik} - A_k) = 0 \quad (4.7)$$

Summed over k , these equations give:

$$\sum_k \lambda_k * (\sum_i n * a_{ik} - A_k) = 0 \quad (4.8)$$

3. Form a function F by addition of this sum to G^t :

$$F = G^t * \sum_k \lambda_k * (\sum_i n * a_{ik} - A_k) = 0 \quad (4.9)$$

Function F is identical to G^t , because the summation term is zero. However, the partial derivatives of F and G^t with respect to n_i are different, because function F incorporates the constraints of the material balances.

4. The minimum value of both F and G^t is found when the partial derivatives of F with respect to n_i are set equal to zero:

$$\left(\frac{\partial F}{\partial n_i}\right)_{T,P,n} = \left(\frac{\partial G^t}{\partial n_i}\right)_{T,P,n} * \sum_k \lambda_k * a_{ik} = 0 \quad (4.10)$$

The middle member is the definition of the chemical potential; whence:

$$\mu_i * \sum_k \lambda_k * a_{ik} = 0 \quad i = (1,2, \dots, N) \quad (4.11)$$

However, for gas-phase reactions and standard states as the pure ideal gases at P^o , the chemical potential is given by Eq. 4.12:

$$\mu_i = G_i^0 + RT \ln \frac{f_i}{P^o} \quad (4.12)$$

If G_i^0 is arbitrarily set equal to zero for all *elements* in their standard states, then for compounds $G_i^0 = \Delta G_{f,i}^0$, the standard Gibbs-energy change of formation for species *i*.

In addition, the fugacity is eliminated in favor of the fugacity coefficient by Eq. 4.13

$$f_i = y_i \times \Phi_i \times P \quad (4.13)$$

Assuming that we are dealing with ideal gas, Φ_i are all unity. Assuming also $P = 1$ bar and also standard state pressure bar $P^\circ = 1$, the equation for μ_i becomes

$$\mu_i = \Delta G_{f,i}^0 + RT \ln y_i \quad (4.14)$$

Where $y_i = n_i / \sum_i n_i$

Combination with Eq. 4.11 gives:

$$\sum_k \lambda_k * a_{ik} + \Delta G_{f,i}^0 + RT \ln \frac{n_i}{\sum_i n_i} = 0 \quad (1,2, \dots, N) \quad (4.15)$$

If species *i* is an element, $\Delta G_{f,i}^0$ is zero. There are *N* equilibrium equations one for each chemical species, and there are *w* material-balance equations, one for each element, for a total of *N* + *w* equations. The unknowns in these equations are the n_i (note that $y_i = \frac{n_i}{\sum_i n_i}$), of which there are *N*, and the λ_k , of which there are *w*, for a total of *N* + *w* unknowns. Thus, the number of equations is sufficient for the determination of all unknowns. The scheme of the final system of equations, characterized for the model developed in this thesis, is shown in figure 4.2. In addition to the *N* + *w* equations herein described, the enthalpy balance of the species brings in a further variable, the adiabatic reactor temperature. Solution of the equations provides a preliminary set of y_i , then the process is repeated to convergence. All calculations are well suited to computer solution. In this procedure, the question of what chemical reactions are involved never enters directly into any of the equations.

4.4 Model parameters

✓ INPUT

- Inlet reactant pre-heating temperature, that is the temperature of reactants entering the catalyst reactor (section 2.2.2)
- lambda, that is a measure of the ratio between inlet methane and oxygen (section 2.2.2)

✓ OUTPUT

- Composition of reaction products, molar fractions and reactor outlet temperature
- CH₄ conversion, H₂ and CO selectivity

✓ HP

- The thermodynamic model is adiabatic and zero-dimensional
- The inlet temperature does not exceed 350-400°C, in order to limit the outlet temperature that otherwise would rise above 1000°C. Such high temperatures are not feasible for the mechanical limit of both reactor materials and stack cells, which usually work in the range 700-900°C.
- The catalyst is already active when the air/fuel mixture enters the reactor (not modelling the startup phase)
- The inlet fuel is methane, CH₄.
- The type of catalyst used for reaction, and hence its design, geometric surface and related support, is taken into account for calculating the thermal capacity of the reactor, k, that enters in the evaluation of the dynamic term (section 4.7)
- The effect of variation in inlet fuel power, cathode cooling air and fuel utilization is considered through a linear regression based on experimental data (section 4.5.1)
- The GHSV, gas hourly space velocity, does not enter in the model,

whose nature is mainly thermodynamic and therefore the kinetic is excluded.

- In the simulation, the mole fraction composition of air was assumed to be 0.2095 O₂ and 0.7905 N₂.

✓ TARGET

- Determine the theoretical conditions that yield to the maximum methane conversion and hydrogen gain in the outlet products, compatibly with the limit set for the reactor outlet temperature. For given operating conditions, the equilibrium temperature of the reactor and the equilibrium compositions have been calculated. The model has been developed in Matlab®/Simulink® environment.

4.5 CPOx model description

T_{iIN} , T_{iREF} respectively, reactant inlet temperature and reference temperature

T_{iOUT} reactor outlet temperature.

\dot{x}_{iIN} molar composition of inlet reactants

\dot{x}_{iOUT} molar composition of outlet products

Reactants Enthalpy and Entropy calculation, at T_{iIN}

$$H_{iTin} = H_{iTref} + a(T_{iIN} - T_{iREF}) + \frac{b}{2}(T_{iIN}^2 - T_{iREF}^2) + * \\ + \frac{c}{3}(T_{iIN}^3 - T_{iREF}^3) + \frac{d}{4}(T_{iIN}^4 - T_{iREF}^4) \quad (4.16)$$

$$S_{iTin} = S_{iTref} + a * \ln \frac{T_{iIN}}{T_{iREF}} + +b(T_{iIN} - T_{iREF}) + \\ + \frac{c}{2}(T_{iIN}^2 - T_{iREF}^2) + \frac{d}{3}(T_{iIN}^3 - T_{iREF}^3) \quad (4.17)$$

Products Enthalpy and Entropy calculation, at T_{OUT} (unknown)

$$H_{i T_{out}} = H_{i T_{ref}} + a(T_{i OUT} - T_{i REF}) + \frac{b}{2}(T_{i OUT}^2 - T_{i REF}^2) + \frac{c}{3}(T_{i OUT}^3 - T_{i REF}^3) + \frac{d}{4}(T_{i OUT}^4 - T_{i REF}^4) \quad (4.18)$$

$$S_{i T_{out}} = S_{i T_{ref}} + a * \ln \frac{T_{i OUT}}{T_{i REF}} + b(T_{i OUT} - T_{i REF}) + \frac{c}{2}(T_{i OUT}^2 - T_{i REF}^2) + \frac{d}{3}(T_{i OUT}^3 - T_{i REF}^3) \quad (4.19)$$

where $H_{i T_{ref}}, S_{i T_{ref}}$ are respectively enthalpy and entropy of formation at reference temperature, and a, b, c, d are tabulate constants [101].

Calculation of reactants Enthalpy and Entropy of formation, at T_{IN}

$$\text{CH}_4 \quad H_{f \text{CH}_4 T_{in}} = H_{\text{CH}_4 T_{in}} - H_{\text{C Tref}} - 2H_{\text{H}_2 Tref} \quad (4.20)$$

$$\text{H}_2\text{O} \quad H_{f \text{H}_2\text{O T}_{in}} = H_{\text{H}_2\text{O T}_{in}} - H_{\text{H}_2 Tref} - \frac{1}{2}H_{\text{O}_2 Tref} \quad (4.21)$$

$$\text{H}_2 \quad H_{f \text{H}_2 T_{in}} = H_{\text{H}_2 T_{in}} - H_{\text{H}_2 Tref} \quad (4.22)$$

$$\text{CO} \quad H_{f \text{CO T}_{in}} = H_{\text{CO T}_{in}} - H_{\text{C Tref}} - \frac{1}{2}H_{\text{O}_2 Tref} \quad (4.23)$$

$$\text{CO}_2 \quad H_{f \text{CO}_2 T_{in}} = H_{\text{CO}_2 T_{in}} - H_{\text{C Tref}} - H_{\text{O}_2 Tref} \quad (4.24)$$

$$\text{O}_2 \quad H_{f \text{O}_2 T_{in}} = H_{\text{O}_2 T_{in}} - H_{\text{O}_2 Tref} \quad (4.25)$$

$$\text{N}_2 \quad H_{f \text{N}_2 T_{in}} = H_{\text{N}_2 T_{in}} - H_{\text{N}_2 Tref} \quad (4.26)$$

$$\text{C} \quad H_{f \text{C T}_{in}} = H_{\text{C T}_{in}} - H_{\text{C Tref}} \quad (4.27)$$

The same equations are applicable to the entropy of formation as well.

Calculation of reactants Enthalpy and Entropy of formation, at T_{OUT}

The calculation is identical to the inlet case, except for the temperature.

Calculation of Gibbs free energy of formation at T_{OUT}, reactor outlet

The inlet energy of formation, evaluated at T_{IN}, does not enter in the final set of equations:

$$G_{f i T_{out}} = H_{f i T_{out}} - T_{out} * S_{f i T_{out}} \quad (4.28)$$

Calculation of delta Gibbs free energy of formation at T_{OUT}, reactor outlet

$$\text{CH}_4 \quad \Delta G_{f \text{CH}_4 T_{out}} = G_{f \text{CH}_4 T_{out}} - G_{f \text{C} T_{out}} - 2G_{f \text{H}_2 T_{out}} \quad (4.29)$$

$$\text{H}_2\text{O} \quad \Delta G_{f \text{H}_2\text{O} T_{out}} = G_{f \text{H}_2\text{O} T_{out}} - G_{f \text{H}_2 T_{out}} - \frac{1}{2}G_{f \text{O}_2 T_{out}} \quad (4.30)$$

$$\text{H}_2 \quad \Delta G_{f \text{H}_2 T_{out}} = G_{f \text{H}_2 T_{out}} - G_{f \text{H}_2 T_{out}} \quad (4.31)$$

$$\text{CO} \quad \Delta G_{f \text{CO} T_{out}} = G_{\text{CO} T_{out}} - G_{\text{C} T_{out}} - \frac{1}{2}G_{\text{O}_2 T_{out}} \quad (4.32)$$

$$\text{CO}_2 \quad \Delta G_{f \text{CO}_2 T_{out}} = G_{\text{CO}_2 T_{out}} - G_{\text{C} T_{out}} - G_{\text{O}_2 T_{out}} \quad (4.33)$$

$$\text{O}_2 \quad \Delta G_{f \text{O}_2 T_{out}} = G_{\text{O}_2 T_{out}} - G_{\text{O}_2 T_{out}} \quad (4.34)$$

$$\text{N}_2 \quad \Delta G_{f \text{N}_2 T_{out}} = G_{\text{N}_2 T_{out}} - G_{\text{N}_2 T_{out}} \quad (4.35)$$

Species mass balance

$$\sum_i n * a_{ik} = A_k \quad (4.36)$$

Where n are the species entering the reactor, k the species elements, A_k atomic mass number of elements k.

In this particular case:

$$\text{C:} \quad nCH_4 + nCO + nCO_2 \quad (4.37)$$

$$\text{H:} \quad 4nCH_4 + 2nH_2O + 2nH_2 \quad (4.38)$$

$$\text{O:} \quad nH_2O + nCO + 2nCO_2 + 2nO_2 \quad (4.39)$$

Calculation and minimization of total Gibbs free energy

$$\frac{\Delta G_{f i T_{out}}}{RT_{out}} + \ln \frac{\dot{x}_{i T_{out}}}{\sum_i^n \dot{x}_{i T_{out}}} + \sum_k \frac{\lambda_k}{RT_{out}} a_{ik} \quad (4.40)$$

where λ_k is a lagrangian constant associated to each element.

Enthalpy balance

The reactor outlet temperature is now unknown and therefore it needs to be calculated through the resolution of the final set of equations. On the contrary, if the heat input to the reactor is known and specified (e.g. in steam reforming reaction when the reactor temperature is fixed), the outlet temperature does not represent an output.

$$\dot{Q} = \Delta H_{reaz T_{in}} - \Delta H_{sens} \quad (4.41)$$

Where:

$$\Delta H_{reaz T_{in}} = \sum_i^n ((\dot{x}_{i out} - \dot{x}_{i in}) * H_{f i T_{in}}) \quad (4.42)$$

$$\Delta H_{sens T_{out}} = \sum_i^n ((\dot{x}_{i out}) * (H_{f i T_{out}} - H_{f i T_{in}})) \quad (4.43)$$

Making explicit the two expressions and introducing the dynamic term, it is yielded:

$$\dot{Q} = \sum_i (\dot{x}_{i\ OUT} * H_{fi\ OUT} - \dot{x}_{i\ IN} * H_{fi\ IN}) + k \frac{dT}{dt} \quad (4.44)$$

When $\dot{Q}=0$, for the Hp. of adiabatic system, the resulting equations, coupled with the mass balance, generate the set of non linear equations shown in figure 4.2. This system, numerically solved, gives the $\dot{x}_{i\ OUT}$ and T_{OUT} unknown.

➤ CH ₄	$\frac{\Delta G_{f\ CH_4\ T_{out}}}{RT_{out}} + \ln \frac{\dot{x}_{CH_4\ T_{out}}}{\sum_i^n \dot{x}_{i\ T_{out}}} + \sum_k \frac{\lambda_k}{RT_{out}} a_{ik}$
➤ CO	$\frac{\Delta G_{f\ CO\ T_{out}}}{RT_{out}} + \ln \frac{\dot{x}_{CO\ T_{out}}}{\sum_i^n \dot{x}_{i\ T_{out}}} + \sum_k \frac{\lambda_k}{RT_{out}} a_{ik}$
➤ CO ₂	$\frac{\Delta G_{f\ CO_2\ T_{out}}}{RT_{out}} + \ln \frac{\dot{x}_{CO_2\ T_{out}}}{\sum_i^n \dot{x}_{i\ T_{out}}} + \sum_k \frac{\lambda_k}{RT_{out}} a_{ik}$
➤ H ₂	$\frac{\Delta G_{f\ H_2\ T_{out}}}{RT_{out}} + \ln \frac{\dot{x}_{H_2\ T_{out}}}{\sum_i^n \dot{x}_{i\ T_{out}}} + \sum_k \frac{\lambda_k}{RT_{out}} a_{ik}$
➤ H ₂ O	$\frac{\Delta G_{f\ H_2O\ T_{out}}}{RT_{out}} + \ln \frac{\dot{x}_{H_2O\ T_{out}}}{\sum_i^n \dot{x}_{i\ T_{out}}} + \sum_k \frac{\lambda_k}{RT_{out}} a_{ik}$
➤ O ₂	$\frac{\Delta G_{f\ O_2\ T_{out}}}{RT_{out}} + \ln \frac{\dot{x}_{O_2\ T_{out}}}{\sum_i^n \dot{x}_{i\ T_{out}}} + \sum_k \frac{\lambda_k}{RT_{out}} a_{ik}$
➤ C:	nCH ₄ + nCO + nCO ₂
➤ H:	4nCH ₄ + 2nH ₂ O + 2nH ₂
➤ O:	nH ₂ O + nCO + 2nCO ₂ + 2nO ₂
➤	$\dot{Q} = \sum_i (\dot{x}_{i\ OUT} * H_{fi\ OUT} - \dot{x}_{i\ IN} * H_{fi\ IN}) + k \frac{dT}{dt} = 0$

Figure 4.2 – System of final equations

As already stated in previous chapters, this method, here described for the CPOx reforming mechanism, is identically applicable to the steam reforming. In this case, in addition to the CH₄, O₂ and N₂ (and eventually residual of CO₂ and CO), the inlet species will include H₂O.

In the figures 4.3 and 4.4 the scheme of both CPOx and SR model is shown.

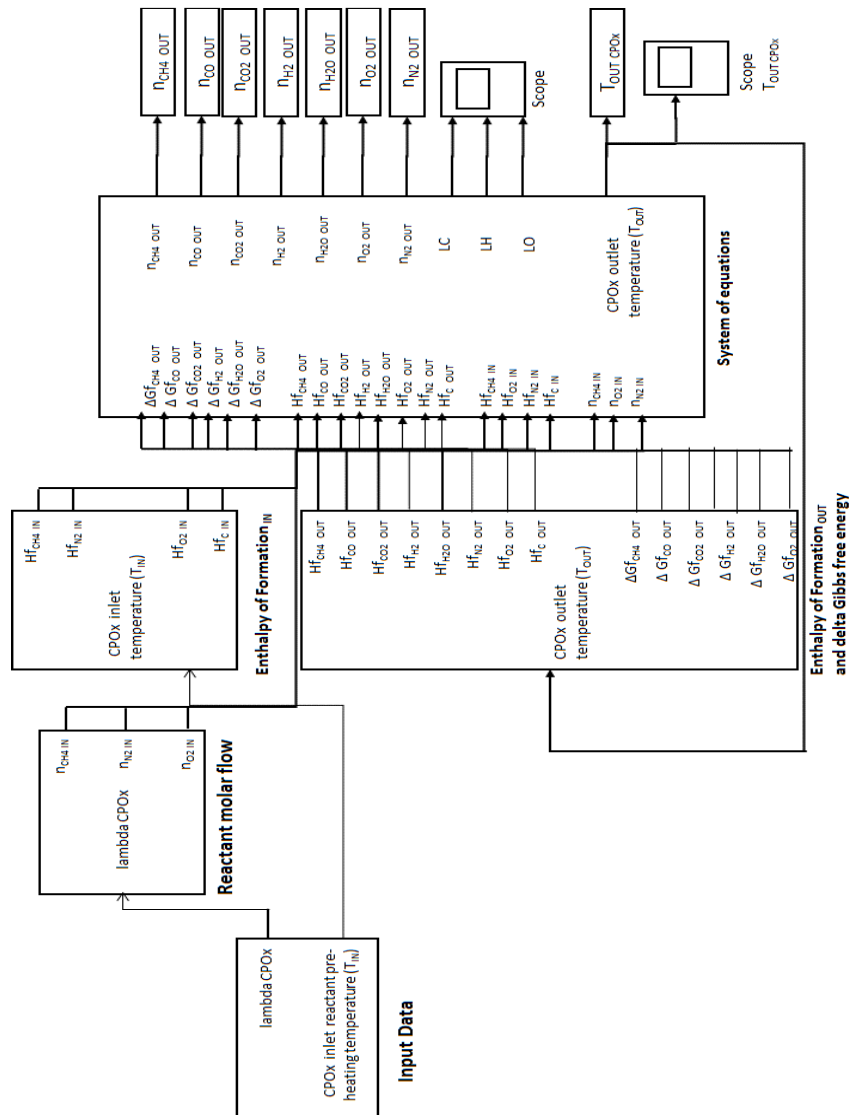


Figure 4.3 – CPOx model scheme

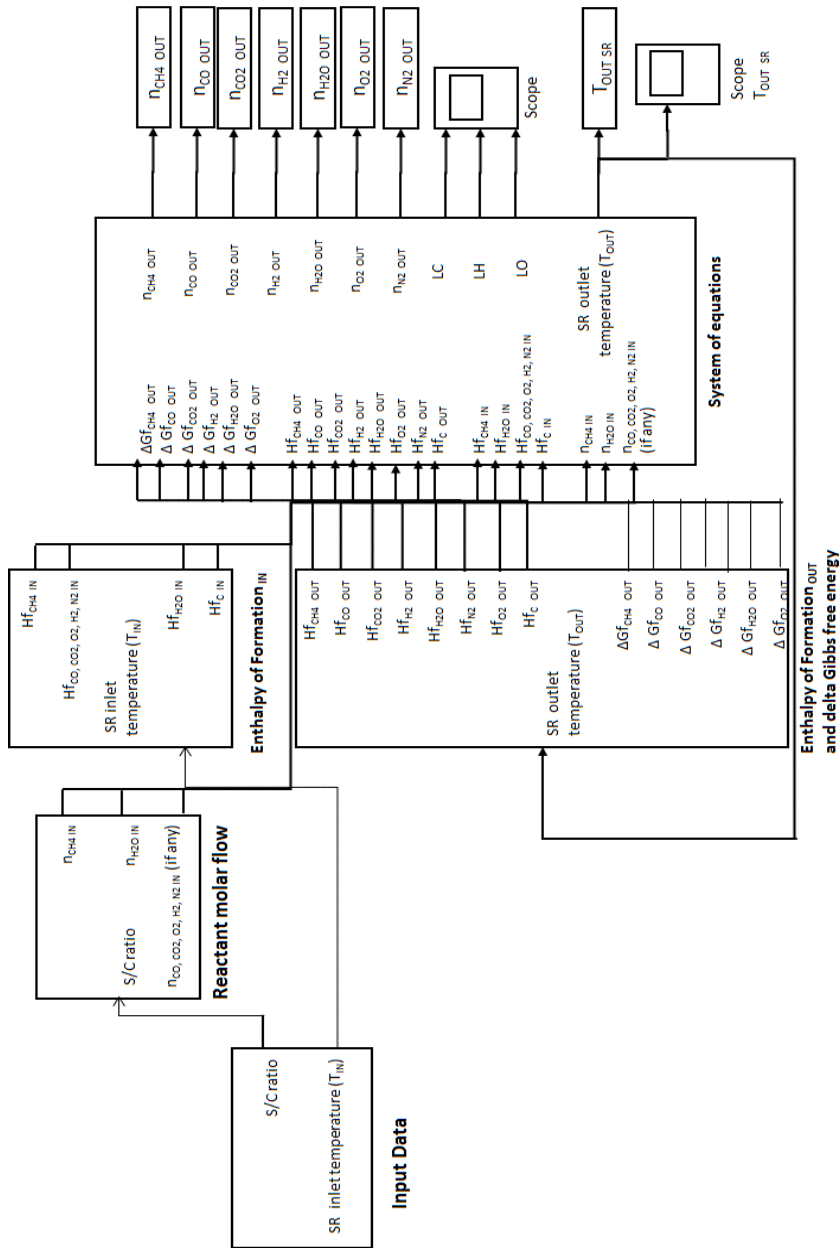


Figure 4.4 – SR model scheme

4.5.1 Linear Regression

The useful range of input values set for the model are as follows:

- **Lambda:** within the range 0.25 - 0.35;
- **Tin reactants:** within the range 20 °C- 350 °C.

The inlet temperature of reactants entering the reactor is not easy to identify, since the pre-heating temperature range is considered as a design parameter by both Hot Box and CPOx reactor manufacturers. The optimal pre-heating contribution is indeed the result of an accurate thermal analysis of heat exchanges occurring inside the Hot Box, verified through simulations and not measured during the tests. The pre-heating of the feeding mixture is carried out usually inside the hot box, through the thermal integration of the inlet plenum or of the pipe that conveys the mixture to the reactor. The heat exchange is due to the heat coming from the stack, or to the cathode air flow after this exits the air pre-heater and before entering the stack itself. When the reactor is external to the Hot Box, the pre-heating is usually carried out by means of electrical resistances wrapped around the CPOx reactor walls (section 3.2.2). It is therefore evident that the pre-heating temperature of reactant species is directly related to many other SOFC system parameters, and its set point can widely vary according to the different operating phases.

For example, during the lab tests (ref. chapter 3, fig. 3.15 – 3.17) it was assessed through experiments that, for the same inlet fuel, different stack currents and cooling air flowrates determine two different temperature values of the products at reactor outlet. During the ramp up of stack power generation, by increasing the current from 1 to 8 A, and the input fuel from 1 to 2.5 Nlpm, the cathode air flow was controlled at 55 Nlpm, while for 9 and 10 A the air flow was raised to 75 Nlpm in order to contrast the stack overheating. In the standby condition, that is when the stack generates only the power needed for the auxiliaries and for maintaining the minimum operating temperatures, with low current generation (1 A), the cooling air was fixed to 85 Nlpm to face the increase in temperature due to extremely low fuel utilization. Increasing the current progressively, and in turns the fuel utilization, the CPOx temperature slightly decreased, being reduced the heating effect due to the offgas burner.

In the CPOx dynamic model here described, all these effects have repercussions on the inlet temperature and have therefore been taken into account through a linear regression.

In order to relate the inlet temperature to the other parameters relevant for a SOFC system, such as:

- Fuel flow input power
- Cathode air flow for stack cooling
- Fuel Utilization (and therefore stack current)
- Temperature at CPOx reactor outlet

a linear regression has been created, comparing the measured outlet CPOx temperature to the value calculated by the model after its validation with the first available data. The linear regression is given by equation 4.45 and accounts for a wide set of different operating conditions of the above parameters, as listed in table 4.1.

Table 4.1 – Linear regression data

Pos	T _{CPOx out} [°C]	SP fuel flow [Nlpm]	PV air cathode [Nlpm]	Current [A]	Uf%	T _{in} (°C)
1	678,3	1	56,1	0	0	84
2	707,8	1,5	52,9	0	0	175
3	701,6	1,5	56,4	1	0,02	172
4	698,8	1,5	54,3	2	18,6	200
5	697,8	1,5	57,1	4	37,2	162
6	713,7	2	55,2	6	41,8	230
7	736,8	2,5	54,3	8	44,6	300
8	725,3	2,5	65,3	8	44,6	284
9	760,9	3	67,1	9	41,8	350
10	757,6	3	74,9	9	41,8	332
11	721,3	2,5	75,2	8	44,6	260
12	687,8	2	73,2	6	41,8	207
13	674,8	1,5	73,4	4	37,2	126
14	685,4	1,5	75,5	1	9,3	150
15	682,1	1,5	90,1	1	9,3	110

$$\begin{aligned}
T_{in} = & \mathbf{b(1)} + \frac{TCPOx}{1000} \times \mathbf{b(2)} + \left(\frac{TCPOx}{1000}\right)^2 \times \mathbf{b(3)} + \frac{Fuel_{in}}{1000} \times \mathbf{b(4)} + \\
& + \left(\frac{Fuel_{in}}{1000}\right)^2 \times \mathbf{b(5)} + \frac{Air_{cat}}{1000} \times \mathbf{b(6)} + \left(\frac{Air_{cat}}{1000}\right)^2 \times \mathbf{b(7)} + \\
& + \frac{Fu}{100} \mathbf{b(8)} + \left(\frac{Fu}{100}\right)^2 \times \mathbf{b(9)}
\end{aligned} \tag{4.45}$$

4.6 - Reactor Design

The internal layout of the CPOx reactor considered for the model derives from design data indicated by reforming systems manufacturer Hysytech [36] and also confirmed by many literature records [80, 82]. The reactor designed by Hysytech is the result of studies and activities carried out within the EFESO project, where this reactor was fabricated and installed in a μ CHP unit, integrated in the Hot Box design (section 3.2.3). Experimental activities over this catalyst have been used for validating the model, both in stand-alone case, where the reactor was tested in lab, wrapped by electrical resistances for the heating phase (see section 3.2.2), and in an Hot Box integrated layout, leading to the final configuration adopted for 1 kW μ CHP (see section 3.2.1-3.2.3).

The reactor considered for this work utilizes extruded monoliths ceramic supports based on Rh catalyst with the specifications reported in table 4.2.

Table 4.2 – Reactor design data [36]

Length	50 mm
Diameter	25 mm
Void grade	52 %
Catalyst	Rh

The extruded monoliths are made of a rigid structure in ceramic material where the metallic catalyst is deposited over α -Al₂O₃ through washcoating, in order to minimize the head losses. This guarantees, at the same time, a robust design for withstanding the frequent start/stop cycles. The support is characterized by a honeycomb structure (fig. 4.5)

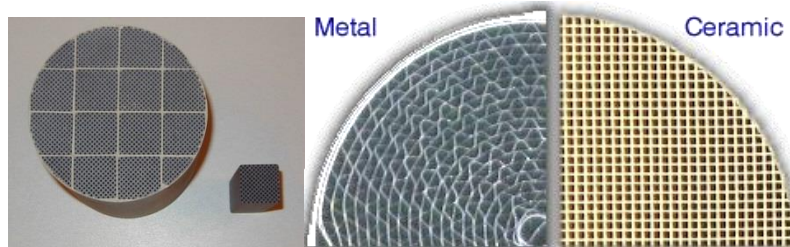


Figure 4.5 – Honeycomb support structure [9]

The metallic housing of the reactor is made out of high-temperature resistant stainless steel with a maximum outer diameter of 3 cm, internal diameter 2.6 cm and a total length of 11.3 cm, properly insulated with Mica, teflon, EPDM or micro-porous material, to prevent any heat losses.

Several reactor layout configurations are commonly available, depending on how the catalyst is positioned respect to the reactor axial dimension (in-out length) [7, 50, 59, 80, 82]. The standard configuration, shown in figure 4.6, considers as follows:

- inert cordierite monolith, uncoated (or foams)
- void space (about 1.5 cm long), it allows to have a good mixing of gas and it prevents the partial occlusion of the channels of the catalytic monolith;
- catalytic monolith (variable). Usually a few grams (e.g. for platinum 5 gram is enough) of active material are deposited over the support through washcoating;
- void space (about 1.5 cm long) with the same function of the void before of catalytic bed;
- inert cordierite monolith, uncoated, which has the function of back heat shield.

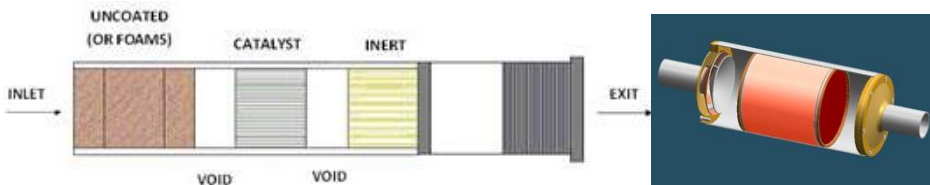


Figure 4.6 – Standard reactor layout configuration [102]

The insulation of the cylindrical reactor can vary depending on the material properties and on the thermal integration. Normally, 10 mm thickness is required.

Upstream and downstream the reactor it is useful to provide a volume of 2-3 reactor diameters, in order to guarantee a proper flow distribution. In fact, in this volume the feeding mixture needs to be distributed along the full section of the reactor; this is also achievable by installing conic fittings or flow conditioning systems, according to the max allowable pressure losses, inlet and outlet diameters. The same is applicable to the reactor outlet.

In this work, the reactor design, as well as the catalyst element and layout configuration, enters in the calculation of the dynamic term, as indicated in paragraph 4.7.

4.7 Dynamic Conditions

The model is configurable for different reactor inlet temperatures and, as stated in par. 4.4, the assumption is that the catalyst is already activated once the air/gas mixture approaches its walls. The common use in CPOx systems is to enable the anode fuel and air only after that the reactor temperature has exceeded a fixed set point, generally over 400-450°C; this is achieved during the startup phase of the system, when the Hot box and stack are heated up by a gas or electrical burner. Theoretically, the reforming reaction could take place even with cold reactor, provided that the ratio between air and methane approaches the stoichiometric combustion ratio (λ tending to 1), but with very slow kinetics and with high risk of catalyst oxidation. The combustion in the preliminary phases would allow reaching the high temperatures needed for lighting up the mixture, and afterwards the λ value can be lowered as the temperature is autothermally maintained.

For what concerns the inlet reactant temperatures, the lower limit corresponds to the ambient temperature. Indeed, it is not strictly necessary a pre-heating of the mixture before entering the reactor, since even at ambient temperature the heat diffusion is achieved by the monolith layers, leading to a slower but feasible ignition. Nevertheless, as shown in the

model results described in chapter 5, in absence of pre-heating the conversion efficiency is lower and the temperature of products exiting the reactor is prevented to reach the desired values. In turn, this leads to work at stack temperatures out of the nominal range, because of the lower temperature of the species entering the anode side of fuel cell.

The dynamic aspect of the model is of vital importance for simulating the transient behavior of the reforming reactor during the fuel cell system operation and on-off cycles. As shown by the experimental test results on 1 kW μ CHP system (see section 3.2.3), during the late start-up phase, when the stack temperature is not yet adequate for the proper electrochemical reaction, the CPOx lambda is higher than during the operation phase. However, even when the startup is over, the lambda can significantly vary with the operating conditions, according to the design parameters set for each phase.

The term kdT/dt enters the energy balance and accounts for the transient response of the system before reaching the steady state.

$$\dot{Q} = \sum_i (\dot{x}_{i\text{OUT}} * H_{fi\text{OUT}} - \dot{x}_{i\text{IN}} * H_{fi\text{IN}}) + k \frac{dT}{dt} \quad (4.46)$$

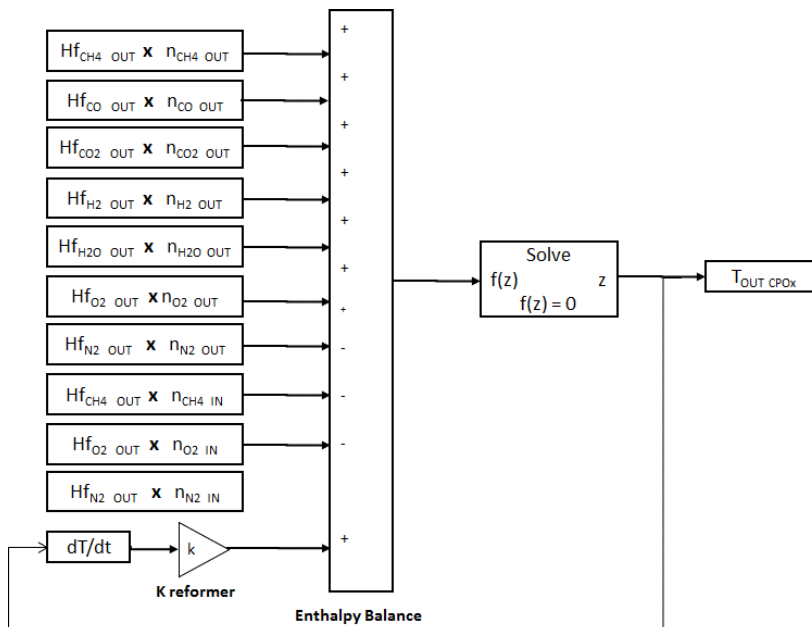


Figure 4.7 – Dynamic model scheme

The scheme representing how the dynamic term is entering the set of final equations is shown in figure 4.7.

The heat capacity of the reactor catalyst, k , is defined as the product of the specific heat, c , by the mass of the catalyst element, m . This in turn is given by the product of the volume, V , per its density, ρ , leading to:

$$k = c \times m = c \times \rho \times V \quad (4.47)$$

By considering a specific heat of 925 J/kgK and a density of 1.38 g/cm³, the calculation yields to a k value of about 31 J/K. Usually, the active metal (Rh, Nickel, Platinum, etc.) is present in very small quantities, approximately 2 to 6 grams.

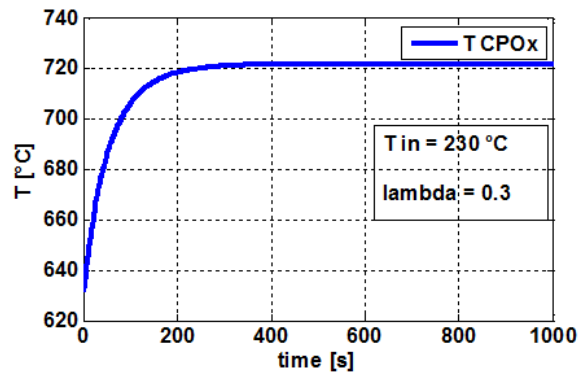


Figure 4.8 – CPOx model temperature output trend

In figure 4.8 the dynamic trend of the reactor outlet temperature, before reaching the stationary value, is shown as yielded on output by the model (inlet fuel 2 Nlpm, current 6 A, T_{in} 230°C and λ 0.29).

Chapter 5

Model Validation and Application

In the following paragraphs the main model results, i.e. chemical and thermal outputs, species selectivity and methane conversion, are shown. These results have been obtained by varying the input parameters, i.e. lambda and inlet reactant pre-heating temperature, in the operating range specified for the application of CPOx reactor in a SOFC system. The model has been validated through the experimental data reported in chapter 3. In addition, the application of the CPOx dynamic model for fault detection and isolation analysis has been evaluated, by taking into account the faults occurred during the tests session.

5.1 - Model results: x_{out} vs T_{out}

The first set of results is achieved by running the model at different lambda to see the effect of the inlet reactant pre-heating temperature on the reactor outlet compositions. The plots report on the x-axis the reactor outlet temperature and on the y-axis the molar outlet compositions. The relation between inlet pre-heating temperature and outlet temperature is also shown for each condition. The simulations are referred to four different lambda values, namely 0.25, 0.27, 0.30 and 0.33, whereas the inlet pre-heating temperature is varied in the range 50 -350 °C.

The analysis of figures 5.1 - 5.4 leads to the following considerations:

- For lambda = 0.25, which is the theoretical optimal value for the CPOx oxidation, the reactor outlet temperature exceeds 700°C only when the pre-heating temperature is very high (350 °C). For lower inlet reactant temperatures, a low lambda does not promote the auto sustaining of CPOx reaction and prevents the stack from reaching the required operating temperatures. Furthermore, the CH₄

conversion is reduced. Thus, working with a lambda of 0.25 does not represent the optimal condition from a thermal point of view. Indeed, it is possible to yield the maximum hydrogen gain, approaching the theoretical reaction efficiency, only for a very high pre-heating temperature. In different conditions, the inlet methane is only partially converted and the residual CH_4 molar fraction is still high. The trend of H_2 concentration (magenta line) shown in figure 5.1 increases with temperature.

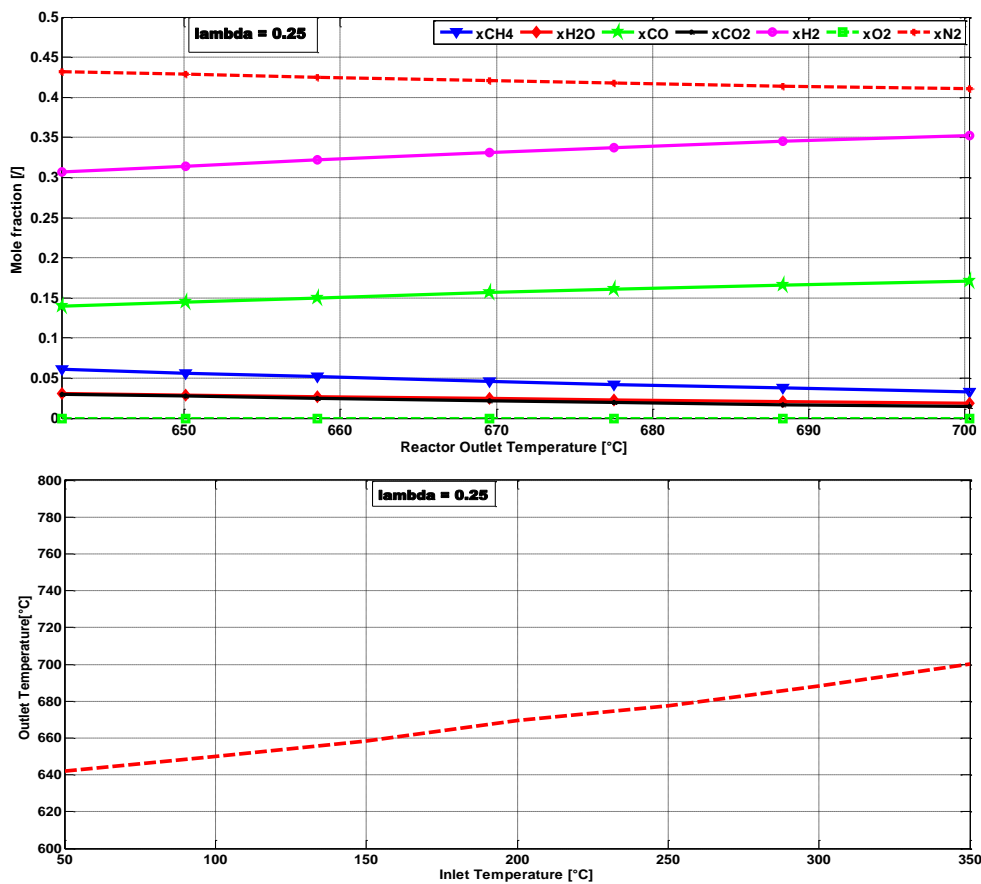


Figure 5.1 – x_{out} vs T_{out} and T_{out} vs T_{in} for $\lambda=0.25$

- Theoretically, as shown in the following figures achieved for higher lambda, the H_2 gain should reach a maximum value, beyond which

the hydrogen is no longer produced. In the plot, it is clear that, for the limit temperature on the x-axis of 700°C, this maximum is not reached yet, and with higher pre-heating temperature (over 350 °C) it would be possible to approach H₂ concentrations around 38%. On the other hand, such conditions for the pre-heating of the reactant mixture are difficult to execute and out of the design specifications, as explained in chapter 2 and 3, reason why they are not taken into account in this analysis.

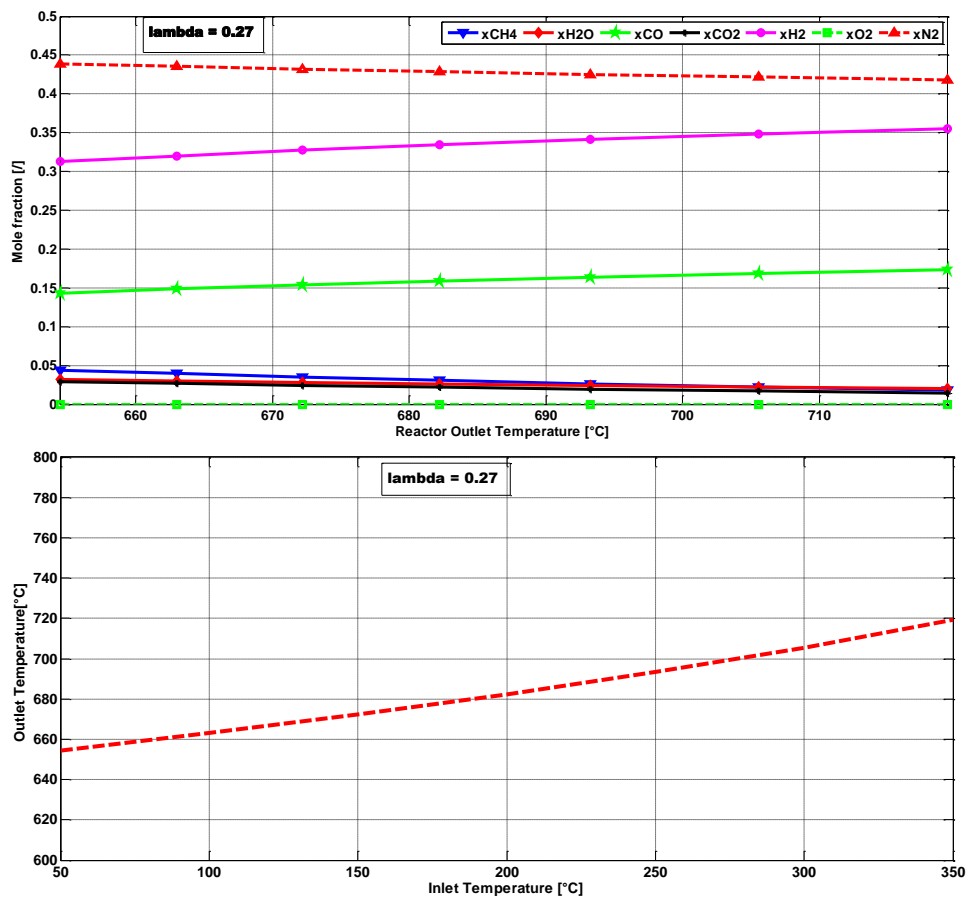


Figure 5.2 – x_{out} vs T_{out} and T_{out} vs T_{in} for $\lambda=0.27$

- The best condition is achieved for a λ of 0.30, figure 5.3. Indeed, in this case the H₂ molar fraction is approaching the

maximum yield (the magenta line is stabilizing around 35%) when the reactor temperature exceeds 720 °C, corresponding to a reactant pre-heating temperature of around 200 °C. The methane is almost completely converted. The same result can be obtained also with a lambda of 0.27 (figure 5.2). In this condition, in order to yield sufficient reactor outlet temperatures, the pre-heating temperature shall be increased over 300 °C, which is more critical for the thermal design of the system.

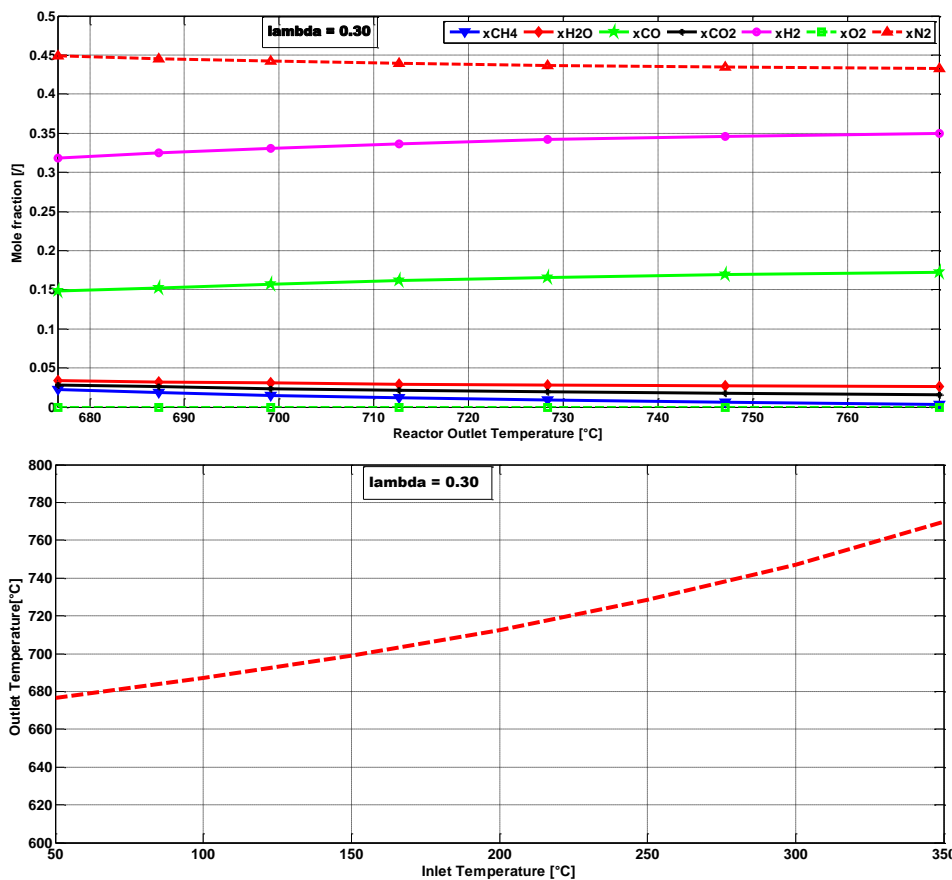


Figure 5.3 – x_{out} vs T_{out} and T_{out} vs T_{in} for $\lambda=0.30$

- For $\lambda = 0.33$, figure 5.4, the H_2 yield is lower than other conditions, even if the conversion of CH_4 is higher. Simultaneously, the reactor outlet temperatures are too high (more than 860 °C for a

pre-heating temperature of 350°C), which implies that this condition is suitable only in the late startup phase, when there is the need to heat up the reactor in order to reach the most suitable conditions.

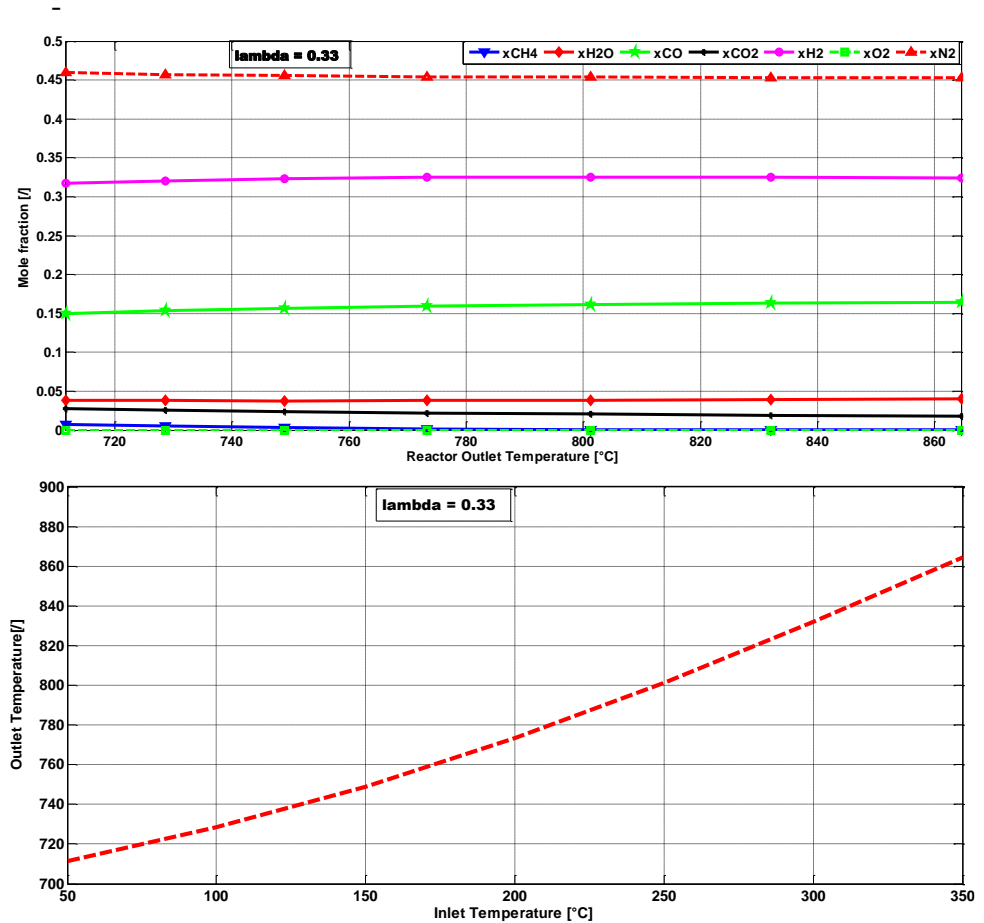


Figure 5.4 – x_{out} vs T_{out} and T_{out} vs T_{in} for $\lambda=0.33$

5.2 - Model results: λ vs T_{out}

The second set of results is obtained by varying the λ in the range 0.25 -0.35, at fixed reactant pre-heating temperatures, in order to evaluate the effect of working at different λ on the outlet temperature and

compositions. Simulations have been carried out at four inlet pre-heating temperatures, namely 50 °C, 150 °C, 230 °C and 300 °C. For each condition, both plots of outlet compositions and CPOx reactor temperature over lambda are shown below (Fig. 5.5 - 5.8).

The analysis of figures 5.5 - 5.8 leads to the following considerations:

- when the reactant pre-heating contribution is small ($T_{in} = 50^{\circ}\text{C}$), the reaction occurs at non optimal temperatures when the lambda is below 0.32; this leads to a lower H_2 and CO outlet yield, resulting in an overall lower conversion efficiency. It would hence be necessary to set a lambda in the range 0.33-0.35 in order to get the maximum selectivity, but also in this case the outlet molar fractions are below the expected margins.

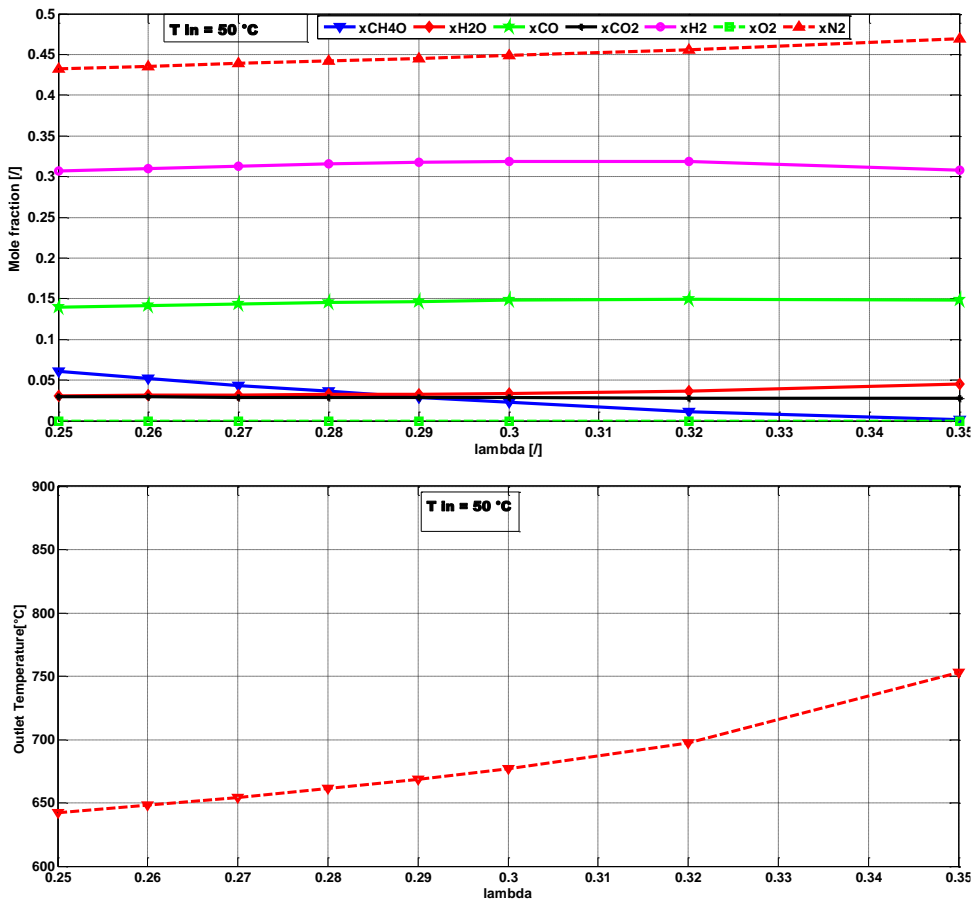


Figure 5.5 – x_{out} vs λ and T_{out} vs λ for $T_{in}=50^\circ\text{C}$

- Working in the intermediate conditions ($T_{in} = 150^\circ\text{C}$ and $T_{in} = 230^\circ\text{C}$) with λ of 0.29-0.31 represents the best option for a CPOx reactor operation. In fact these parameters allow operating at an adequate reactor temperature, in the range $680\text{-}750^\circ\text{C}$, with high efficiencies and $\text{H}_2\text{-CO}$ selectivity.

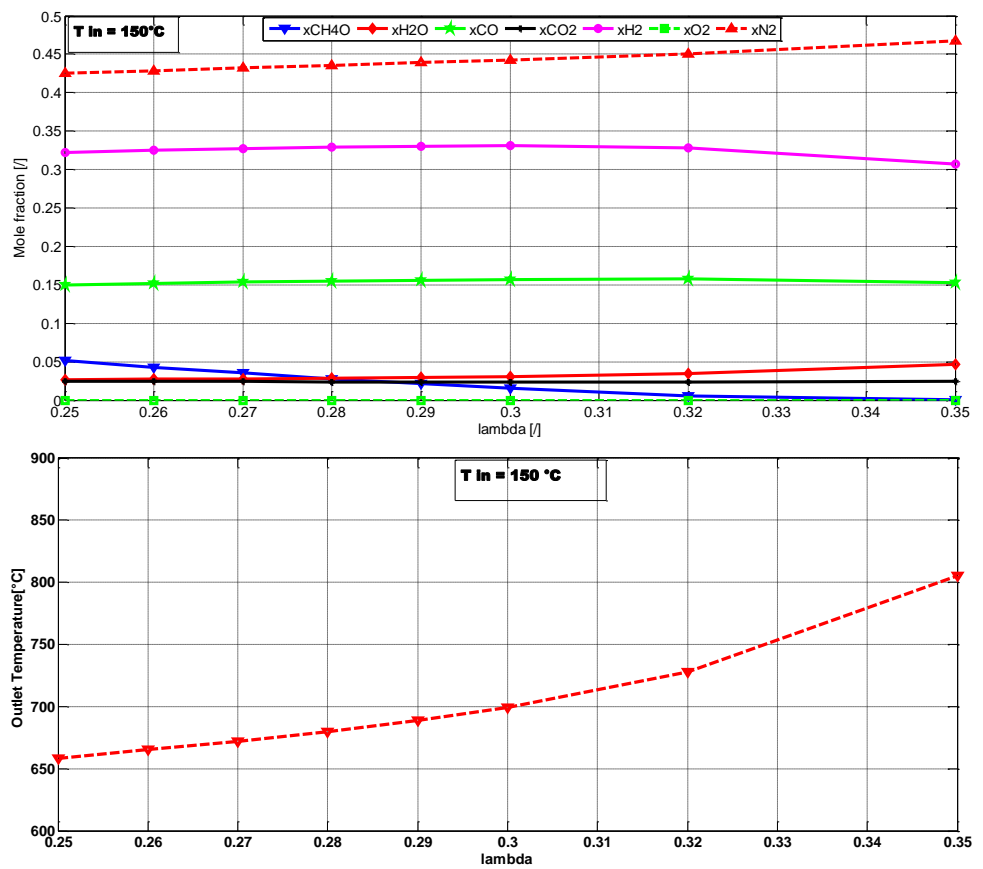


Figure 5.6 – x_{out} vs λ and T_{out} vs λ for $T_{in}=150^\circ\text{C}$

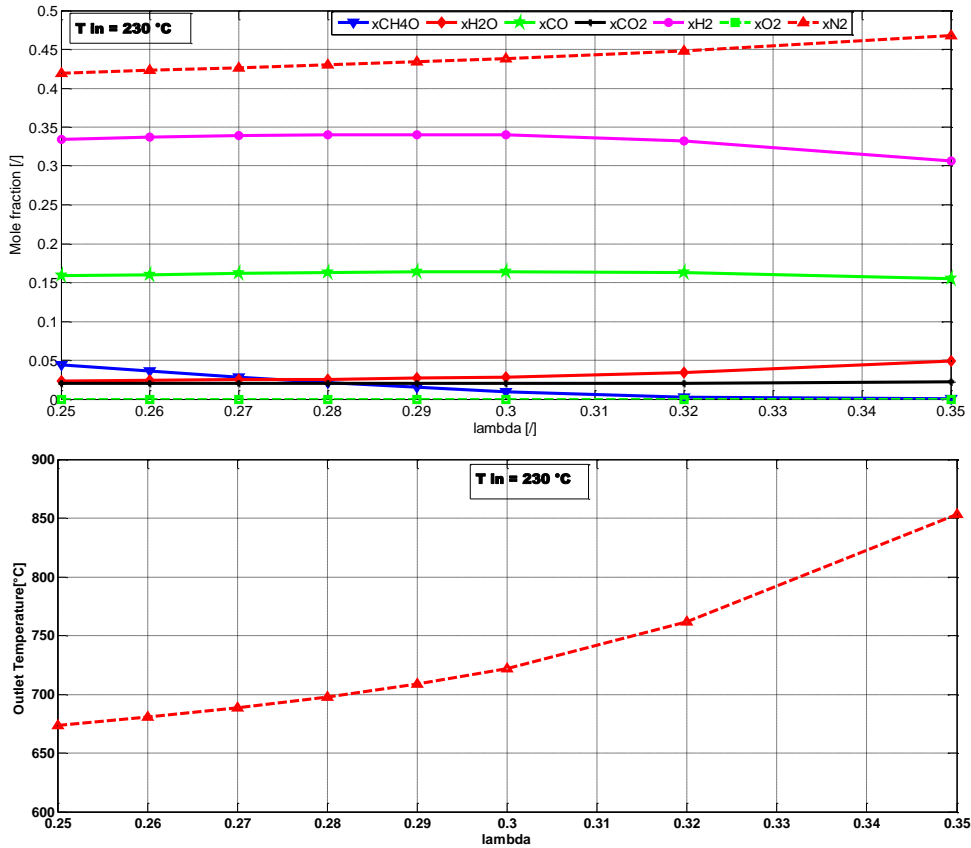


Figure 5.7 – X_{out} vs λ and T_{out} vs λ for $T_{in}=230^\circ\text{C}$

- To a higher reactant pre-heating temperature ($T_{in} = 300^\circ\text{C}$) corresponds the maximum H_2 and CO gain, up to a λ of 0.3. Beyond this value, it is not worthy working with both high pre-heating temperature and high λ . Indeed, the outlet H_2 and CO concentrations decrease and in addition the reactor temperature reaches dangerous values, close to 900°C for a λ of 0.35.

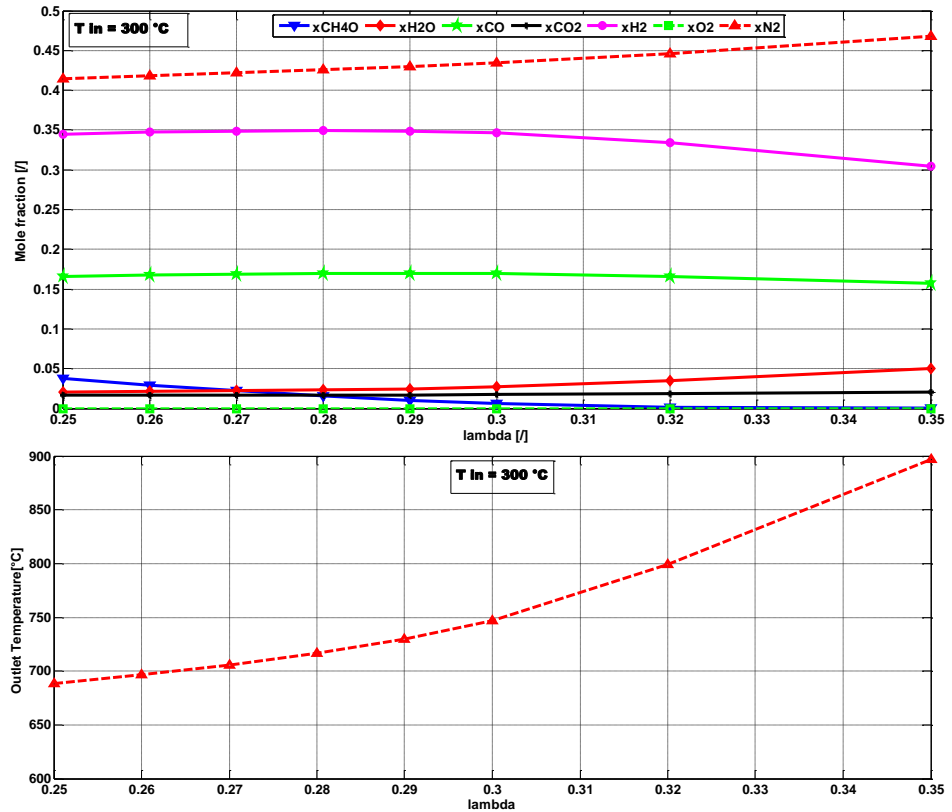


Figure 5.8 – x_{out} vs lambda and T_{out} vs lambda for $T_{in}=300\text{ }^{\circ}\text{C}$

5.3 - H_2 , CO Selectivity and CH_4 conversion

Other relevant outputs of the model, not directly entering in the final set of equations but directly computable starting from the products outlet compositions, are the H_2 and CO selectivity and the CH_4 conversion. These parameters are well suited to properly describe the efficiency of a CPOx reaction and give immediate indication about the optimal variables range. Indeed, the general trend is to define the enhanced operating conditions at which the fractional conversion is more than 0.99, while the durability of the reformer system is guaranteed [8].

The methane conversion, H_2 and CO selectivity are defined as

follows:

$$CH_{4conv} = (\dot{n}_{CH_4 in} - \dot{n}_{CH_4 out}) / (\dot{n}_{CH_4 in}) \quad (5.1)$$

$$H_{2sel} = (\dot{n}_{H_2 out}) / [2 \times (\dot{n}_{CH_4 in} - \dot{n}_{CH_4 out})] \quad (5.2)$$

$$CO_{sel} = (\dot{n}_{CO out}) / (\dot{n}_{CH_4 in} - \dot{n}_{CH_4 out}) \quad (5.3)$$

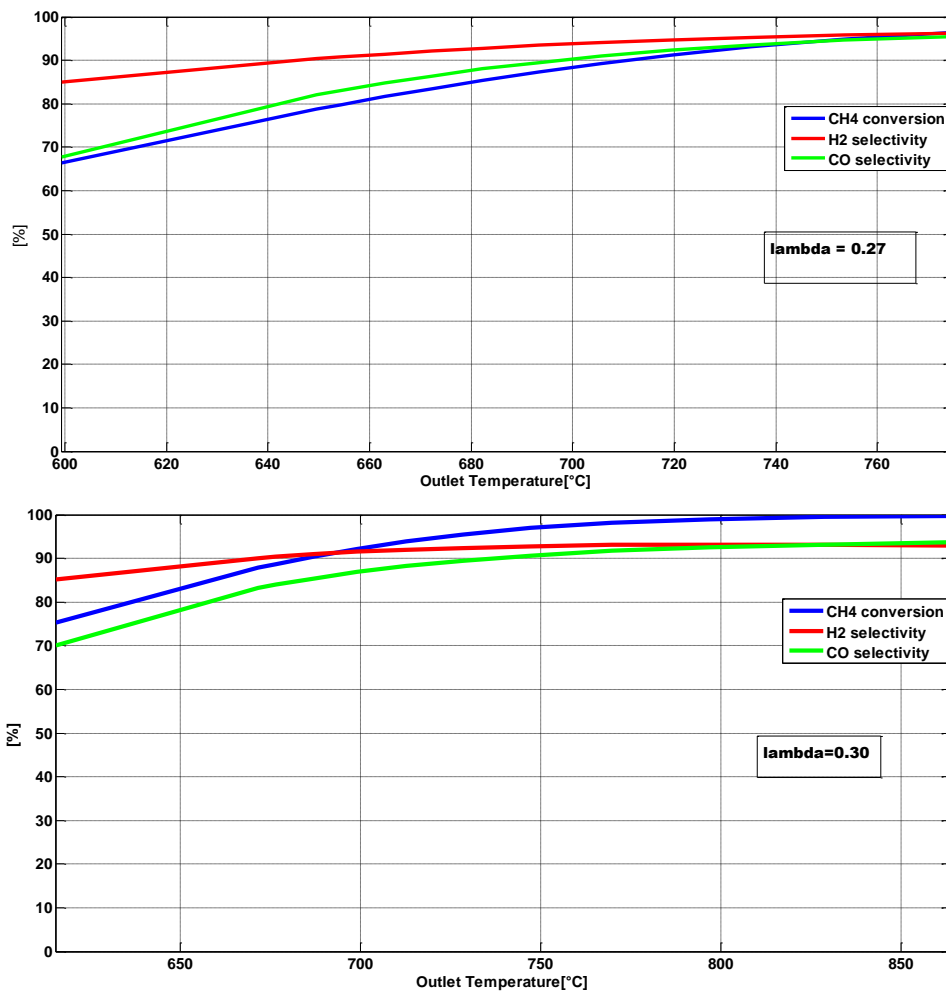


Figure 5.9 CH₄ conversion, H₂ and CO selectivity vs for T_{out} different lambda

Figure 5.9 shows the methane conversion, H₂ and CO selectivity for fixed lambda values (0.27 and 0.30) and variable reactant pre-heating temperature. The x-axis reports the reactor temperature. On the other hand, figure 5.10 represents the variation of the above mentioned parameters with respect to lambda, for two fixed preheating temperatures (50 °C and 230 °C).

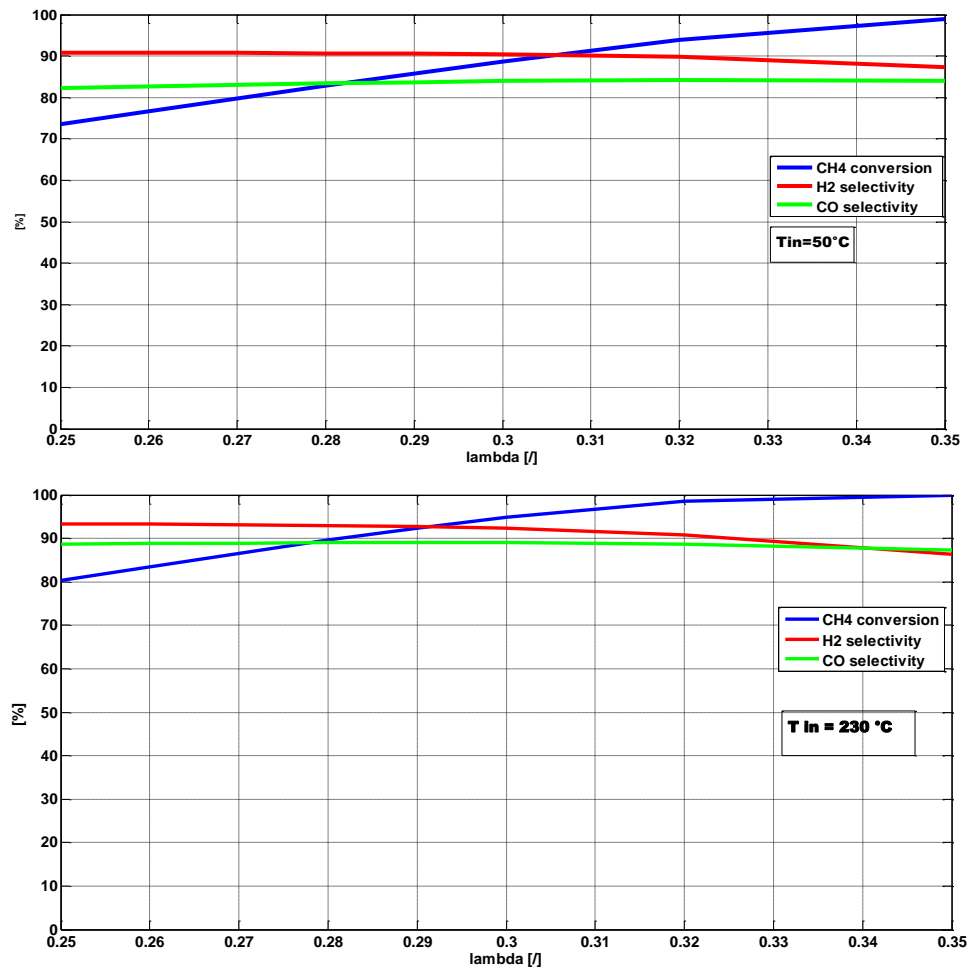


Figure 5.10 CH₄ conversion, H₂ and CO selectivity vs lambda for different reactant pre-heating temperature

Figures 5.9 and 5.10 indicate that the H₂ yield decreases with lambda, resulting in a lower quality of the reformat exiting the reactor.

The maximum H₂ gain, for each inlet reactant pre-heating temperature, corresponds to the theoretical maximum value of $\lambda = 0.25$. The CO selectivity trend is decreasing with λ as well, even if less markedly than H₂, and increases with the pre-heating temperature. It can also be noted that raising the inlet temperature of the reactants improves the CH₄ conversion, and the same happens for high values of λ . The optimal conditions mentioned in the previous paragraphs, which are λ in the range 0.29-0.30 and a reactor outlet temperature within 680-750°C, correspond to values of CH₄ conversion above 95% and H₂, CO selectivity are both over 90%.

5.4 Model validation

The CPOx model was validated through the experimental data reported in chapter 3. As shown in the figures 5.11 -5.17, the simulation results follow accurately the test outcomes for each operating condition and well reproduce the real reaction mechanisms occurring in a CPOx reactor, either integrated in a SOFC Hot Box or external and heated up by electrical resistances (section 3.2.1-3.2.3). At high pre-heating temperatures, the model becomes less accurate for high λ values, over 0.5, which are however far enough from the useful range of parameters typical of a catalytic partial oxidation reaction, as described in chapters 2 and 3. This can be explained considering that by increasing both λ and the inlet preheating temperature, the conditions inside the reactor promote the total oxidation with respect to the reforming reaction. The model is not developed to follow operating conditions close to the combustion regime, for which the initial temperature set as starting point for the numerical resolution of the non-linear set of equation should be changed accordingly. Same is valid for the initial solutions represented by the outlet concentrations. Therefore, in order to reproduce the proper system operating for λ approaching the combustion reaction values, it is necessary to adjust the initial conditions inside the model.

5.4.1 - Comparison with experimental data of tests case a (ref. section 3.2.1)

In section 3.2.1, the tests performed by the CPOx reformer manufacturer Hysytech and by the Hot Box integrator SOFC Power have been described. The outcomes of these tests, indicated as test case a, have given useful data for the comparison with the model results. Figure 5.11 reports the comparison between simulated and measured outlet compositions for different reactor outlet temperatures. As may be seen in Table 5.1, the deviation between real and simulated products concentrations is always below 5%, for each reactor outlet temperature, being higher for the species whose molar fraction is lower. Indeed, CO₂, CH₄ and H₂O outlet concentrations tend to zero as long as the reactor temperature increases, therefore the error is higher due to a lower order of magnitude of both measured and simulated values. Figure 5.12 shows the correlation between experimental data and model results.

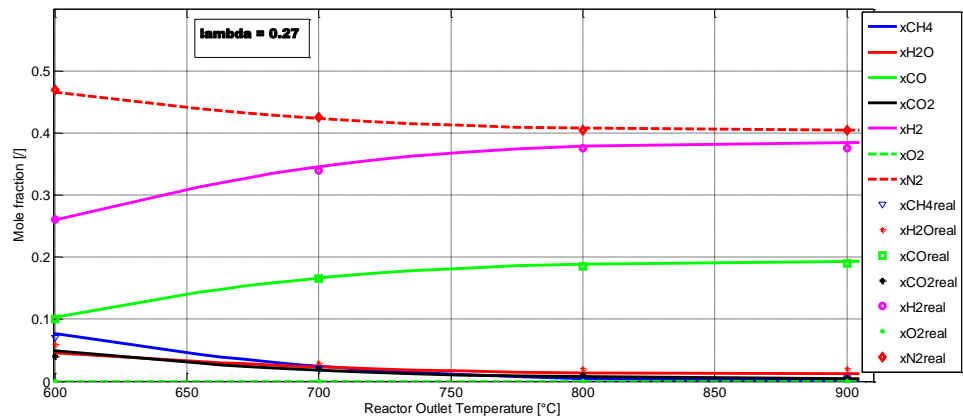


Figure 5.11 – x_{out} vs T_{out} for $\lambda=0.27$: comparison with real data (test case a)

Table 5.1 – Deviation between experimental and model results for $\lambda=0.27$

T	error H2%	error CO%	error CO2%	error H2O%	error CH4%	error N2%
600	1,7	3,0	4,2	1,3	2,8	1,2
700	2,1	3,0	4,9	4,3	2,8	1,9
800	2,0	2,9	4,8	2,3	4,9	0,8
900	2,0	1,9	4,9	4,6	3,1	1,0

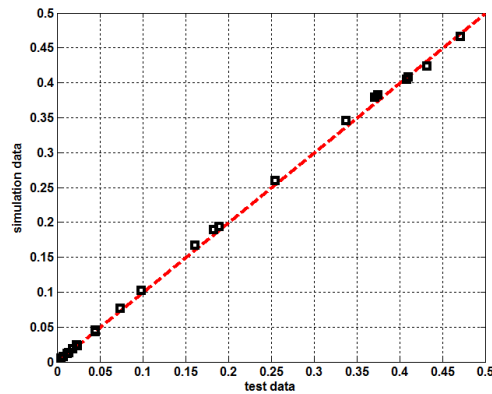


Figure 5.12 – Correlation between experimental and model results for $\lambda=0.27$

Similar conclusions can be drawn for a λ of 0.30. As may be observed in figure 5.13 and 5.14, the deviation is below 1% when comparing species whose molar fraction is higher, such as N_2 and H_2 . On the contrary, the error becomes higher when moving to lower order of magnitude.

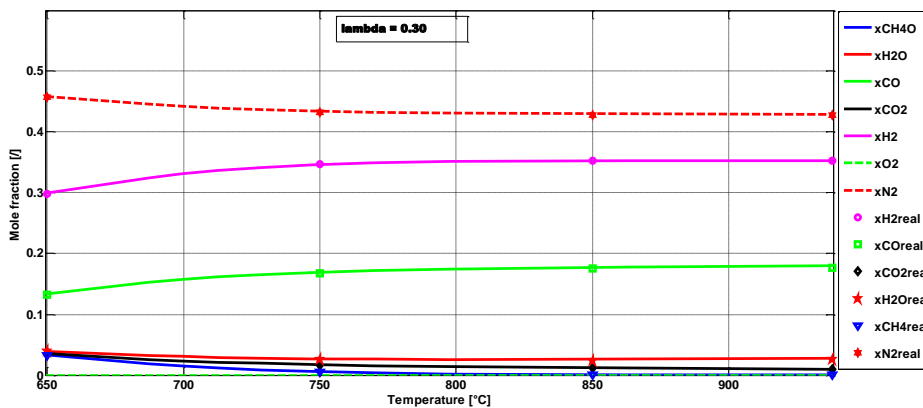


Figure 5.13 – x_{out} vs T_{out} for $\lambda=0.30$: comparison with real data (test case a)

Table 5.2 – Deviation between experimental and model results for $\lambda=0.30$

T	error H2%	error CO%	error CO2%	error H2O%	error CH4%	error N2%
650	0,3	1,2	4,1	0,7	2,8	0,2
750	0,3	1,1	4,6	4,2	4,3	0,3
850	0,4	0,7	4,1	4,3	3,9	0,2
950	0,6	2,0	4,6	3,7	4,5	0,2

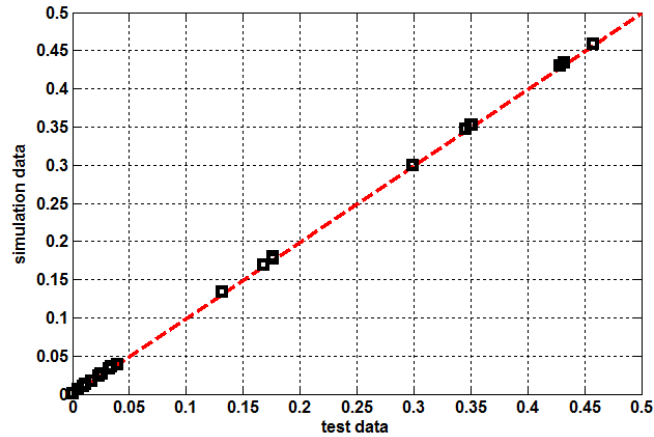


Figure 5.14 – Correlation between experimental and model results for $\lambda=0.30$

In order to analyze the accuracy of the model in reproducing the relationship between inlet pre-heating temperature and the reactor temperature, a comparison has been made with the experimental data reported in figure 5.15 (black squares). These data were measured by SOFC Power for the integrated Hot Box configuration, with the CPOx reactor thermally integrated within the stack module. The tests were performed at a λ of 0.29. Figure 5.15 reports the comparison between the experimental data and the model outputs for the same λ . The correlation appears extremely accurate for temperatures up to 200 °C, whereas the simulated outlet temperature slightly exceeds the measured one for the last point (temperature over 200 °C).

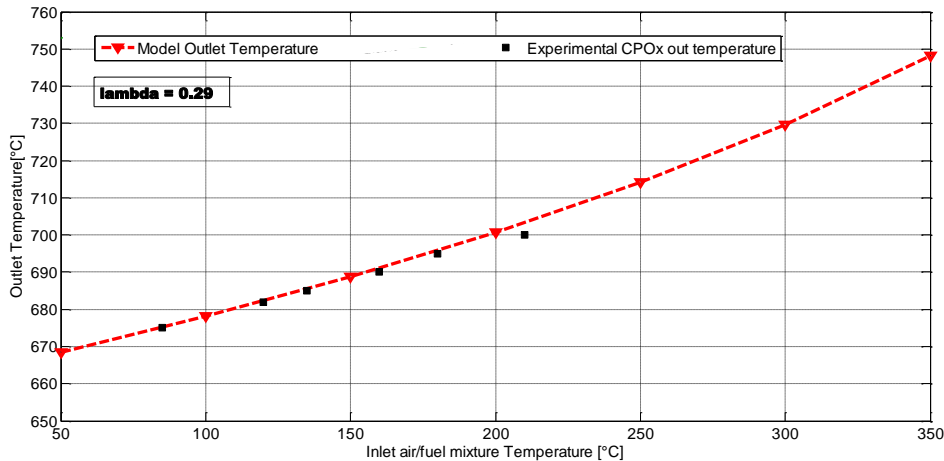


Figure 5.15 – T_{out} vs T_{in} for $\lambda=0.29$: comparison with real data

The model validation with experimental results referred to the test case a can be concluded by considering the experimental results given by Hysytech and reported in table 3.2 of section 3.2.1. This table, here reproduced and indicated as table 5.3, reports the equilibrium composition and adiabatic reaction temperature for different λ and with same pre-heating mixture temperature.

Figure 5.16 reports the model results at the same reactant inlet temperatures (230 °C), for different λ , together with the experimental data included in table 5.3. They are depicted through black markers, different for each λ (triangle, square and right arrow respectively for λ of 0.25, 0.27 and 0.30).

Table 5.3 – Test measurements for different λ at $T_{in} = 230^{\circ}\text{C}$ [36]

λ	$T_{in} = 230^{\circ}\text{C}$						T_{out}
	CH4	CO	CO2	H2O	N2	H2	
0.25	4,4%	15,65%	2%	2,36%	42%	33,42%	673,5
0.27	2,80%	16,16%	2%	2,52%	42,65%	33,87%	688,71
0.3	1%	16,39%	2%	2,85%	43,78%	33,97%	721,77

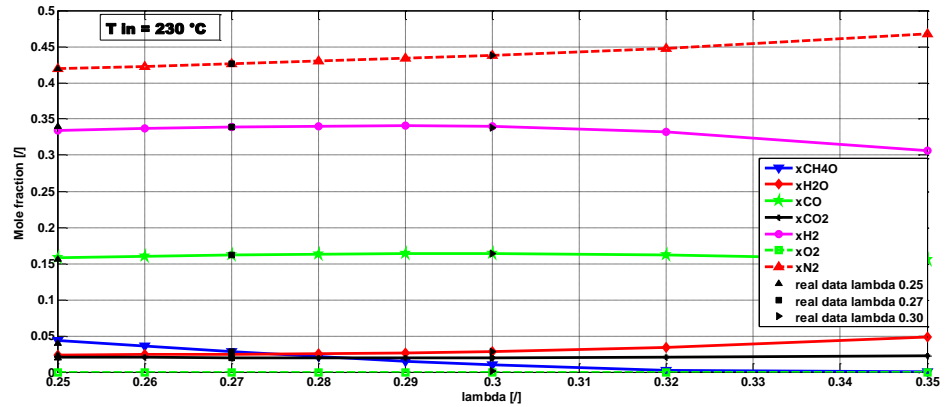


Figure 5.16 – x_{out} vs lambda for $T_{in}=230^{\circ}\text{C}$: comparison with real data

The products molar fractions well fit the experimental measurement for each operating condition.

5.4.2 - Comparison with experimental data of tests case b (ref. section 3.2.2)

The experimental data available for the model validation in test case b are shown in section 3.2.2. They were taken from tests on the CPOx reactor performed by Environment Park at Hysylab. In this case, as explained in section 3.2.2, a fair simulation was not possible because of the different catalyst reactor design with respect to what implemented into the model. Moreover most of the experiments were carried out at high lambda (0.4 and 0.5), which are operating conditions not suitable for real on-field use with SOFC systems; only two sets of measures, taken at lambda of 0.29, are adapt to be reproduced by the model. To further evaluate the accuracy of the model developed, a comparison analysis was done for such tests with different inlet fuel flow rates (see table 5.4).

Table 5.4 – Comparison between model and test results on CPOx reactor external to Hot Box

	Fuel input [kW]	lambda	Tout [°C]	H2 [%]	CH4 [%]	CO [%]	CO2 [%]	N2 [%]	H2O [%]
Model	0,8	0,29	672	32	2	14	2	44	3
Test	0,8	0,29	677	26	5	14	1,5	53	NA
	Fuel input [kW]	lambda	Tout [°C]	H2 [%]	CH4 [%]	CO [%]	CO2 [%]	N2 [%]	H2O [%]
Model	1,2	0,29	700	33	2	17	2	44	2
Test	1,2	0,29	690	30	4	18	1	47	NA

The temperature measurement at the middle of catalyst reactor is comparable with the simulated values for similar input conditions (considering an external reactor temperature of 700°C), whereas the products compositions are slightly different. The residual CH₄ was quite higher respect to the model results and also to the other tests results shown in sections 3.2.1 and 3.2.3. This may be caused by a poor active surface of the catalyst that was not sufficient to convert part of the CH₄ for that lambda. Also, the outlet H₂ molar fraction was slightly below the expected target for the nominal operating conditions. It is worth to remark that the results of the experiments for that catalyst configuration motivated a new design with a higher active surface. Such a new design was then adopted for the CPOx reactor installed in the final μ CHP prototype. The higher conversion activity of this catalyst is confirmed through the results shown in section 3.2.3.

The reasons for the mentioned discrepancies between the tests results here described and the experimental data measured for the μ CHP and integrated HB tests, and with respect to the model as well, are as follows:

- The reactor was warmed up instantaneously by electrical resistances, and the same is valid for the pre-heating of reactant gases. This did not allow a complete and homogenous heating of the whole reactor, as confirmed by the marked differences in the surface temperature in both active area and upstream/downstream

the catalyst. On the other hand, when the reactor is thermally integrated inside the Hot Box, the reactor is activated gradually during the startup and maintained at operating temperature by means of a proper insulation and engineered thermal integration.

- The adiabatic temperature calculated by the model is comparable with the T_{mid} of experimental tests, measured at the center of reactor, as shown by figure 3.11 in section 3.2.2. In the same figure, it is possible to note that the T_{up} , measured at reactor outlet, downstream the catalyst surface, is slightly lower as it reflects the decrease in temperature led by the cooling suffered by the products exiting the reactor. In the model, due to the adiabatic hypothesis, this aspect is not taken into account.
- During tests, the H_2O outlet concentration of the outlet products was not measured. Indeed, the products exiting the reactor flowed first through a condenser where the H_2O was separated and after were conveyed to the gas chromatographer. This is because the gas chromatographer measured the dry gas.
- The methane used for the tests had high purity and thereby no desulphurizers were needed.

5.4.3 - Comparison with experimental data of tests c (ref. section 3.2.3)

The most interesting tests for characterizing the performance and diagnostics of a SOFC based application are those carried out on the μ CHP prototypes realized as milestone of the EFESO project, described in section 3.2.3. As recalled in chapter 3, the final aim of EFESO project was to design, assemble and test on field four μ CHP units, thereby tests on the single components were all finalized to check individually the correct operation and functionalities of the subsystems before their assembling in the final prototype. By exploiting the experimental data of test case a (section 3.2.1) and b (section 3.2.2), the model has been validated in steady

state conditions, as explained in sections 5.4.1 and 5.4.2. It was assumed that the transient phase was already completed when comparing the measured reactor temperature with the CPOx model result obtained for each lambda and reactant inlet temperature. On the contrary, the tests on the final μ CHP (section 3.2.3) were extremely useful to characterize and validate the dynamic model in the transient states. When testing the μ CHP, the target was to reproduce the real conditions which are likely to occur when the unit is installed for residential application use. The fuel cell stack was therefore stressed to evaluate the electrical performance of the SOFC system (power and efficiency). The phase when the electrical current is progressively raised from zero (idle state, stack operating in open circuit voltage) to 9 A goes under the name of “power ramp up” phase. It is shown in figure 5.17 and lasts approximately 40 minutes, from minute 250 to about 290. When stepping up the current, and therefore the electrical power, the complete variations of fuel cell inputs, relevant parameters and outputs are shown in section 3.2.3, figures 3.15 – 3.17, whereas the trend for some of them is here reproduced, in figures 5.18 and 5.19.

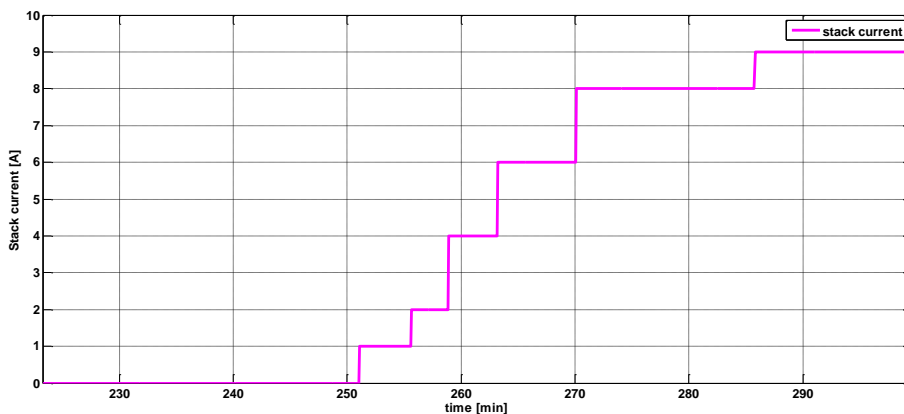


Figure 5.17 – stack current vs time in μ CHP power ramp-up phase: measured data

The plots in figures 5.18, 5.19 and 5.20 show respectively the trend of cathode air flow, anode air and fuel flows and lambda and during the power ramp up phase. It is useful recalling that, in the figures legend, the term PV indicates present value, which is the current value measured by the system sensors, whereas SP stands for Set Point, that is what has been fixed in the tuning and design phase. The set points for the SOFC unit

startup and operation phases are reported in table 3.4 (section 3.2.3). By displaying both information for the same parameter, it is possible to detect when a fault or an abnormal behavior is occurring, as ascertained for both fault scenarios described in par. 3.3.

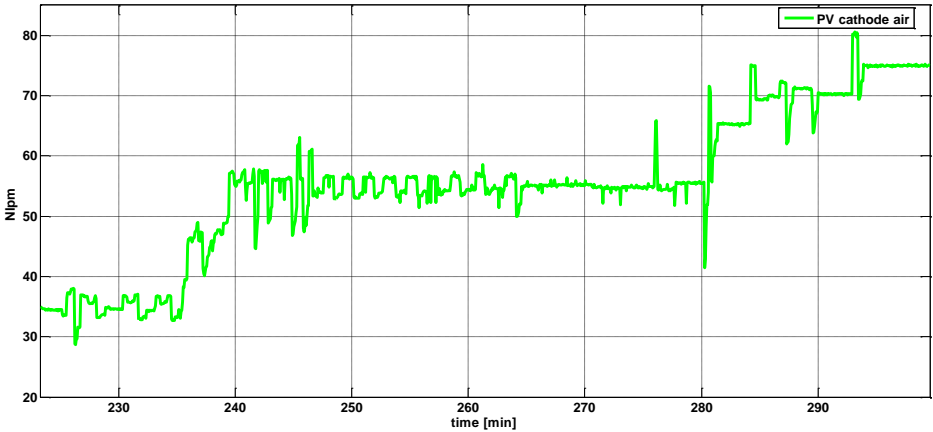


Figure 5.18 – cathode air flow vs time in μ CHP power ramp-up phase: measured data

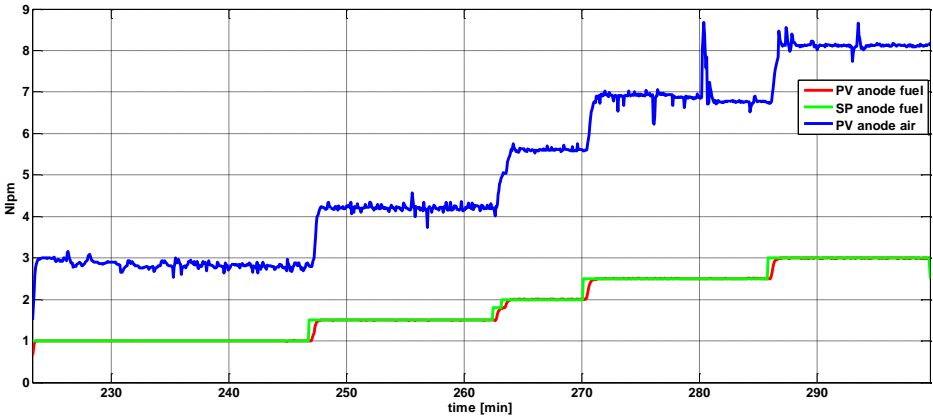


Figure 5.19 – anode fuel and air flow vs time in μ CHP power ramp-up phase: measured data

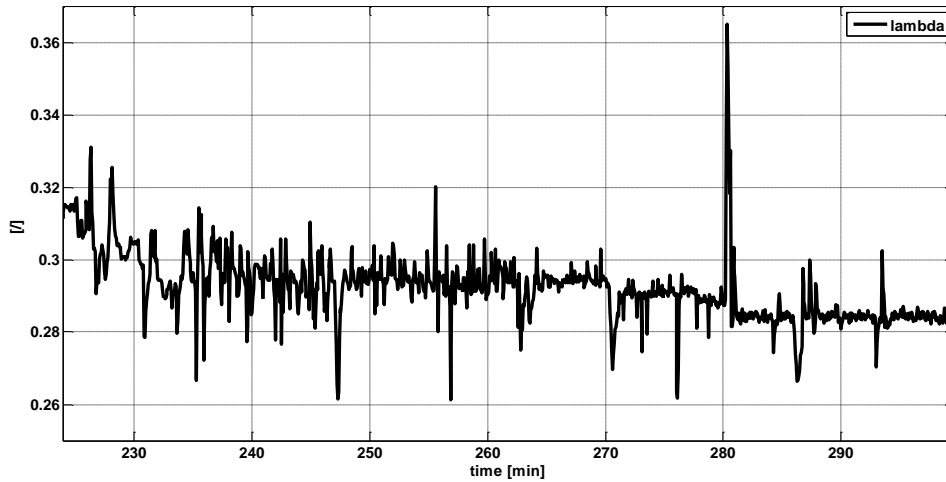


Figure 5.20 – lambda vs time in μ CHP ramp-up phase: measured data

In order to evaluate the dynamic application of the model and validate its transient results, during the tests the CPOx reactor temperature and its dynamic trend were measured for each condition. The information about molar flows at reactor outlet did not enter in this analysis, because the purpose of the tests was to evaluate the thermal and electrical performance of the unit without focusing on the molar gas composition entering the fuel cell. Only the composition of the discharge flue was measured at the system exhaust, to check whether the emissions were within the acceptable values and compliant with the international standards.

This dynamic trend of CPOx reactor outlet temperature was properly and accurately followed by the model, as might be observed in figure 5.21. The red line represents the temperature measured on the CPOx reactor through a contact thermocouple, whereas the blue line is the transient behavior of the model when the operating conditions vary and switch from one set point to the consecutive. For the entire power ramp up phase, the dynamic trend given by the model before reaching the steady state value is compared with the transient time measured in the real system. The dynamic validation is possible only for positive gradients (temperature raising during the power ramp up), due to the hypothesis of adiabatic CPOx model. Hence, the power ramp down phase and the cooling phases described by decreasing temperature (e.g. from minute 238 to minute 247

of figure 5.21) are not simulated. This explains why the simulated T_{CPOx} , blue line in figure 5.21, is not shown in the cooling phase intervals.

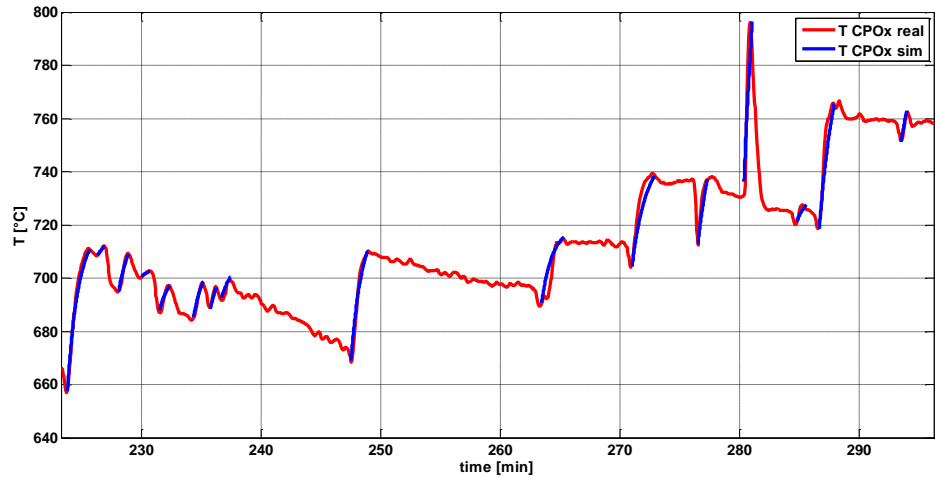


Figure 5.21 – T_{out} vs time in μCHP ramp-up phase: comparison between measured and simulated transients

An analysis of the test results is already given in section 3.2.3. However, here additional considerations are given, with a focus on the behavior of the system in transient times. By analyzing the trends of reactor outlet temperature, lambda and the anode flows (Fig. 5.19 – 5.21), it might be seen that the starting point for the graphs corresponds to the late startup phase (minutes 220 – 230). During the system startup, a conventional gas burner is ignited and utilized to warm up the system, making the temperature suitable to enable the anode fuel and air flows. Indeed, the CPOx reactor shall be activated before feeding it with the air/fuel inlet mixture, and this is achieved through the Hot Box enclosure warm up brought by the startup burner. As reported in table 3.4 (section 3.2.3), in order to proceed with the transition from startup to operating phase, it is also required that the stack temperatures exceed 700°C , to activate the electrolyte placed between cell anode and cathode. In the late startup phase, the startup burner is shut off, the anode air and fuel valves are enabled and the reactor temperature, together with the stack operating temperatures, starts to increase, even if no power is drawn from the stack. In figure 5.20 it may be observed as the initial lambda set point is higher than the optimal values (0.29-0.30). Indeed, as already explained, as soon as the reactor is

enabled, the lambda holds at high values, around 0.4, to promote the combustion reaction over the reforming one, as the target here is to heat up the system rather than enhancing the H₂ conversion. The lambda is then progressively reduced, by decreasing the anode air as long as the reactor temperature stabilizes over 650°C. After this initial assessment phase, when the stack temperatures have reached a certain stability, it is possible to start the power ramp up phase and draw current from the stack. The average lambda oscillates around 0.30 up to minute 270 (current 6A), except for some outliers and undesired peaks which are due to the hysteresis of anode fuel and air valve opening control. Each step in current, variation in air/fuel flowrates and cooling air has effects on the reactor temperature, and these are properly reflected by the model. The reactor temperature in this phase never exceeds 720°C. After minute 270, the air and fuel flow are increased and, in turn, the current is raised to 8 A. The lambda is further reduced (0.29-0.285) to account for an increase in the hydrogen selectivity and fuel cell electrical efficiency. Around minute 280, an uncontrolled opening of air valve leads to an increase in the anode air present value and thereby lambda. This causes a peak in the reactor temperature, which is accurately chased by the simulated results. It is worth to remark that the temperature peak has a time delay, which is properly simulated by the dynamic model. The cathode air is hence increased to reestablish the operating conditions held before this event. At minute 285, the last phase of ramp up is characterized by a rise in the anode air and fuel flowrates and a further reduction in lambda (to 0.282), with the aim to move closer to the nominal operating conditions. The stack power in this case is approaching 500W. The CPOx reactor temperatures has a considerable boost to over 760°C. This is the last step taken before starting the power ramp down phase and complete the electrical cycle. The operating parameters are then progressively decreased, following the same but reverse steps of the ramp up phase, until the μ CHP unit is brought to the standby operating mode (generating only power needed for the auto-sustaining).

5.5 - Fault 1- Carbon deposition: model based fault detection and isolation

In order to prove the feasibility of the model to simulate and detect faults likely to occur in a CPOx reactor, the faults experienced in the experimental test session have been investigated. Herein the carbon deposition event described in paragraph 3.3.1 has been taken into account. Figure 5.22 shows the detection of the fault, occurring around minute 261. The anode fuel flowrate and lambda trends show a considerable change in the current operating conditions (PV) with respect to the design ones (SP).

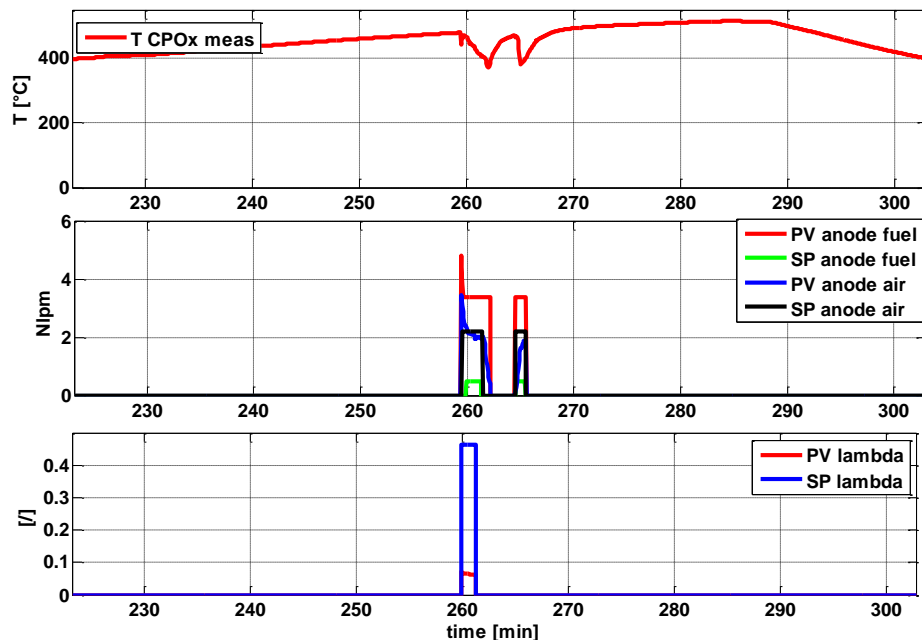


Figure 5.22 – Fault 1 detection: T_{CPOx} , anode air and fuel flows, lambda vs time

As soon as the fault occurred, the excessive anode fuel flowrate led to a remarkable decrease in the CPOx temperature, visible around minute 263. A detailed description of the plots reported in figure 5.22 is already given in chapter 3.3.1.

After the fault has occurred, it is possible to evaluate the ability of

the model to isolate this event and identify its magnitude. Indeed, in the μ CHP startup afterwards the fault event, the CPOx temperature shows a trend different from the nominal conditions, as confirmed by figure 3.22 (section 3.3.1) and figure 5.23 reported below. It is evident that the reforming system was not behaving properly and its performance were below the expectations. When the model is used to evaluate the output results for the same input conditions, it is possible to compare the simulated reactor temperature with the measured one and analyze their trends (temperature plot in figure 5.23). It can be noted that the measured temperature (red line) is indicating an abnormal behavior of reforming reactor; on the contrary, the simulated temperature (blue line) is properly representing the nominal operating conditions, which the system would have achieved if no fault had occurred. The deviation between real and simulated CPOx reactor temperatures is approximately 300 °C up to minute 450, whereas it reduces between minutes 460 and 580, when anode air and fuel flowrates are increased. The ability of the model to determine the theoretical trend of CPOx outlet temperature corresponding to the given set points enables the fault diagnosis.

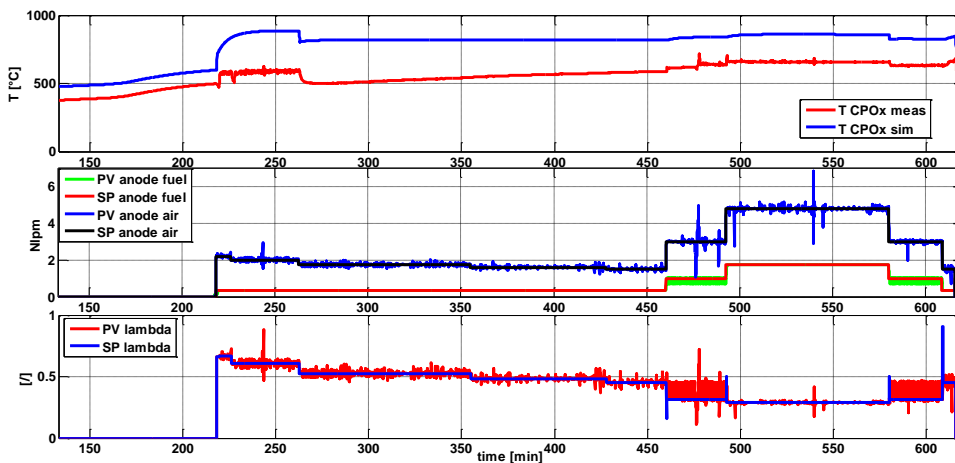


Figure 5.23 – Fault 1 isolation: T_{CPOx} measured and simulated, anode air and fuel flows, lambda vs time in the μ CHP startup afterwards the fault occurrence

A clear indication that the reforming reaction was not occurring properly is given by the long time needed for the reactor to be heated up. When the anode flows are enabled (around min 220), for a lambda of 0.6,

the model predicts a remarkable peak in CPOx temperature, over 900°C, due to the exothermic character of catalytic partial oxidation reaction, whereas the measured temperature barely approached 600°C. As recalled in previous sections, such a high lambda is adopted only for first ramp up (or late startup) phase, after the air/fuel mixture is fed to the reactor, in order to instantaneously raise the temperatures to promote the reforming reaction. In addition to the deviation of almost 300 °C between measured and simulated reactor temperatures, another factor which brings to account for a carbon deposition fault is the very long transient time (over 450 min) required by the reactor to exceed 600 °C, even if the lambda was maintained quite higher with respect to the normal design status. Indeed, in nominal operating conditions the temperature should have exceeded 700 °C, as indicated by the simulated results and confirmed by the rise in the temperature observed at minute 220, just after the anode line enabling. It is worth noting that, since the temperature in the reactor was not increasing sufficiently, for all the test duration the startup burner was hold ignited, also during the operation phase, with the aim to exploit its contribution for the reactor thermal heating. After 480 min, with increasing anode fuel and air flowrates, the oxidation reaction characterizing the indirect CPOx mechanism was promoted in the still active catalyst sites, leading to a slight increase in the temperature.

By examining all these aspects and the temperatures graph in figure 5.23, it appears logical that the reforming reaction was not happening properly inside the reactor. The unique reason for this abnormal behavior can be addressed to the reduction of the catalyst active area. This consideration is consistent with the hypothesis that a carbon deposition event occurred. In this case, in order to investigate about the entity of the fault, it is required to look also to other experimental variables. Indeed, sometimes the difference in CPOx temperature trends between measured and simulated results might not be sufficient to isolate and identify the fault: a CPOx temperature trend below the expectations can be experienced also for other abnormal events, such as catalyst oxidation, described in paragraph 3.3.2. In order to identify the type of fault occurred in the system and to prove that a carbon deposition phenomenon took place, the temperatures plots shall be associated to the information about stack voltage (figure 5.24).

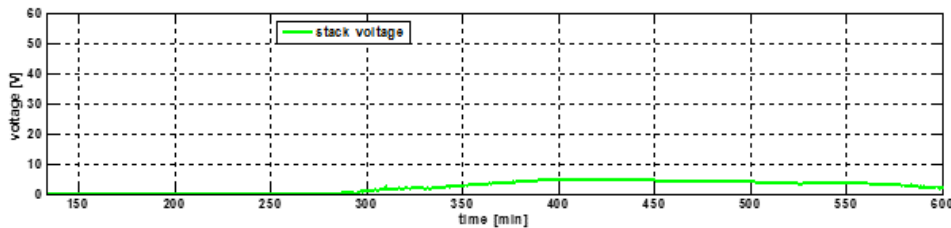


Figure 5.24- Fault 1 isolation: stack voltage in the μ CHP startup afterwards the fault occurrence

As explained in section 3.3.1 and here recalled, the stack voltage shown in figure 5.24 was heavily below the theoretical OCV value registered in the previous startup (60 V). This means that the inlet methane was not totally converted into hydrogen, and in turn the fuel cell anode did not have the ability to carry out the electrochemical reaction which generates electrical current. Most of the fuel entering the CPOx reactor left the same unconverted and reached the fuel cell anode compartment. Here, it could either react inside the stack with the anode air not consumed into the CPOx reactor, or directly burn inside the offgas burner. A combination of both phenomena is also feasible. When the model is included in a large-scale SOFC system dynamic model, the drop in stack voltage might be observed through the variation of the anode inlet composition (reduced H_2 molar fraction).

5.6 - Fault 2- Catalyst oxidation: model based fault detection and isolation

The second fault simulated by the model is the catalyst oxidation, described in paragraph 3.3.2. Figure 5.25 shows the occurrence of the above mentioned fault during the operating phase of μ CHP, with the CPOx reactor temperature approaching undesired and dangerous levels. The fault detection is very simple and immediate in this case, since it happens while operating at steady state conditions and not during the startup phase as experienced for fault 1.

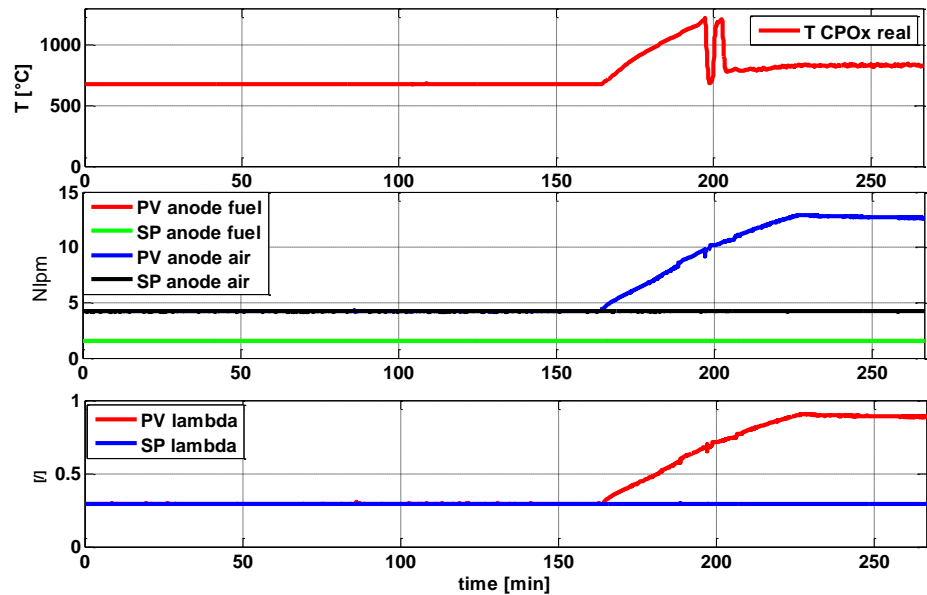


Figure 5.25 – Fault 2 detection: T_{CPOx} , anode air and fuel flows, lambda vs time

A detailed description of the plots reported in figure 5.25 was already given in chapter 3.3.2.

As in the previous case of carbon deposition fault, by investigating the μ CHP performances after the occurrence of this fault it is possible to understand whether this event has caused severe consequences for the CPOx reactor of fuel cell stack. The comparison between measured data and simulated results permits then the fault diagnosis, to acknowledge the ability of the developed model to be used as tool for the fault analysis application. The fault detection and isolation is carried out by looking at the difference between model output temperature and the experimental data measured in the μ CHP start up subsequent to the fault event, shown in figure 5.26.

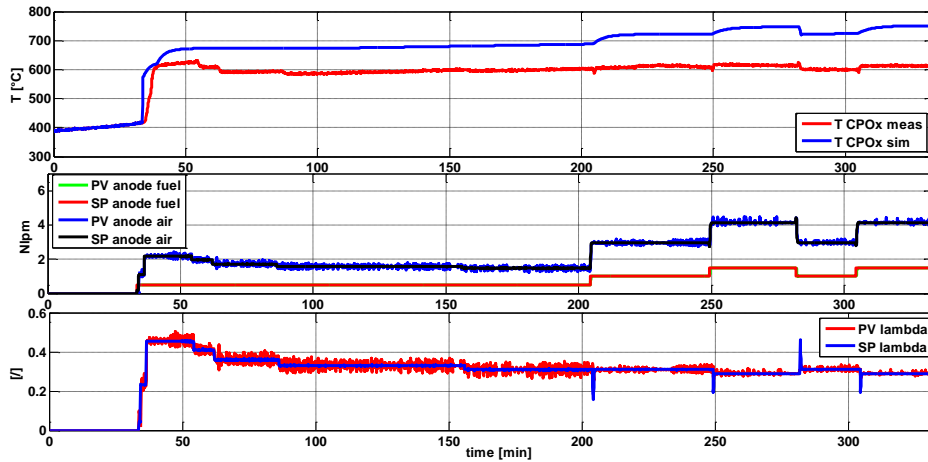


Figure 5.26 – Fault 2 isolation: T_{CPOx} measured and simulated, anode air and fuel flows, lambda vs time in the μ CHP startup afterwards the fault occurrence

The complete temperature trends for this μ CHP startup attempt are shown in figure 3.17 of section 3.3.2. For the model based diagnosis application here considered, only a restricted time frame is taken into account. The fact that the CPOx reactor was working in abnormal conditions is evident. Indeed, the real reactor temperature oscillated around 600°C for each input condition, against the nominal trend expected for the CPOx temperature given by the model, which always keeps around 700°C . Respect to what displayed in the graph 5.23 (carbon deposition fault), in this case the gap between measured and simulated temperature tends to be constant all over the startup and run operating phase. Moreover, the deviation between both trends is lower than the previous case: the maximum offset between nominal and measured reactor temperature is 138°C at minute 318 (750°C the simulated temperature and 612°C the real one). The average deviation for the entire operating period is around 100°C , against the 300°C obtained in the case of carbon deposition. The first peak in the real CPOx temperature trend (minute 34), visible as soon as the anode feeding system is enabled, is properly reproduced by the model. After that, when reducing the lambda value (which however was kept below 0.4 over the entire operating range), the real temperature stabilized around 600°C , whereas the nominal value given by the model approaches 700°C . Nevertheless, the exothermic reforming reaction was taking place inside the reactor, and this is confirmed by the difference respect to the

previous case, where both a higher lambda and the contribution of the startup burner to heat up the reactor were required. The gradient between real and theoretical temperatures increases when moving to the run phase (after min 210), when both air and fuel flowrate were increased and the stack was generating power.

The above considerations lead to conclude that also here some active sites of CPOx catalysts were not working properly. However, differently from the carbon deposition event, the reactor hold its temperature almost constant for each operating condition, even if below the nominal trend offered by the model. This implies that the exothermic reforming reaction was occurring inside the CPOx reactor, but with lower efficiency. This is confirmed by analyzing the stack voltage trend shown in figure 5.27, as done for the diagnosis of carbon deposition fault. Differently from the previous case, in the μ CHP startup carried out just after the fault was detected the stack voltage kept slightly below the nominal OCV value of 60V and the power drawn by the stack was about 340W.

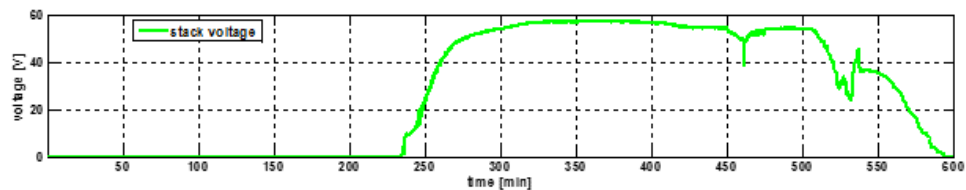


Figure 5.27- Fault 2 isolation: stack voltage in the μ CHP startup afterwards the fault occurrence

The ability of the stack to generate power brings to isolate and identify the fault as catalyst oxidation. In fact, this confirms the hypothesis that the catalyst surface was only partially affected by the fault and the reforming reactions were taking place, even if with a different efficiency and conversion respect to the nominal conditions. The catalyst was therefore partially damaged by the fault and only some active sites were poisoned by the oxide. The likely combustion which occurred inside the reactor when the lambda grow up out of control (between minute 160 and 240 in figure 5.25) could have only in part damaged the catalyst, the seals and the insulating materials. In spite of this, the CPOx reforming however occurred, with reduced conversion and lower H_2 molar fraction yield and also, in turn, reduced electrical stack performances.

Similarly to the previous case, the confirmation of the type of fault

is given by the following test sessions, reported in paragraph 3.3.2. During the subsequent μ CHP startup attempts, the system continued to operate and generate power, with performance progressively reduced, until the stack ended up to be finally damaged after four startup attempts. Several stack clusters have eventually suffered a reduction in the electrical performances and the replacement of the whole cell module was required.

Conclusions

In this thesis an investigation of the reforming methods available for Solid Oxide Fuel Cell (SOFC) systems and their basic concepts has been carried out. The three main reforming mechanisms for SOFC applications have been classified as steam reforming (SR), catalytic partial oxidation (CPOx) and autothermal reforming (ATR). For each method, the reactions involved, the main operating parameters together with the main advantages and the critical issues have been described. Moreover, the thermodynamics and the kinetics of the reaction mechanisms have been analysed, with particular focus on the CPOx reforming, which is the main topic of this thesis.

The Catalytic Partial Oxidation (CPOx) technology has been identified as the most attractive process for the production of syngas or hydrogen in both small-medium scale SOFC applications and Micro Combined Heat and Power (μ CHP) systems. This is due to the ability of the CPOx reaction to be carried out in compact reactors with rapid dynamic response and with low heat capacity. The reaction is slightly exothermic and therefore does not require external heat to take place. In addition, CPOx technology does not require steam, as the media required for the reforming reaction is air, which is easily available for residential application. This mainly means that CPOx is independent from an external water source and any heating source. On the other hand, catalytic partial oxidation is less efficient than steam reforming, therefore it is most suitable for applications where the system simplicity is a priority with respect to high hydrogen yield.

For this mechanism, an analysis of reactor catalysts and supports typically used for SOFC systems has been performed. The Rhodium has been identified as the best noble metal because of its high selectivity to H_2 , low volatility and resistance to coke formation. The best support that can be associated to the Rhodium catalyst in order to maintain the dispersion of the active phase and ensure thermal stability in severe working conditions has resulted to be α - Al_2O_3 .

The general analysis of the CPOx reforming process has allowed the identification of the main parameters to take into account when considering fault diagnosis of reformer based on this technology. The most common fault events likely to occur inside a CPOx reformer for SOFC

systems have been analysed through a Failure Mode and Effect Analysis (FMEA) and a Fault Tree Analysis (FTA). These analyses are aimed at identifying the main events responsible for the catalyst deactivation, together with their causes and effects on the SOFC system performance.

The Catalytic Partial Oxidation mechanism has then been explored from both modelling and experimental points of view, with the aim to simulate the reforming process and identifying the thermodynamic optimal operating conditions at which natural gas may be converted to hydrogen. At the same time, the main fault scenarios likely to occur during the reforming phase have been analysed, both in experiments and during simulations, to evaluate the capability of the developed model in performing effective fault detection and isolation for on-board diagnostic application.

The CPOx dynamic model developed in this thesis is based on the minimization of Gibbs free energy and can be easily reconfigured for describing a steam reforming mechanism. The approach adopted for the thermodynamic model is zero-dimensional (i.e. grey-box model), which is suitable to evaluate the impact of inlet composition (λ) and inlet reactant pre-heating temperature on the product gas fractions and on the reactor outlet temperatures required as outputs. The inlet reactant pre-heating temperature has been linked to the other parameters relevant to the SOFC system (input fuel flow rate, cathode air flow for stack cooling, fuel utilization and CPOx reactor outlet temperature) through a linear regression based on experimental data. The reactor layout adopted in the model assumes the catalytic system most suitable and efficient for the partial oxidation of methane to synthesis gas. The catalyst considered is Rhodium (Rh) deposited over α -Al₂O₃ extruded monoliths ceramic supports with a honeycomb structure.

The model results are useful to identify the conditions that yield to the maximum methane conversion and hydrogen gain in the outlet products according to the limit set for the reactor outlet temperature. For given operating conditions, the equilibrium temperature of the reactor and the equilibrium compositions are calculated. These results are obtained by varying the input parameters, i.e. λ and inlet reactant pre-heating temperature, in the operating range specified for the application of CPOx reactor in a SOFC system.

The first set of results was achieved by running the model at fixed λ in the range 0.25 - 0.33, to evaluate the effect of the inlet reactant

pre-heating temperature (varied in the range 50 - 350 °C) on the reactor outlet compositions and temperature. It was observed that working with a lambda of 0.25 yields the maximum hydrogen gain. However, this does not represent the optimal condition for SOFC applications, as the reactor outlet temperature exceeds 700 °C only when the pre-heating temperature is very high (350 °C). Furthermore, the CH₄ conversion is reduced.

The best conditions are achieved for a lambda in the range 0.29-0.30, leading to a reactor outlet temperature within 680-750°C. Indeed, in these cases the H₂ molar fractions are approaching the maximum yield (around 35%) with reduced reactant pre-heating temperatures, and moreover the methane is almost completely converted (CH₄ conversion above 95%). Both H₂ and CO selectivity are over 90%. For lambda higher than 0.30, the H₂ yield is lower than other conditions, even if the conversion of CH₄ is higher. Simultaneously, the reactor outlet temperatures are too high (more than 860 °C for a pre-heating temperature of 350°C with lambda of 0.33), which implies that this condition is suitable only in the late startup phase, when there is the need to heat up the reactor in order to reach the most suitable conditions.

The second set of results is obtained by varying the lambda in the range 0.25-0.35, at fixed reactant pre-heating temperatures (between 50 and 300 °C), in order to evaluate the effect of working at different lambda on the outlet temperature and compositions. It was found that when the reactant pre-heating contribution is small ($T_{in} = 50^{\circ}\text{C}$) and the lambda below 0.32, the reaction occurs at non optimal temperatures; this leads to a lower H₂ and CO outlet yield, resulting in an overall lower conversion efficiency. Working in the intermediate conditions ($T_{in} = 150^{\circ}\text{C}$ and $T_{in} = 230^{\circ}\text{C}$) with lambda of 0.29-0.30 represents the best option for a CPOx reactor operation. Indeed, these parameters allow operating at an adequate reactor temperature with high efficiencies and H₂-CO selectivity. For each inlet reactant pre-heating temperature, the H₂ yield decreases with increasing lambda (the maximum is for lambda of 0.25), resulting in a lower quality of the reformat exiting the reactor. The CO selectivity trend is decreasing with lambda as well, even if less markedly than H₂, and increasing with the pre-heating temperature.

The model is dynamic and therefore accounts for the transient variations in input conditions, i.e. air and fuel ratio over the startup and run time, in order to describe the CPOx temperature ramp up.

The model has been validated through experimental data gained in three different test cases:

- a)* Internal tests on CPOx reactor integrated in the Hot Box;
- b)* Lab tests on CPOx reactor external to the Hot Box, heated up by electrical resistances;
- c)* Tests on 1 kW planar μ CHP unit.

Tests *a* were performed at Hysytec/SOFC Power facilities on CPOx reactors integrated inside the Fuel Cell Module. The thermal integration allows the reactor to reach the operating temperatures required for its activation through the contribution of the startup burner. In addition, it enables the pre-heating of the reactant gas mixture before entering the reactor. These tests were finalized to evaluate in detail the temperature distribution inside the reactor and to measure the products gas composition via spectral analysis.

Tests *b* were carried out at Hysylab laboratories (Environment Park). In these test sessions, the reactor was separated by the Hot Box. In order to approach the appropriate operating temperature for the CPOx reaction, the mixture entering the reactor and the reactor itself were heated up by means of three electrical resistances. The tests allowed the measurement of products concentrations and temperatures in five different locations inside the reactor for different operating conditions.

The tests performed at Ariston Thermo facilities on the μ CHP final units (tests *c*) were the most complete. Indeed, in addition to the local information directly related to the CPOx reactor, i.e. reactor outlet temperature and lambda, other relevant parameters for the entire SOFC system such as inlet fuel, stack current and cathode air were measured.

The model validation has shown that the simulation results follow accurately the experimental tests for each operating condition and well reproduce the real reaction mechanisms occurring in a CPOx. In transient analysis, the dynamic trend of the CPOx reactor temperature was properly and accurately followed by the model as well.

During the test activities on the planar 1 kW μ CHP (case *c*), two faults, namely carbon deposition and catalyst oxidation, occurred and their effects on the system were evaluated.

The catalyst oxidation fault did not cause irreversible damage as resulted for carbon deposition event; in the former case the SOFC system

is still able to operate for a certain time after the fault occurrence, though out of the nominal range. On the other hand, the catalyst oxidation phenomenon may affect also the stack if not detected in the due time, whereas in case of a carbon deposition event the stack replacement can be avoided.

The faults occurred during the test sessions have been taken into account in the model, with the purpose to evaluate the application of the CPOx dynamic model for fault detection and isolation analysis. Indeed, the diagnosis algorithm has been tested by comparing the real effect of the faults on the reforming reactor parameters with the nominal results given by the model, in order to verify that the fault diagnosis is properly accounted by the simulated conditions. The results shown in the thesis have proven the feasibility of the model to simulate and detect faults likely to occur in a CPOx reactor and thereby have demonstrated its capability to be used as fault detection and isolation tool in SOFC systems.

Ringraziamenti

Al termine del lavoro realizzato, credo sia doveroso esprimere riconoscenza verso le persone che mi hanno costantemente sostenuto ed aiutato in questi anni, permettendomi di superare le difficoltà ed i problemi sorti in corso d'opera.

Un ringraziamento speciale va al Prof. Cesare Pianese, per l'impegno, la competenza, la disponibilità e la pazienza con cui mi ha continuamente seguito e consigliato in ogni fase di realizzazione del lavoro.

Ringrazio l'Ing. Dario Marra, per la costanza e la pazienza con cui mi ha seguito ed aiutato dal primo all'ultimo giorno di lavoro. Senza le sue brillanti idee e le competenti delucidazioni non sarei stato in grado di portare a termine il lavoro.

Ringrazio il Prof. Marco Sorrentino, per la preziosa collaborazione e per gli utili consigli.

Ringrazio Ariston Thermo, gruppo in cui ho lavorato per due anni e mezzo, per avermi dato la possibilità di coniugare il lavoro in azienda con l'attività di dottorato, consentendomi di utilizzare i dati resi disponibili dal progetto EFESO per lo sviluppo della mia tesi. In particolare, ringrazio Lorenzo Marra e Doriano Tabocchini, per avermi aiutato a crescere professionalmente mettendo a disposizione la loro esperienza e competenza, e per la fiducia riposta nei miei confronti.

Sempre nell'ambito del progetto EFESO, ringrazio tutti i partner coinvolti che hanno acconsentito all'utilizzo dei risultati conseguiti ed alla divulgazione degli stessi nel mio lavoro di tesi. Grazie a Massimo Bertoldi ed Andrea Leonardi (SOFC POWER), Massimiliano Antonini e Marco Mori (Hysytech), Sabina Fiorot ed Alessandro Graizzaro (Environment Park), Stefan Wirth e Tony Litka (Acumentrics).

Grazie a Giada, amb, per avermi sostenuto e motivato costantemente per tutta la durata del dottorato, incitandomi nei momenti difficili ed aiutandomi quando richiesto, come soltanto la persona con cui sai di voler condividere ogni momento della tua vita sa fare.

Ringrazio i miei genitori e mia sorella Marianna, che sono da sempre i miei punti di riferimento e non mi hanno mai fatto mancare il loro affetto ed il loro sostegno.

References

- [1] M. Sorrentino, C. Pianese, 2007, "Control Oriented Modeling of SOFC Auxiliary Power Unit for Transportation Applications". Proceedings of the ASME 5th International Conference on Fuel Cell Science, Engineering and Technology New-York, NY, USA 18-20 giugno 2007 Vol.1, Pag.1-12
- [2] M. Sorrentino, 2005, "Development of a Hierarchical Structure of Models for Simulation and Control of Planar Solid Oxide Fuel Cells".
- [3] R. Isermann, 2006, "Fault Diagnosis System, An Introduction from Fault Detection to Fault Tolerant".
- [4] M. Witczak, 2003, "Identification and Fault Detection of Non-Linear Dynamic Systems".
- [5] G. Rizzoni, P. Pisu, R. Scattolini, 2008, "Fault Detection and Diagnosis in Mechatronic Systems".
- [6] A.Di Filippi, 2010, Master Thesis: "Fault Tree Analysis and development of a Fault Detection and Isolation scheme for SOFC systems"
- [7] R.J. Braun, 2002, PhD Thesis: "Optimal Design and Operation of Solid Oxide Fuel Cell Systems for Small-scale Stationary Applications"
- [8] Y.S. Seo, A. Shirley, S.T. Kolaczekowsky: "*Evaluation of thermodynamically favorable operating conditions for production of hydrogen in three different reforming technologies*"; Journal of Power sources, 108 (2002) 213-225.
- [9] M.Martinelli, PhD Thesis, "Application of the spatially resolved sampling technique to the analysis and optimal design of a CH₄-CPO reformer with honeycomb catalyst".
- [10] J.I.Gazzarri, 2007, "Impedance Model of a Solid Oxide Fuel Cell for Degradation Diagnosis".
- [11] J.Larminie, A.Dicks, "Fuel Cell Systems Explained-Second Edition", 2003.
- [12] Adris A.M., Pruden B.B., Lim C.J., Grace J.R.: "*On the reported attempts to radically improve the performance of the steam methane reforming reactor*"; Can. J. Chem. Eng., 74 (1996) p. 177.
- [13] A. Heinzl, B. Vogel, P. Hubner: "*Reforming of natural gas-hydrogen generation for small scale stationary fuel cell systems*"; Journal of

- Power Sources, 105 (2002) 202-207.
- [14] Schmidt L.D., Bharadwaj S.S.: “*Catalytic partial oxidation of natural gas to syngas*”; Fuel processing technology, 42 (1995) 109-127.
- [15] Y. Matsumura, T. Nakamori: “*Steam reforming of methane over nickel catalysts at low reaction temperature*”; Applied Catalysis A: General, 258 (2004) 107-114.
- [16] Bizzi M., Saracco G., Schwiedernoch R., Deutschmann O.: “*Modeling the Partial Oxidation of Methane in a Fixed Bed with Detailed Chemistry*”; AIChE J., 50 (2004) 1289-1299.
- [17] S.S. Bharadwaj L.D. Schmidt - *Catalytic partial oxidation of natural gas to syngas*. - Fuel Proc. Techn. 42, 109-127 (1995).
- [18] I. Bobrova, N. Bobrov, V. Chesnokov, V. Parmon: “*Catalytic Steam Reforming of Methane: New Data on the Contribution of Homogeneous Radical Reactions in the Gas Phase: II. A Ruthenium Catalyst*”; Kinetics and Catalysis, Vol. 42, No. 6 (2001) 805–812.
- [19] Tavazzi I., Maestri M., Beretta A., Groppi G., Tronconi E.: “*Steady-State and Transient Analysis of a CH₄-Catalytic Partial Oxidation Reformer*”; AIChE J., 52 (2006) 3234-3244.
- [20] L.V. Mattos, E.R. de Oliveira, P.D. Resende, F.B. Noronha, F.B. Passos: “*Partial oxidation of methane on Pt/Ce–ZrO₂ catalysts*”; Catalysis Today, 77 (2002) 245–256.
- [21] Schmidt L.D., Hickman D.A.: “*Steps in CH₄ Oxidation on Pt and Rh surfaces: High temperatures reactor simulations*”; AIChE J., 39 (1993) 7.
- [22] R. Horn, K.A. William, N.J. Degenstein, L.D. Schmidt.- *Syngas by catalytic partial oxidation of methane: mechanism conclusion from spatially resolved measurement and numerical simulations* - Journal of Catalysis 242(2006), 92-102.
- [23] Prette M., Eichner C., Perrin M.: “*The catalytic oxidation of methane to carbon monoxide and hydrogen*”; Chem. Rev. 1940; 27; 1.
- [24] Heitnes K., Lindberg S., Rokstad O.A., Holmen A.: “*Catalytic partial oxidation of methane to synthesis gas*”; Catalysis Today, 24 (1995) 211-216.
- [25] G. Veser, J. Frauhammer, U. Friedle: “*Syngas formation by direct oxidation of methane Reaction mechanisms and new reactor concepts*”; Catalysis Today, 61 (2000) 55-64.
- [26] A.M. De Groote, G.F. Froment: “*Simulation of the catalytic partial oxidation of methane to syngas*”; Applied Catalysis A: General, 138

(1996) 245-264.

- [27] F. Basile, G. Fornasari, F. Trifirò, A. Vaccari: “*Partial oxidation of methane. Effect of reaction parameters and catalyst composition on the thermal profile and heat distribution*”; *Catalysis Today*, 64 (2001) 21-30.
- [28] Z. Chen, Y. Yan, S. S.E.H. Elnashaie, 2004, “Catalyst deactivation and engineering control for steam reforming of higher hydrocarbons in a novel membrane reformer”, *Chemical Engineering Science* 59 (2004) 1965 – 1978.
- [29] H.-J. Jahn, W. Schroer, 2005, “Dynamic simulation model of a steam reformer for a residential fuel cell power plant”, *Journal of Power Sources* 150 (2005) 101–109.
- [30] P. Dokamaingam, S. Assabumrungrat, A. Soottitantawat, 2008, “Modeling of SOFC with indirect internal reforming operation: Comparison of conventional packed-bed and catalytic coated-wall internal reformer”, *international journal of hydrogen energy*.
- [31] M. Prettre, Ch. Eichner and M. Perrin - *Trans Faraday Soc.* 42, 335, 1946.
- [32] S.S. Bharadwaj L.D. Schmidt - *Catalytic partial oxidation of natural gas to syngas.* - *Fuel Proc. Techn.* 42, 109-127 (1995).
- [33] W.Wang, S.M. Stagg-Williams, F.B. Noronha, L.V. Mattos, F.B. Passos, *Catal. Today* 98 (2004) 553
- [34] L. Ma, D. Trimm: “*Alternative catalyst bed configurations for the autothermic conversion of methane to hydrogen*”; *Applied Catalyst A: General*, 136 (1996) 265-273.
- [35] J. Xu, G.F. Froment: “*Methane Steam Reforming, Methanation and water Gas Shift: Intrinsic Kinetics*”; *AIChE Journal*, 35 (1989) n°1, 88-102.
- [36] Hysytech (Hydrogen System Technology) srl, deliverables and work packages reports of EFESO project, 2011-2013. <http://www.hysytech.com/>
- [37] SOFC Power spa, deliverables and work packages reports of EFESO project, 2011-2013. www.solidpower.com
- [38] Acumentrics Corporation, deliverables and work packages reports of EFESO project, 2011-2013. www.acumentrics.com
- [39] R.P. Aldaco, 2007, “A Model based framework for Fault Diagnosis and Prognosis of dynamical systems with an application to helicopter transmissions”.

- [40] S.C. Singhal, K.Kendall, 2004, "High Temperatures Solid Oxide Fuel Cells: Fundamentals, Design and Applications".
- [41]] Bijan F. Hagh: "*Optimization of autothermal reactor for maximum hydrogen production*"; International Journal of Hydrogen Energy, 28 (2003) 1369-1377.
- [42] Hoang D.L., Chan S.H., Ding O.L.: "*Hydrogen production for fuel cells by autothermal reforming of methane over sulphide nickel catalyst on a gamma alumina support*"; J. Power Sources, 159 (2006) 1248-1257.
- [43] Tomishige K., Nurunnabi M., Maruyama K., Kunimori K.: "*Effect of oxygen addition to steam and dry reforming of methane on bed temperature profile over Pt and Ni catalysts*"; App Cat. A: Gen., 85 (2004) 1103-1120.
- [44] Hoang D.L., Chan S.H.: "*Experimental investigation on the effect of natural gas composition on performance of autothermal reforming*"; Int. J. Hydrogen Energy, 32 (2007) 548-556.
- [45] M. Souza, M. Schmal: "*Autothermal reforming of methane over Pt/ZrO₂/Al₂O₃ catalysts*"; Applied Catalysis A: General, 281 (2005) 19–24.
- [46] Li B., Maruyama K., Nurunnabi M., Kunimori K., Tomishige K.: "*Temperature profile of alumina-supported noble metal catalyst in autothermal reforming of methane*"; App. Cat. A: Gen., 275 (2004) 157-172.
- [47] Joensen, F., Rostrup-Nielsen, J. (2002) "*Conversion of hydrocarbons and alcohols for fuel cells*". J. Power Sources 105, 195-201.
- [48] P.M. Biesheuvel and G.J. Kramer, "*Two-section reactor model for autothermal reforming of methane to synthesis gas*" AIChE J. 49, 1827-1837 (2003).
- [50] L.Salemme, PhD Thesis, "*Produzione di idrogeno a partire da metano in un reattore autotermico*".
- [51] Lin ST, Chen YH, Yu CC, Liu YC, Lee CH. "*Dynamic modeling and control structure design of an experimental fuel processor*" Int J Hydrogen Energ 2006;31(3):413–26.
- [52] Wei ZhengWeng, Qian Gu Yan, Chun Rong Luo, Yuan Yan Liao and Hui Lin Wan." "*The concentration of oxygen species over SiO₂-supported Rh and Ru catalysts and its relationship with the mechanism of partial oxidation of methane to synthesis gas*" Catalysis Letters Vol. 74, No. 1–2, 2001

- [53] J. Zhua, D. Zhanga,*, K.D. King: “*Reforming of CH₄ by partial oxidation: thermodynamic and kinetic analyses*”; Fuel 80 (2001) 899-905
- [54] Q.G. Yan , T.H. Wub, W.Z. Weng, H. Toghiani , R.K. Toghiani, H.L. Wan,*, C.U. Pittman Jr.: “*Partial oxidation of methane to H₂ and CO over Rh/SiO₂ and Ru/SiO₂ catalysts*”; Journal of Catalysis 226 (2004) 247–259
- [55] Dissanayake, D., Rosynek, M.P., Kharas, K.C.C., & Lunsford, J.H. (1991). “*Partial oxidation of methane to CO and H₂ over a Ni/Al₂O₃ catalyst*”. J. Catal., 132, 117-127.
- [56] Dissanayake, D., Rosynek, M.P., & Lunsford, J.H. (1993). *Are the equilibrium concentrations of CO and H₂ exceeded during oxidation of CH₄ over a Ni/Yb₂O₃ catalyst* J. Chem. Phys., 97, 3644-3646.
- [57] Joelmir A.C. Dias, José M. Assaf:” *The advantages of air addition on the methane steam reforming over Ni/_-Al₂O₃*”; Journal of Power Sources 137 (2004) 264–268
- [58] Joelmir A.C. Dias, José M. Assaf “*Autothermal reforming of methane over Ni/ γ -Al₂O₃ promoted with Pd: The effect of the Pd source in activity, temperature profile of reactor and in ignition*”, Applied Catalysis A General 01/2008; 334(s 1–2):243–250.
- [59] Johnson Matthey Catalysts, *The catalyst technical handbook*, 2008
- [60] Pio Forzatti , Luca Lietti, ” *Catalyst deactivation*”, Catalysis Today 52 (1999) 165-181
- [61]H. Liander - Trans. Faraday Soc. 25, 462, 1929.
- [62]C. Padovani, P. Facchinetti - Giorn. Chem. Ind. Appl. Catal. 15, 429, (1933).
- [63]A.P.E York, T. Xiao, and M.L.H. Green - *Brief overview of partial oxidation of methane to synthesis gas*. - Topics in Catalysis, 22
- [64]D.A Hickman, L.D. Schimdt – *Synthesis gas formation by direct oxidation of methane over Pt monoliths* - J. Catal., 138, 267, 1992.
- [65]D.A. Hickman, L.D. Schmidt - AlChE J. 39 (1993), 1164.
- [66]Edwards N., Ellis S.R., Frost J.C., Golunski S.E., van Keulen A.N.J., Lindewald N.G., and Reinkingh J.G. (1998) “*Onboard hydrogen generation for transport applications: the HotSpot methanol processor*”, Journal of Power Sources, 71(1–2), 123–128.
- [67]Dvorak K., van Nusselrooy P.F.M.T., Vasalos I.A., Berger R.J., Olsbye U., Verykios X.E., Roberts M.P., Hildebrandt U., and

- Hageman R. (1998) “*Catalytic Partial Oxidation of Methane to Synthesis Gas*”, report of EU Contract JOF3-CT95-0026.
- [68] Kumar R., Ahmed S., and Krumpelt M. (1996) “*The low temperature partial oxidation reforming of fuels for transportation fuel cell systems.*” Proceedings of the US Fuel Cell Seminar, Kissimee, Florida, November, pp. 17–20.
- [69] Schmidt L.D., Klein E.J., O’Connor R.P., and Tummala S. (2001) “Production of hydrogen in millisecond reactors: combination of partial oxidation and water-gas shift”, *Abstracts of Papers of the American Chemical Society*, 222 (FUEL Part 1) 111.
- [70] P.D:F: Vernon, M.L.H. Green, A.K. Cheetham, A.T. Ashcroft - *Catal. Lett.* 6 (1990)181.
- [71] Dong W.-S., Roh H.-S., Jun K.-W., Park S.-E., Oh Y.-S., “*Methane reforming over Ni/Ce ZrO₂ catalysts: effect of nickel content*”, *Applied Catalysis A: General* Volume 226, Issues 1–2, 28 March 2002, Pages 63–72
- [72] Tianli Zhu, Maria Flytzani-Stephanopoulos, “*Catalytic partial oxidation of methane to synthesis gas over Ni–CeO₂*”, *Applied Catalysis A: General* 208 (2001) 403–417
- [73] D.L. Trimm, “*Catalysts for the control of coking during steam reforming*”, *Catalysis Today* 49 (1999)
- [74] Konrad Herbst , Gurli Mogensen, Florian Huber, Martin Østberg, Martin Skov Skjøth- Rasmussen – *Challenges in applied oxidation catalysis* – *Catalysis Today* 157 (2010), 297- 302.
- [75] Hamada K, Mizusawa M., and Koga K. (1997) “*Plate Reformer*” US Patent no. 5,609,834.
- [76] Shinke N., Higashiguchi S., and Hirai K. (2000) *Fuel Cell Seminar Abstracts*, Courtesy Associates Inc., Portland, Oregon, pp. 292–295.
- [77] Goulding P.S., Judd R.W., and Dicks A.L. (2001) 8UK Patent Application GB 2353801.
- [78] Ogden J.A. (2001) “*Review of Small Stationary Reformers for Hydrogen Production,*” International Energy Agency Report No. IEA/H2/TR-02/002
- [79] By J. W. Jenkins and E. Shutt, *The Hot Spot TM Reactor: hydrogen generation using a novel concept*, Johnson Matthey Technology Centre, 1989
- [80] Van Hook J.P. (1980) *Catalysis Review/Science and Engineering*, 21.

- [81] Rostrup-Nielsen J.R. (1984) in J.R. Anderson and M. Boudart (eds.) “*Catalytic Steam Reforming*” Catalytic Science and Engineering. Vol. 5, Springer-Verlag, Copenhagen.
- [82] Twigg M. (1989) *Catalyst Handbook*, 2nd ed., Wolfe, London.
- [83] De Falco, Marrelli, Iaquaniello, *Membrane Reactors for Hydrogen Production Processes*, 2011, XII, 235 p.
- [84] V.M. Janardhanan, V. Heuveline, O.Deutschmann a, “*Performance analysis of a SOFC under direct internal reforming conditions*”, Journal of Power Sources 172 (2007) 296–307
- [85] I. Arsie, A. Di Filippi, D. Marra, C. Pianese, M. Sorrentino, in: “*Fault Tree Analysis aimed to design and implement on-field Fault Detection and Isolation schemes for SOFC systems.*” ASME 2010 Eighth International Fuel Cell Science, Engineering and Technology Conference
- [86] P. Polverino , C. Pianese, M. Sorrentino, D. Marra, “*Model-based development of a fault signature matrix to improve solid oxide fuel cell systems on-site diagnosis*”, Journal of Power Sources 280 (2015)
- [87]K. Ho Lee a, R. K. Strand, 2009, “*SOFC cogeneration system for building applications, part 1: Development of SOFC system-level model and the parametric study*”, Renewable Energy 34 (2009) 2831–2838.
- [88] Scognamiglio D, Russo L, Maffettone PL, Salemme L, Simeone M, Crescitelli S. “*Modelling and simulation of a catalytic autothermal methane reformer with Rh catalyst*”. Int J Hydrogen Energy 2012;37:263e75
- [89]Ramaswamy , Ramachandran, Dudukovic “*Modeling catalytic partial oxidation of methane to syngas in short-contact-time packed-bed reactors*” Ind Eng Chem Res 2007;46:8638e51.
- [90]Donazzi A, Maestri M, Beretta A, Groppi G, Tronconi E, Forzatti P. “*Microkinetic analysis of CH4 CPO tests with CO2- diluted feed streams*” Appl Catal A Gen 2011;391:350e9.
- [91] M. Nielsen, S. Kaer, *Modeling a PEM Fuel Cell Natural Gas Reformer*, in: Proceedings of the 16th International Conference on Efficiency, Costs, Optimization, and Environmental Impact of Energy Systems (ECOS), Copenhagen, Denmark, 2003.
- [92] J.E.P. Navalho, I. Frenzel, A. Loukou, J.M.C. Pereira, D. Trimis, J.C.F. Pereira, “*Catalytic partial oxidation of methane rich*

- mixtures in non-adiabatic monolith reactors*”, international journal of hydrogen energy, 38 (2013).
- [93] Maestri M, Beretta A, Groppi G, Tronconi E, Forzatti P. “*Comparison among structured and packed-bed reactors for the catalytic partial oxidation of CH₄ at short contact times*” Catal Today 2005;105:709e17.
- [94] Dalle Nogare D, Degenstein NJ, Horn R, Canu P, Schmidt LD. “*Modeling spatially resolved profiles of methane partial oxidation on a Rh foam catalyst with detailed chemistry*” J Catal 2008;258:131e42.
- [95] Beretta A, Groppi G, Lualdi M, Tavazzi I, Forzatti P. “*Experimental and modeling analysis of methane partial oxidation: transient and steady-state behavior of Rh-coated honeycomb monoliths*” Ind Eng Chem Res 2009;48:3825e36.
- [96] Lee ST, Aris R. “*On the effects of radiative heat transfer in monoliths*”. Chem Eng Sci 1977;32:827e37.
- [97] Modest MF. *Radiative heat transfer*. New York: McGraw-Hill; 1993.
- [98] I. Istadi, Didi D., Nor Aishah Saidin, Wei Ling, “*Catalyst Deactivation Simulation Through Carbon Deposition in Carbon Dioxide Reforming over Ni/CaO-Al₂O₃ Catalyst*” Bulletin of Chemical Reaction Engineering & Catalysis, 6 (2), 2011, 129 – 136
- [99] J. T. Pukrushpan, A.. Stefanopoulou, S.Varigonda, L.Pedersen, S.Ghosh, H.Peng,” *Control of Natural Gas Catalytic Partial Oxidation for Hydrogen Generation in Fuel Cell Applications*”
- [100] V. Liso, A.C.Olesen, M.P.Nielsen, S.K. Kær,”*Performance comparison between partial oxidation and methane steam reforming processes for solid oxide fuel cell (SOFC) micro combined heat and power (CHP) system*”, Energy 36 (2011) 4216e4226
- [101] R.H.Perry, Don W.Green, “*Perry’s Chemical Engineers’ Handbook*”, 7th edition, 1997
- [102] Environment Park, deliverables and work packages reports of EFESO project, 2011-2013.
www.envipark.com
- [103] Ariston Thermo spa, deliverables and work packages reports of EFESO project, 2011-2013.
www.ariston.com